UNIVERSITA' DEGLI STUDI DI PADOVA

DIPARTIMENTO DI SCIENZE CHIMICHE

CORSO DI LAUREA MAGISTRALE IN CHIMICA

The use of thermally activated delayed fluorescence (TADF) emitters in light-mediated strain release processes.

Relatore: Prof. Luca Dell'Amico

Controrelatore: Prof. Antonio Barbon

LAUREANDO: Visentini Stefano

ANNO ACCADEMICO 2022 / 2023

Table of Contents

Preface

In modern chemistry, one of the most exciting concepts is the interaction between light and matter. The last decades of the 20th century, known as ‘Golden age of photochemistry’, brought to the scientific community a massive development of photochemical and photocatalytic reactivity. This led to several and detailed studies on the light sources and materials, the photocatalyst nature and the reaction mechanisms. The interest in the field of photochemistry grown rapidly just as the number of publications. Consequently, in the recent years a huge number of transformations and photocatalysts has been produced, particularly in the field of organic synthesis, where photochemistry has found its major application. The possibility to achieve incomparable reactivity with respect to the traditional polar and thermal chemistry represents for the photochemistry a very powerful tool to build organic structures. This is also due to the possibility of using milder reaction conditions, due to the use of a ‘greener’ energy source with respect to heat, and the avoidance of utilizing dangerous and toxic reagents. This thesis project aims to go into the details of the development of a photocatalytic transformation, investigating the roles of the key parameters of the process with a particular focus on the choice of the photocatalyst.

Another important concept regards the role of saturated aza-strained-cycle in the scientific environment. Azetidines, organic compounds composed by a four-member nitrogen containing cycle, represent a relevant scaffold for bio-active compounds. It is present in natural product and, in the last 20 years, also in agrochemicals and drugs discovery. It has been demonstrated that the azetidine motif has enhanced physicochemical and pharmacokinetic properties with respect to the corresponding extended saturated and unsaturated cycle. However, their use is limited due to the lack of efficient synthetic methods, that usually requires harsh conditions (high temperature, long reaction times, over stoichiometric amounts of reagents). This thesis project aims to provide a new synthetic methodology to access the azetidine moiety, with the use of photocatalytic conditions, visible light and at room temperature.

1. Introduction

1.1 Photochemistry

Photochemistry, the branch of chemistry that deals with chemical reactions initiated by the absorption of light, has revolutionized the field of organic synthesis and catalysis. [1] The possibility to use light as an energy source offers numerous advantages over traditional thermal methods, including milder reaction conditions, enhanced selectivity, and the ability to access unique reaction pathways (Figure 1). [2],[3]

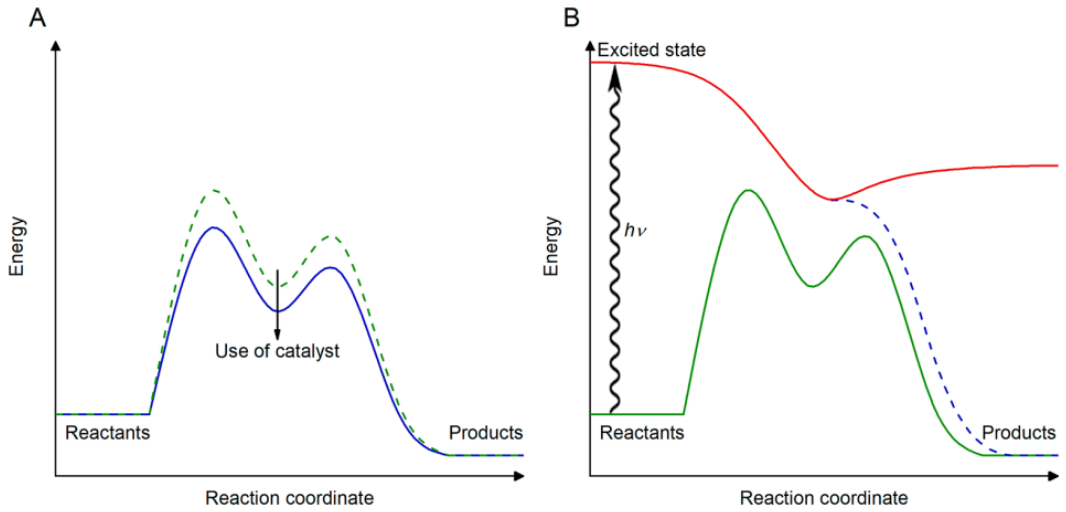

***Figure 1**. Thermal reaction vs photochemical reaction energy diagram. Reproduced from [3].*

When exposed to light, molecules undergo electronic excitation, leading to a significant rearrangement of their electron distribution compared to their ground state. Consequently, the chemical properties and reactivity of these molecules change, resulting in a broader range of reaction outcomes depending on the nature of the starting materials. [4] When using photochemical steps into a synthesis can considerably shorten it while facilitating the formation of complex, polycyclic, or highly functionalized structures. Such photochemical transformations offer new possibilities for accessing product families or libraries that are challenging to achieve with ground-state reactions, providing novel prospects for discovering biologically active compounds. This

feature makes photochemical reactions particularly attractive in the context of green chemistry, aligning with sustainable and environmentally friendly principles. Additionally, some of these reactions can be performed using visible light or sunlight as a renewable energy source, a concept initially considered by Giacomo Ciamician almost a century ago in 1912. [5]

1.1.1. General concepts of photophysics

In order to initiate a photochemical reaction, the light must be absorbed by a chemical compound, when a molecule is excited to a high-energy state, an electronic transition occurs. This event can occur only if the transition dipole moment is different to zero, following the Fermi's Golden Rule, [6] that says that the transition rate depends upon the strength of the coupling between the initial and finale state and upon the density of the final states of the system The probability of the electronic transition is also related to the overlap between the vibrational wavefunctions of the ground and excited-state, defined by the Franck-Condon factor. [7] The initial and the final spin states must be equivalent, so after the absorption of a photon, a molecule is excited from the singlet ground state S_0 to a singlet excited state S_n. As depicted in the Jablonski diagram [8] (Figure 2), the molecule in the S_n state can undergo different decays to regenerate its ground state.

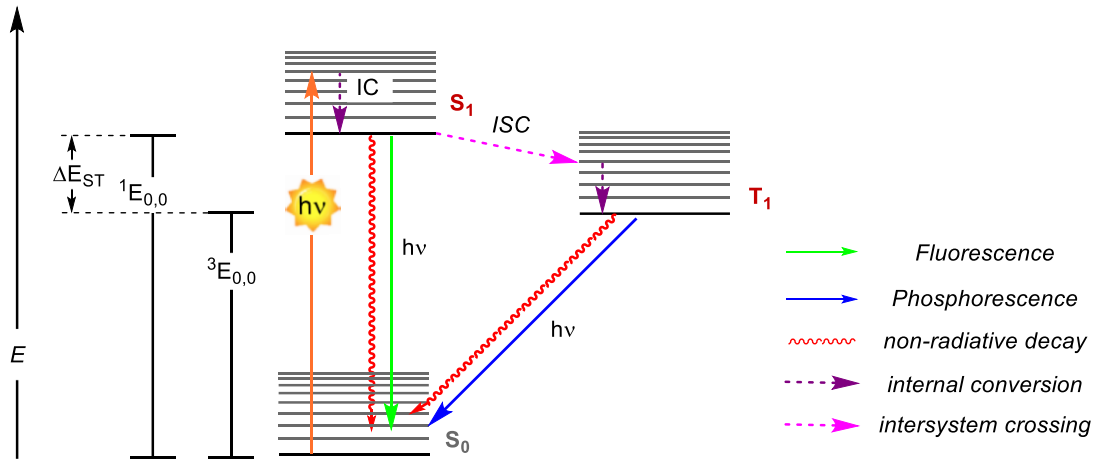

Figure 2. *Jablonski diagram.*

The faster process is usually the internal conversion (IC), that occurs in picoseconds (ps) scale time, that brings the molecule to the lowest vibrational level of the excited singlet state S_1. This could evolve through radiative (fluorescence) or non-radiative decay to reform the S_0 state. Another possible pathway from the S_1 state is the spin-forbidden intersystem crossing to the triplet excited state T_1, that for most of organic molecules is more stabilized and more long-lived with respect to the S_1 state. Finally, the T_1 state, as the S_1, could evolve through radiative (phosphorescence) or non-radiative decay to restore the S_0 state.

1.1.2 *Direct Photochemistry in Organic synthesis*

When the light is absorbed directly by the species that undergo the chemical transformation, we talk about direct photochemistry, a general photochemical reaction could be described as depicted in Scheme 1:

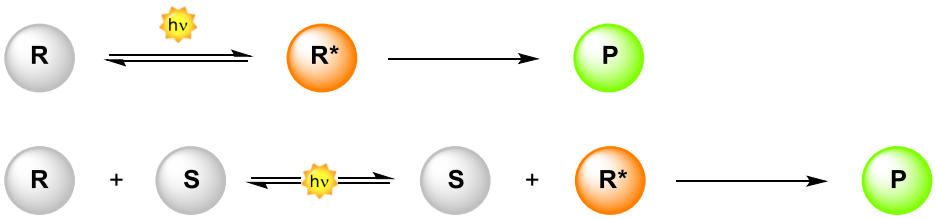

***Scheme 1**. General photochemical reaction.*

The light is absorbed by a general reactant **R**, that reaches the excited state **R*** that evolves directly, or through a chemical reaction with a substrate **S**,to the final product **P**. The interest in photochemistry had a huge improve during the 20th century, scientists developed several transformations, such as pericyclic reactions, photoisomerizations, photodimerizations and Norrish type reactions. A tangible example of this can be found in the chemistry of Santonin (**1**), depicted in Scheme 2, one of the first reported compound involved in light-induced reactivity. [4] It's an anthelmintic sesquiterpene lactone. It occurs in the leaves and flower buds of various species of artemisia and is the active ingredient of Levant wormseed which was widely used in medicine. It was isolated for the first time in the 1830 by Kahler and Alms, [9],[10] a few years later

Trommsdorff [11] observed the change of the color after exposition to light, and he got interested in the wavelength dependency of the transformation. The santonin and its yellow photo-photoproduct (**2**) were characterized only 100 years later thanks to the work of Sestini and Cannizzaro, [12],[13] which also observed the photodimerization products (**3**) and (**4**).

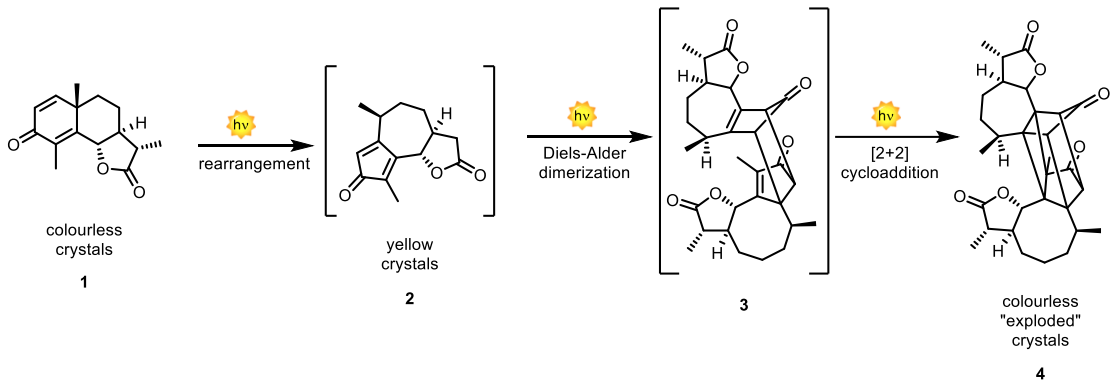

***Scheme 2**. Photochemistry of Santonin.*

While direct photochemistry offers notable advantages, it does come with certain limitations that warrant consideration. Primarily, there must be light absorption by at least one of the reactants; if this criterion is weakly fulfilled or absent, the desired transformations can become difficult or impossible to achieve. Conversely, selectivity poses another potential concern, as it may lead to the formation of unintended products or even degradation. When multiple species within the same mixture are excited, divergent pathways may be explored, compromising the overall cleanliness and selectivity of the transformations.

Furthermore, the compatibility of substrates may be constrained. The utilization of multiple functional groups could prove unfeasible due to stability issues arising from the requirement for UV light, since not all the organic molecules have chromophores in their structure able to absorb the visible light. Consequently, the range of applicable substrates might be limited, thereby hampering the scope of potential reactions.

The advent of photocatalysis has effectively addressed and improved upon many of these limitations.

In the next section, the focus turns to photocatalysis as a distinct field. Here, the multifaceted nature of photocatalytic reactions will be thoroughly explored, with the focus on the diverse pathways that these reactions can traverse.

1.1.3 Photocatalysis

The principles of photocatalysis involve the activation of a photocatalyst, that could be either transition-metal based or purely organic, by absorption of photons. [14] The resulting high energy state transient species can participate in a variety of photochemical transformations. The photocatalyst can act as an electron donor or acceptor, mediating the transfer of electrons or energy to substrate molecules, initiating a cascade of chemical transformations. This unique mode of reactivity allows for the selective activation of specific bonds, facilitating the synthesis of complex and valuable organic molecules with high precision.

Photocatalysis has emerged as a versatile and sustainable tool for driving organic transformations and has gained significant attention in recent years. [14] The growing interest in photocatalysis came from the urgent need for more sustainable and environmentally friendly approaches to chemical synthesis. By employing less energetic wavelengths, milder conditions can be achieved, enhancing the stability of reactants. Notably, selectivity is improved as the photocatalyst is selective excited, diminishing the number of possible reaction pathways. [15] Additionally, the substrate scope widens, tolerating a greater variety of functional groups. This expansion of compatibility is facilitated by the photogenerated catalytic species.

Efficiency also experiences a marked increase, owing to the photocatalyst's higher quantum yield and superior absorption properties compared to conventional organic substrates. Moreover, reaction rates are accelerated, as the photocatalyst acts as an effective mediator the transformation kinetics. [16] Photocatalysis provides an attractive alternative by utilizing readily available and non-toxic catalysts that can efficiently convert light energy into chemical transformations. [17]

The versatility of photocatalysis is exemplified by its broad applicability in diverse areas of organic synthesis. From the construction of carbon-carbon and carbon-heteroatom bonds to the functionalization of “inert” C-H bonds, photocatalysis has enabled the development of new synthetic strategies and the synthesis of complex molecules that were previously challenging or impossible to access. Additionally, the compatibility of photocatalysis with various reaction conditions and functional groups unlocks opportunities for late-stage functionalization and reducing the number of synthetic steps. [18]

Despite its tremendous potential, the field of photocatalysis in organic synthesis is still relatively young, and many fundamental aspects remain to be explored. The design and development of efficient and selective photocatalysts, understanding the underlying mechanistic pathways, and optimization of reaction conditions are key areas of research that demand further investigation. Furthermore, the scalability and practicality of photocatalytic processes for large-scale applications need to be addressed to facilitate their implementation in industry.

There are various mechanisms that govern the interactions between light, photocatalyst, and reagents. Here, we describe some of the different mechanisms commonly observed in organic photocatalysis:

Single Electron Transfer (SET). In SET type mechanism, the PC donates or accepts an electron to or from a reactant, generating active radical species. [19] These species initiate the subsequent reaction steps, such as bond formation or cleavage. The excited PC is either a better oxidant or a better reductant with respect to its ground state form as depicted in Figure 3. Upon excitation, two singularly occupied molecular orbitals (SOMO) are formed, the lowest in energy is more stabilized with respect to the highest occupied molecular orbital (HOMO) of the ground state form, resulting in a higher oxidative power of the PC*, on the contrary, the highest SOMO is more destabilized with respect to the Lowest unoccupied molecular orbital (LUMO) of the ground state, resulting in an enhanced reductive power of the PC*.

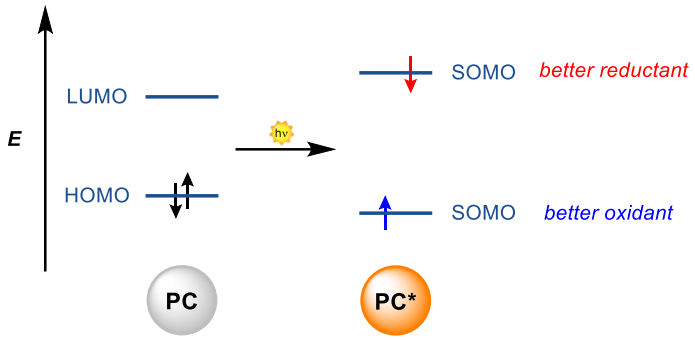

Figure 3. *Energy level comparison between ground state and excited state of a PC.*

Consequently, the PC* is able to donate or accept an electron to or from a substrate that is the ground state, following one of the two possible cycles depicted in Scheme 3.

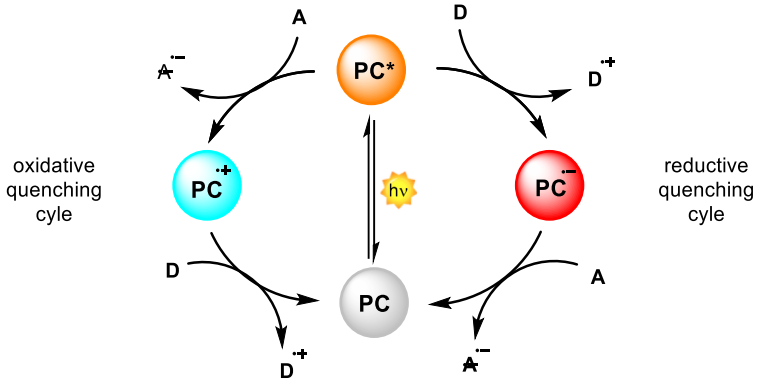

Scheme 3*. SET photocatalytic cycle.*

In the oxidative quenching cycle, the excited PC (PC*) donates an electron to an acceptor, forming the radical cation form of the PC and the radical anion form of the substrate that can undergo subsequent transformations. The PC has to be restored to its ground state form with another SET process that requires the presence of a donator. In the reductive quenching cycle, the PC* promotes an oxidation of the substrate that in this case is a donor moiety, generating the radical anion form of the PC that, upon a subsequent SET event can restore the PC in the ground state form. This type of mechanism requires a PC with the right redox properties, so if the PC works as a photoreductant (oxidative quenching cycle), it must have an oxidation potential lower than the reduction potential of the substrate. If a PC works as a photooxidant (reductive

quenching cycle), it must have a reduction potential higher than the oxidation potential of the substrate.

Proton-Coupled Electron Transfer (PCET). In PCET, both an electron and a proton are transferred simultaneously. [20] The excited photocatalyst transfers an electron while, promoting proton transfer, resulting in the generation of substrates radical species that drive the reaction forward, while the PC in the radical anion/cation form needs to be oxidized/reduced to close the catalytic cycle, as shown in Scheme 4.

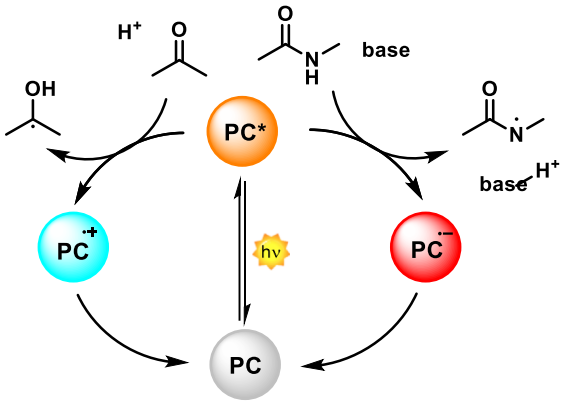

Scheme 4. *PCET photocatalytic cycle.*

Hydrogen Atom Transfer (HAT). HAT involves the transfer of a hydrogen atom from a reactant to the excited state of the PC. [21] The resulting radical species of the PC is then able to transfer the H atom to another substrate, resulting in a formal HAT. After this the PC is back to the ground state form and, upon excitation, is able to start a new catalytic cycle. This mechanism, shown in Scheme 5, is commonly observed in reactions where hydrogen abstraction is a key step, leading to the formation of radicals and subsequent transformations.

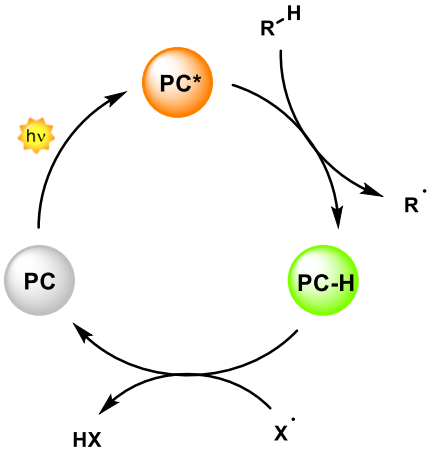

Scheme 5. *HAT photocatalytic cycle.*

Energy Transfer (EnT): In this mechanism, depicted in Scheme 6, the excited state of the PC that in this manifold is usually called photosensitizer (PS), transfers its energy to the reactant molecule, promoting the desired reaction (Scheme 6). Energy transfer can occur through various pathways, such as Förster resonance energy transfer (FRET) or Dexter electron transfer. The PC absorbs light and rapidly transfers its energy to the reactant, which then undergoes the intended transformation. The project developed in the present thesis is related to a transformation induced by an energy transfer manifold, in the next section it will be discussed more into the details.

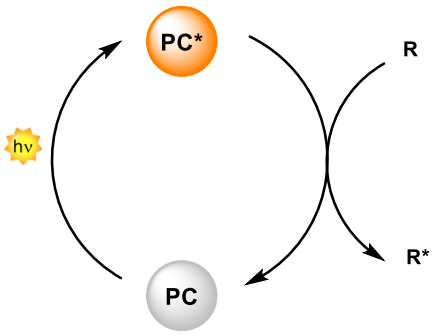

Scheme 6. *EnT photocatalytic cycle.*

1.1.4 Energy transfer (EnT) in Photocatalysis

Energy transfer is defined as the photophysical phenomenon in which the excited state in one molecule (referred to as the donor D) undergoes

deactivation to the ground state level. This deactivation occurs through the transmission of energy to another molecule (the acceptor A), that brings the acceptor to a high energetic state, as shown in Scheme 7. [22],[23]

***Scheme 7**. General EnT mechanism from a donor unit (D) to an acceptor unit (A).*

In photocatalytic conditions, the photocatalyst resembles the donor, which is excited by the direct absorption of visible light (while the direct excitation of a common organic substrate would often require more energetic light, in the UV region). The excited photocatalyst can subsequently transfer its excited state energy to the respective substrate (the acceptor), which is ‘‘indirectly excited’’ or ‘‘sensitized’.

To transfer its energy to a substrate molecule, the photocatalyst, typically referred as a triplet energy donor in its excited triplet state must find an appropriate energy acceptor. The donor molecule should possess a higher triplet energy level than the substrate molecule, facilitating energy transfer without undergoing any chemical changes itself, but the triplet excited state of the photocatalyst must be long-lived enough to allow the energy transfer process to happen. In the context of energy transfer, two main mechanisms can be identified: Dexter exchange and Förster resonance energy transfer:

- *Förster resonance energy transfer* (FRET)

Förster resonance energy transfer, also known as ‘Fluorescence resonance energy transfer’, is a quantum mechanical process dependant from the distance between the two interacting molecules, usually chromophores. [24] It proceeds through a dipole-dipole coupling mechanism, shown in Figure 4 in which an excitation energy exchange between the electronic states of the two molecules occurs. [25]

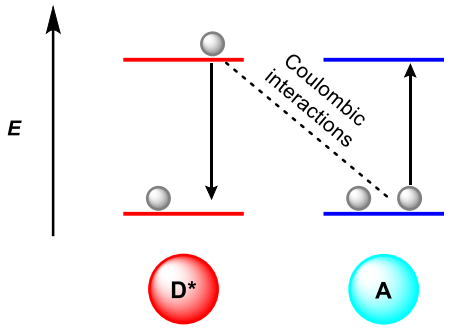

Figure 4. *FRET mechanism.*

In this mechanism, the two partners, forming a FRET pair, are recognized as a donor, that upon excitation is able to transfer the energy to another molecule that is named acceptor. Electronic oscillation in the excited electronic state donor (D*) can induce electronic oscillation in the ground state acceptor (A) through space. If this interaction is in resonance, D can relax with electronic excitation of A at the same time. This event requires a spectral overlap between the donor emission and the acceptor excitation spectra, also the efficient is highly dependent from the distance between the two partners, following the Eq.1 usually in the 1nm to 10nm range scale. [26]

$$E = \frac{1}{1 - (\frac{r}{R_0})^6} \qquad \text{[Eq.1]}$$

In this equation E is the efficiency of FRET, r represents the distance between D and A, while R_0 is the radius of 50% transfer efficiency (Förster radius).This mechanism is not applicable to a photocatalytic process between a PC* in the triplet state (PC^*T_1) and a substrate in solution, because the $PC^*(T_1)$ should go back to the S_0 ground state and, simultaneously, an excitation of the acceptor from the S_0 ground state to the T_1 excited state should occur, so two spin-forbidden transitions should occur with special separation, violating the of Wagner's spin conservation rules. FRET is usually applicated in fluorescence microscopy and spectroscopy to investigate the interactions and conformational changes of donor-acceptor molecules, such as ligands, proteins or lipids. [27],[28]

- *Dexter energy transfer mechanism*

Dexter energy transfer mechanism is a non-radiative process in which, a donor moiety (D), upon excitation, is able to transfer the energy to an acceptor molecule (A), but it proceeds through a completely different mechanistic pathway. If in FRET there is a Coulombic interaction between two dipoles, while in a Dexter EnT the process goes through a simultaneous intermolecular exchange of two electrons, the D* donates an electron to the LUMO of A, while, at the same moment, A donates an electron to the HOMO of D, resulting in a final excitation of A → A* and the D is back to its ground state form, as shown in Figure 5. [29],[30]

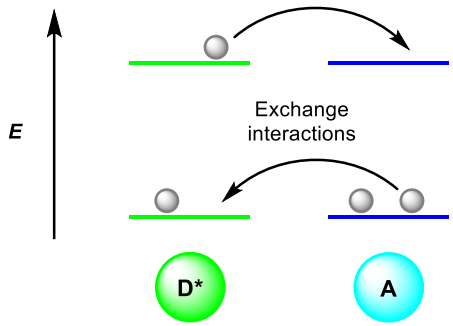

Figure 5. *Dexter exchange mechanism.*

In this process, spin multiplicity and excited state energy are transferred, so no spin and energy conservation rule are violated. The kinetic of the process is described by Eq.2:

$$k_{EnT} = K \cdot J \cdot e^{-\frac{2R_{DA}}{L}} \qquad \text{[Eq.2]}$$

in which the parameter K is specific for the orbital interactions between donor and acceptor, J is the spectral overlap integral and in particular it depends on the normalized emission spectra of the donor and the absorption spectra of the acceptor, it could be estimate experimentally based on the energy gap between excited triplet states of D and A, following Eq.3: [23]

$$\Delta E_T = E_T(A) - E_T(D) \qquad \text{[Eq.3]}$$

the exponential $e^{-\frac{2R_{DA}}{L}}$ is related to the distance between the two partners of the process. Since it has an exponential decay, the distance to obtain an efficient EnT is usually in the order of 10Å, on the contrary, the FRET has a distance dependency to the sixth power, so the distance between D and A could be higher. The behaviour in solution is shown in Figure 6.

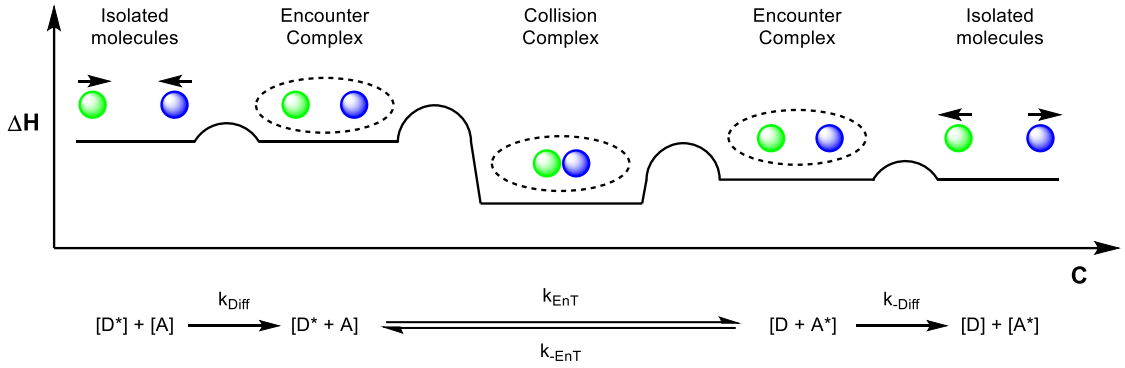

Figure 6. *Dexter EnT in solution.*

The substrates must encounter each other through diffusion, then collision can occur, leading to the orbital overlap between the two species and forming the collision complex, highly stabilized by dispersion interaction due to the high polarizability of molecules in the excited state. The formation of this complex is necessary to bring the D* and the A sufficiently close to each other, leading to the Dexter EnT. This process in usually reversible, so upon dissociation of the collision complex, the system can go through both the encounter complexes, or exciplexes: [D*+A] or [D+A*]. [31] Both evolve to the isolated products or starting materials after diffusion out of the solvent cage. Notably, the D* in the triplet excited state has to be long lived enough to have the possibility to get in contact with the acceptor, before having radiative quenching of the excited state. [32] The solvent plays also an important role since it is fundamental to favour the formation of the exciplex. Upon successful energy transfer, the substrate molecule is promoted to its excited triplet state, which is now primed for subsequent photochemical reactions. The energy stored in the excited triplet state of the substrate can trigger a variety of transformations, including bond dissociation, radical formation, and

rearrangement reactions. Understanding the intricate details of the triplet-triplet energy transfer mechanism in photocatalysis is essential for rational catalyst design and optimization. The choice of appropriate donor molecules, along with the selection of photocatalysts with suitable energy levels, can significantly impact the overall efficiency and success of the photocatalytic process. This is why, elucidating the factors influencing the rate and efficiency of energy transfer aid researchers to develop strategies to improve the performance of photocatalytic systems, leading to more sustainable and selective synthetic strategies.

1.1.5 Photocatalysts in triplet-triplet energy transfer (TTEnT)

To be used in a TTEnT manifold, a photocatalyst should possess the following properties:[33]

1) High absorption in the desired wavelength range (usually UV-Vis).
2) Higher triplet excited state with respect to the substrate [E_t (PC) > E_t (substrate)].
3) Efficient ISC from the S_1 excited state to the T_1 excited state.
4) The lifetime of T_1 must be feasible with the timescale of the EnT process.

In literature, some structures are known to be good photosensitizers for EnT mediated transformations, the nature of the PC can be both metal based or fully organic, and some of them have been described as useful photocatalysts in photoredox processes. [18],[23] In the more recent years a new class of compounds have been investigated as photocatalysts in both photoredox and photosensitization reactions: Thermally activated delayed fluorescence (TADF) emitters. The latter have their main applications in OLED manufacturing, [34],[35] but recently their behaviour as photocatalysts has been investigated as well. TADF compound could have different natures: organic, metal-based or organometallic, we will focus only in the fully organic ones. In Figure 7, a selection of commonly used photosensitizers and TADF emitters is shown: [36],[37],[23]

Commonly used photosensitizers

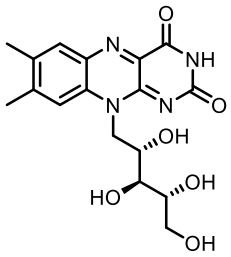

Riboflavine
E_T = 2.17 eV
PC1

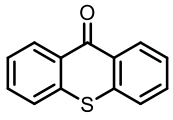

Thioxanthone
E_T = 2.75 eV
PC2

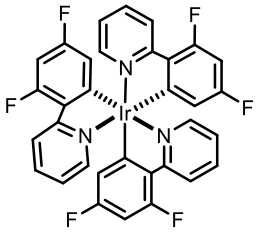

***fac*-[Ir(dF-ppy)$_3$]**
E_T = 2.75 eV
PC3

TADF emitters

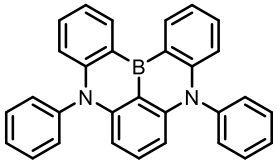

DABNA-1
E_T = 2.59 eV
PC4

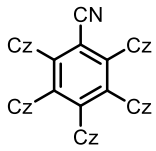

5CzBN
E_T = 2.83 eV
PC5

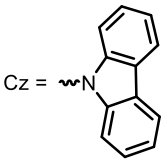

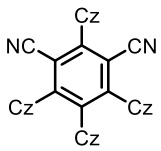

4CzIPN
E_T = 2.43 eV
PC6

Figure 7. *Selection of commonly used PC in TTEnT manifold and TADF compounds.*

For common organic molecules it's reasonable to assume that the S_1 excited state is higher in energy than the T^1 state, by approximatively 0.5 – 1 eV. A key feature of TADF compounds is the very small energy gap between the singlet and the triplet excited states (ΔE_{ST}). This feature favours the reverse intersystem-crossing process (RISC), the molecule is able to go back from the T_1 to the S_1 excited state, and from here it can relax to the S_0 by the 'delayed fluorescence'. [38] These excited states are reachable by intramolecular charge transfer character of the systems containing spatially separated donor and acceptor unities. These molecules are carefully designed in a way to minimize the overlap between the HOMO and the LUMO, that are well localized and separated, leading to small values of ΔE_{ST}. [39]

Generally, this scenario should not lead to an effective TTEnT process, based on the previously mentioned "ideal-properties" for photosensitizers, since the

triplet excited state of these photocatalysts will be much less lived. However, in some cases this could be represent a particular advantage.

1.1.6 Application of TTEnT in Organic Synthesis

In the last 20 years, several reactions promoted by TTEnT were investigated in the field of organic synthesis. [40],[41] In particular, using this activation pathway, the sensitization of both σ and π bonds was reported to be feasible, with differences on the outcome of the reactions in which they are involved. The main categories of transformations will be discussed briefly next.

- *Cyclization and cycloaddition reactions*

Traditionally, photochemical cyclizations and cycloadditions require the use of highly energetic UV light, leading to undesirable side-reactions or degradation of the starting materials, which limits the synthetic applicability. [42],[43] The use of photocatalytic conditions allows to perform these types of reactions in milder conditions with the application of visible light, by which the PC can be selectively excited avoiding uncontrolled side reactions. These transformations enable the formation of new C-C and C-heteroatom bonds, after the activation of the π system, that, in the triplet state, act as a diradical species (**6**) and (**7**), interacting inter or intramolecularly to form the final cyclobutane derivative (**8**) following the mechanism depicted in Scheme 8.

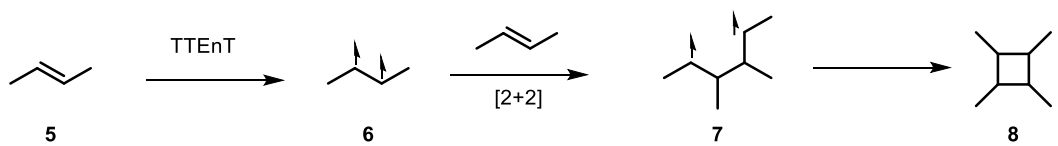

Scheme 8. *General [2+2] photocycloaddition through TTEnT manifold.*

As example, we reported the work of You and co-workers [44] Scheme 9, where an intramolecular light-mediated [2+2] cycloaddition that leads to the formation of cyclo-butane dearomatized indole derivatives (**10**), through a photosensitization manifold on substrate (**9**)

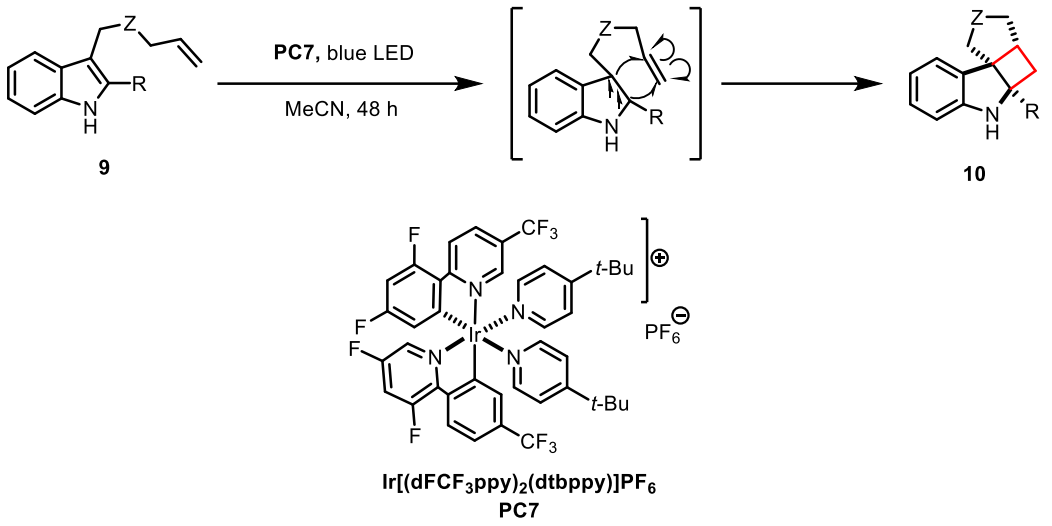

Scheme 9. *You's work: intramolecular light.mediated [2+2] cycloadditon with an [Ir]-PC.*

- *Photoisomerization of olefins*

This class of reaction is one of the most used applications of energy transfer catalysis. Traditionally, harsh UV light and stoichiometric amount of sensitizer were necessary, consequently, the substrate scope were usually limited due to the low tolerance to most of the commonly used functional group. [45] The reaction goes through an energy transfer from the photocatalyst to the olefin, after that, the olefin in the triplet state is characterized by the presence of an electron in a π* orbital, while losing an electron from a π orbital. This causes a decrease in the bond order of the olefin, allowing the rotation around the σ bond and resulting in an isomerization of the olefin. In recent years, this strategy was obtain using mild-visible-light condition, such as in the work of Gilmour and co-workers, [46] Scheme 10, which reported an interesting E→Z isomerization catalysed by riboflavin of activated olefins (**11**) to the corresponding product (**12**), taking inspiration from the natural isomerisation process of retinal that occurs in our eyes. [47]

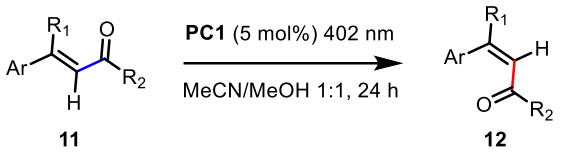

Scheme 10. *Gilmour's work: photocatalytic isomerization of olefins with a natural photocatalyst.*

- *σ bond dissociation*

All the previous strategy described employed the activation of π systems, but TTEnT has been demonstrated to be a powerful tool also for the cleavage of σ bonds with the subsequent generation of radical active species that can undergo further transformations. The limit of this approach is the unpredictability of the bond cleavage after the energy transfer process. Indeed, comparing the energy of the triplet state of the substrate with the one of the photocatalyst is a fast way to check di feasibility of the process. Once the triplet excited state of the substrate is formed, it's difficult to say whether the bond dissociation will take place or not, usually a parameter for this purpose is the bond dissociation energy (BDE), and, in particular, a bond dissociation is more likely to occur if BDE < E_T. [40] The number of publications containing this activation mode of energy transfer is currently quite limited, some of these cases will be described.

In this regard, in 2018 and 2020, the group of Glorius described the σ bond cleavage of disulfides (S-S bond) and oxime esters (N-O bond), [48],[49] respectively, as shown in Scheme 11. Upon photosensitization S-S bonds (**13**) and (N-O) bonds (**16**) can dissociate, the radicals formed can be trapped with other substrates leading to new functionalized products (**15**), (**17**), (**18**). To access this type of reactivity, the authors took advantage of a metal-based photocatalyst, after the cleavage of the bonds the active radicals intermediate were trapped with different partners to form new C-C and C-heteroatom bonds.

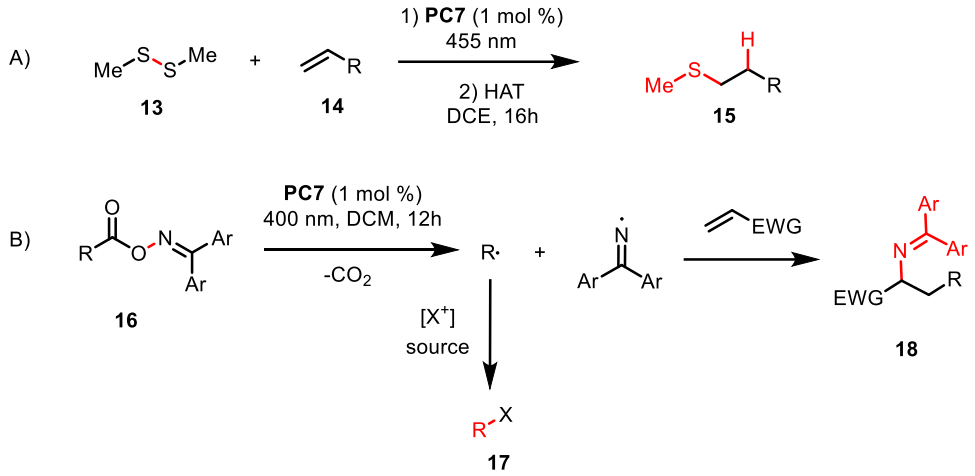

Scheme 11. *Glorius' works: A) S-S σ bond cleavege. B) N-O σ bond dissociation.*

In 2022, Willis and co-workers reported a mild-visible-light mediated sensitization of sulfonylimines, [50] with the use of a fully organic photocatalyst (**PC5**), generating a sulfonyl radical (**20**) after the cleavage of S-N σ bond of substrate **19** that subsequently can be trapped with an electron-poor olefin, leading to the product formation (**21**) as shown in Scheme 12.

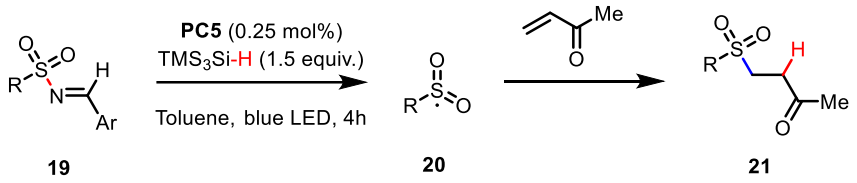

Scheme 12. *Willis' work: S-N sigma bond dissociation of N-sulfonylimine with a fully organic photocatalyst.*

1.2 Compounds of interest

1.2.1 Azetidines

Azetidines are four-member saturated nitrogen containing cycles, and the recent years, the pharmaceutical and drug discovery communities have gained interest in the properties and in the synthesis of this particular scaffold. [51],[52] This interest relies in their presence in bioactive natural products but also in medicinal chemistry for the preparation of drugs. [53],[54] In Figure 8 some of

these compounds are depicted, all containing the azetidine motif with diverse functionalization patterns.

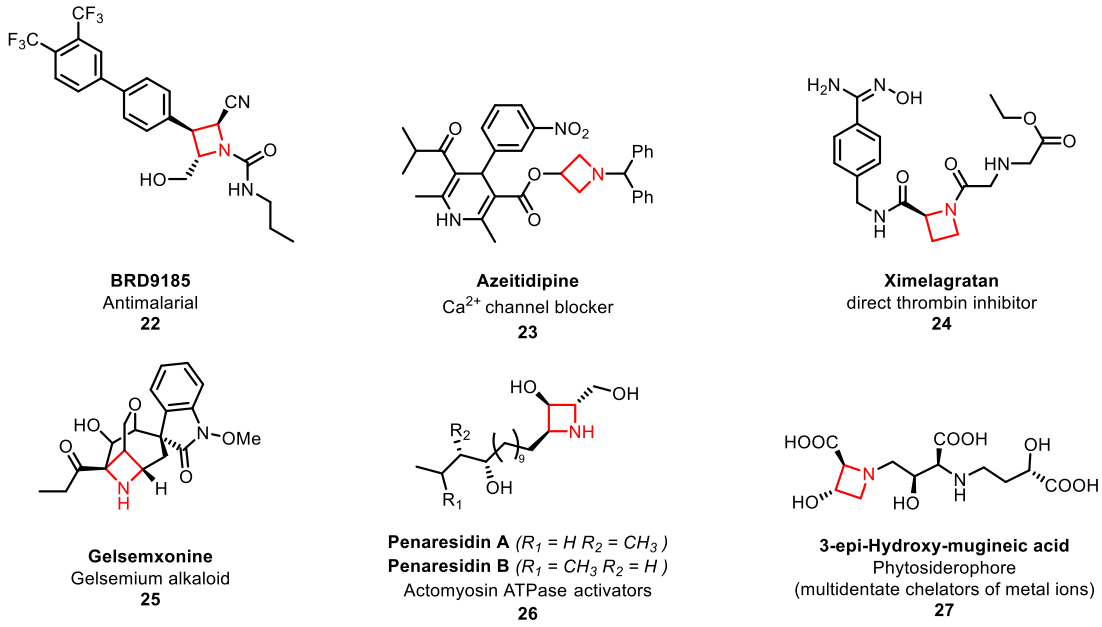

Figure 8. *Selected examples of bio-active and drugs compunds containing the azetidine motif.*

The drug development area has increased the demand for a major degree of saturation and consequently the three-dimensionality of drugs candidates and intermediates. Indeed, it has been demonstrated that 3D shaped molecules possess better pharmacokinetics and physicochemical properties, such as improved solubility, permeability, and reduced lipophilicity with respect to the unsaturated and planar analogues. [55],[56] Most of the drugs containing saturated N-bearing heterocycles present five- and six-membered rings, pyrrolidine and pyridine, respectively, despite azetidines have been demonstrated to possess enhanced pharmacokinetics properties and metabolic stability. The limited use of the azetidine motif might be related to the lack of efficient preparation methods, in particular for the synthesis of 1,3-substituted azetidines, featured in the current drug discovery programmes but with very challenging manipulation that limit the possible applications. The reason of the challenging synthesis of azetidines is mainly due to the strain that have a huge impact in the ring formation, among the series of N-containing saturated heterocycle, the four member one has the smallest tendency to cyclization (5 > 3 > 6 > 7 = 4). [57]

Regarding the preparation of azetidines, four main strategies are mainly used in organic synthesis, depicted in Scheme 13, herein they will be briefly discussed:

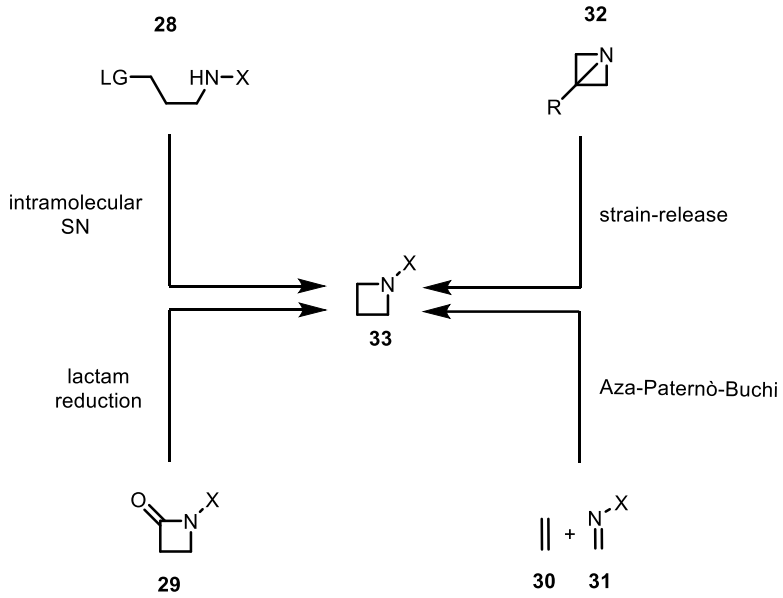

Scheme 13. *Common synthetic strategies to achieve azetidines*.

- I*ntramolecular cyclization via nucleophilic substitution*

This strategy follows the mechanism shown in Scheme 14 in which an intramolecular nucleophilic attack occurs with the exit of a proper leaving group from **28** forming the four-member cycle **33**. [58],[59]

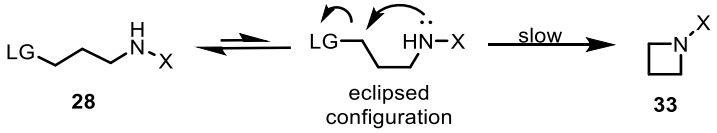

Scheme 14. *Intramolecular cyclization via nucleophilic substitution for the synthesis of azetidines.*

While this synthetic pathway is efficient for the formation of three- five- and six-member heterocycles, it is not as good for the preparation of azetidines, the reactivity is indeed disfavoured by the conformation of the acyclic precursor **28** that, to be reactive in this sense, requires the eclipsed conformation shown in Scheme 14, which, due to eclipsing interactions, has a higher energy with respect to the not-eclipsed form.

- *Reduction of β-lactam*

This strategy is a powerful tool for the formation of azetidines by reduction of 2-azetidinones with a nucleophilic hydride, [60] as depicted in Scheme 15.

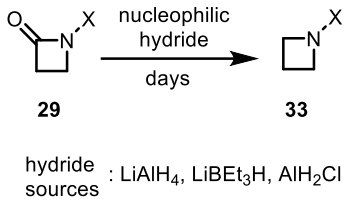

Scheme 15. *Reduction of β-lactams for the preparation of azetidines.*

However, the limitation of this process is due to the side reactions that leads to the formation of γ-amino alcohols. Another critical issue of this transformation is that requires often reflux conditions and very long reaction times (in the order of days).

- *Aza Paternò-Buchi reaction*

This legendary transformation is a photochemical transformation that leads to the formation of N-containing heterocycles through a [2+2] cycloaddition after the excitation of an imine (**31**) which reacts with an alkene (**30**) leading to the final functionalized azetidine **33** [61] as shown in Scheme 16.

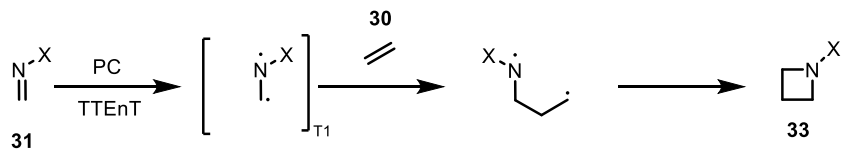

Scheme 16. *Photocatalysed Aza Paternò-Buchi reaction for the synthesis of azetidines.*

In the recent years, the research group of Schindler has devoted great efforts in the design and development of this transformation in photocatalytic conditions trough a TTEnT manifold, using metal-based (Ir and Ru) photosensitizers to activate the imine (**34**) in mild-visible-light conditions

obtaining the functionalized azetidines (**35**) with high diasterotopic control, [62] Scheme 17.

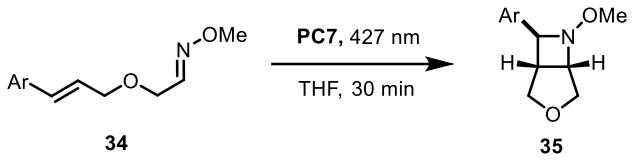

Scheme 17. *Schindler's work: Synthesis of functionalized azetidines through Aza Paternò Buchi reaction activated by metal-based PCs.*

Despite the great advances that have been achieved, several limitations remain to be tackled under this reaction manifold, such as the study of intermolecular versions and the impossibility of accessing monocyclic cores.

- *Strain-release of azabicyclobutanes*

Azabicyclo[1.1.0]butanes (ABB) are uncommon but relevant precursors of azetidines, taking advantage of a strain-release strategy. Traditionally, the functionalization of ABB by means of strain-release is performed in a polar fashion with the use of electrophiles and/or nucleophiles. This strategy will be explored in photocatalytic conditions in this thesis project, in the next paragraph the current state of the art of ABB functionalization will be discussed more into the details.

1.2.2 *Azabicyclo[1.1.0]butanes functionalization driven by strain-release*

In the literature diverse transformations regarding the strain-release of *Azabicyclo[1.1.0]butanes* are described. [63] Herein, some of those will be discussed focusing on the reaction partners.

It is known that Azabicyclo[1.1.0]butanes (**36**) can undergo electrophilic addition through the N-C_3 σ bond, forming a cationic intermediate (**37a** e **37b**) that can be trapped by a nucleophile leading to the di-functionalized 1,3-azetidine (**38**), [64],[65] as shown in Scheme 18.

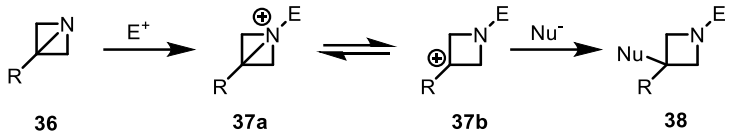

Scheme 18. *ABB functionalization through polar chemistry driven by strain-release.*

This transformation was discovered in the 70s when Kurz, Gillard and co-authors [66],[67] studied the kinetic of the acid-catalyzed solvolysis of 3-phenyl-1-azabicyclo[1.1.0]butanes in water, they hypothesized a protonation of the N of the bicycle followed by the cleavage of the N-C_3 bond through nucleophilic attack of the solvent. Recently, Baran and Gianatassio reported a one-pot procedure in which the order of addition could be reversed, in which a strong nucleophile, such as turbo-Hauser amides are firstly able to attack the C_3 of the bicycle with subsequent electrophilic trapping of the resulting amide anion. [68] Over the years, several electrophile/nucleophile couple were employed leading to different functionalization both on the N atom and the C_3 atom.
Additionally, Gianatassio's group [69] explored the direct alkylation at the C3 position, after an in-situ preparation of the ABB (**40**) from **39**, with the use of organomagnesium or organozinc compounds, that, upon addition at the C3, followed by the reactions with several electrophiles leading to 1,3-difunctionalized azetidines (**41**). This strategy is shown in Scheme 19.

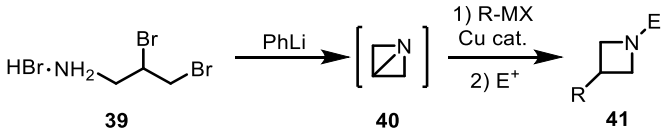

Scheme 19. *ABB functionalization with the use of organometallic reagents driven by strain-release.*

Despite the importance of ABBs as convenient precursors to access azetidine scaffolds, the use of superstoichiometric loadings of organometallic species under harsh conditions, still prevents the drug discovery community to entirely embrace this strategy as the most convenient one. In this regard, the lack of photocatalyzed protocols to access azetidines via strain-release resulted as a major scientific motivation. In this thesis project this strategy was explored.
In the next paragraph, the objectives of the thesis project will be summarized.

1.3 Objectives of the thesis

This thesis project aimed to investigate a new photocatalytic methodology to access densely functionalized azetidines through a visible-light-mediated process driven by strain-release of azabicyclo [1.1.0] butanes. The latter, to the best of our knowledge, has never been explored in photocatalytic conditions, consequently its behaviour has to be completely investigated. The project in this regard included the synthesis of the substrates and the optimization of the key parameters of the reaction, such as stoichiometry, solvent, temperature, photocatalyst nature and loading, temperature. The model product characterization will be shown, after that the reaction scope will be conducted to demonstrate a certain generality of the process under study.
Regarding the photocatalyst, a rational design of the ideal photocatalyst for the transformation under study will be investigated, starting from the synthesis of new structures and the subsequent full characterization of the photo-physical properties of the best photocatalyst at the end of the optimization step.
Finally, mechanistic investigations such as luminescence quenching studies (Stern-Volmer analysis) will be performed, seeking for fine experimental data, enabling the proposal of a rational reaction mechanism.

2 Results and discussion

2.1 *Development of the project*

The project started with the investigation of the reactivity depicted in Scheme 20 of 3-phenyl-1-azabicyclo[1.1.0]butane (**42**) in the presence of a radical source (**43**) and a photocatalyst to determine if the functionalization by means of strain-release was achievable through a photochemical manifold, targeting the azetidine derivative (**44**).

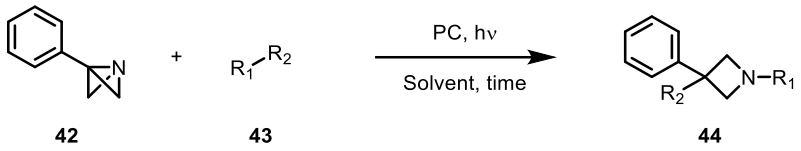

Scheme 20. *General ABB functionalization strategy through a photocatalytic manifold.*

As a radical source we took inspiration from the work of Willis in which described the use of sulfonylaldimines as a sulfonyl radical source. [50] In our case, a N-sulfonylketimine was selected, that is reported to undergo N-S homolytic bond dissociation through an EnT process promoted by the photocatalyst. Subsequently, we wanted to explore whether the two formed radicals could be trapped by the ABB, resulting in a di-functionalized azetidine (**44**). After the synthesis and characterization of the desired starting materials (see *Section 4*), a preliminary test, depicted in Scheme 21, was performed using substrates (**42**) and (**45**) and the same photocatalyst of Willis' work, the 5CzBN (**PC5**), a fully organic photocatalyst, also known to possess TADF properties. [70],[71]

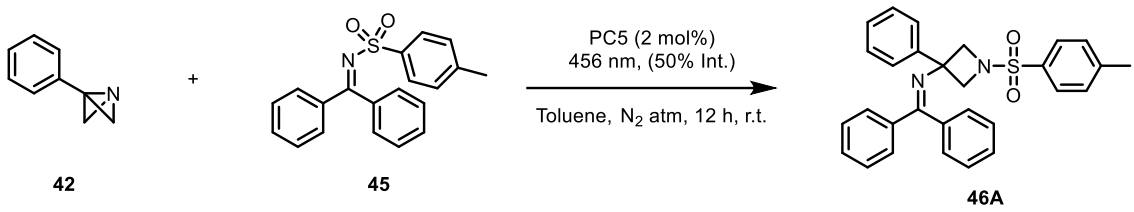

Scheme 21. *Preliminary test: Investigation for ABB reactivity in the presence of a radical source.*

The reaction was performed under nitrogen atmosphere, avoiding the presence of oxygen, as it is known to be an excellent triplet state quencher, that would deactivate the photocatalyst [72],[73]. The reaction was conducted in Toluene, for 12 hours under the 456 nm Kessil lamp at 50 % of intensity.

The reaction crude was then analysed by NMR, that shows new peaks in the aromatic region, and, most importantly, a new coupling system that we suspected was related to the two CH_2 groups of in α position to the N of the resulting azetidine product (Figure 11).

After the purification by flash chromatography column, we were able to isolate three compounds. These species were assigned to:

The expected compound (**46A**) in which the sulfonyl radical was added to the N, position 1 of the bicycle, and the iminyl radical was added to the C_3 position, forming the final di-functionalized azetidine.

The dimerization product (**46B**) that probably comes from the radical homocoupling of the iminyl radical formed after the σ bond dissociation of the starting N-sulfonylimine (**45**).

Ketone (**46C**), which is probably formed upon hydrolysis of 45, due to the presence of traces of water in the reaction media.

The three structures are reported in Figure 9.

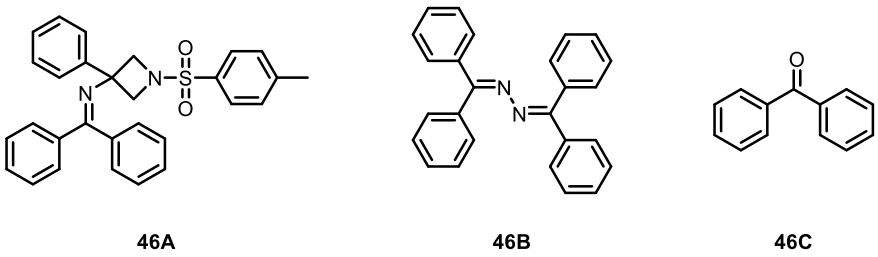

Figure 9. *Structures of the three isolated product.*

This exciting result was a good starting point for the optimization step, that will be described in the next section.

Interestingly, the reaction leads to the formation of only one of the two possible regioisomer, the one with the sulfonyl moiety attached to the nitrogen atom of the azetidine, while the iminyl moiety is bonded to the C_3 position of the four membered ring. This experimental evidence could be explained by the free energy difference of formation of the two regioisomers, as shown in Figure 10.

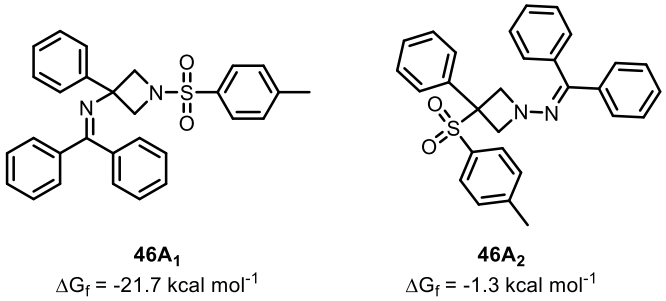

Figure 10. *Structures of the two possible regioisomers.*

The values obtained by DFT calculation (see *Section 4.1* for details), show that the regioisomer **46A$_1$** is more than 20 kcal mol^{-1} thermodynamically more stable with respect of **46A$_2$**, and this could explain why we obtained only one of the two possible regioisomers.

In order to increase the yield and selectivity of the reaction, we envisioned that an optimization of the key parameters of the photocatalytic transformation, such as the solvent, stoichiometry of the two reactants, the nature and the loading of the photocatalyst and finally the temperature could push the reaction towards the desired product, producing less amount of the homocoupling adduct (**46B**). The optimization is based on the NMR-yield of the azetidine

product (**46A**), with the use of trichloroethylene as internal standard (I.S.), [74] as shown in Figure 11.

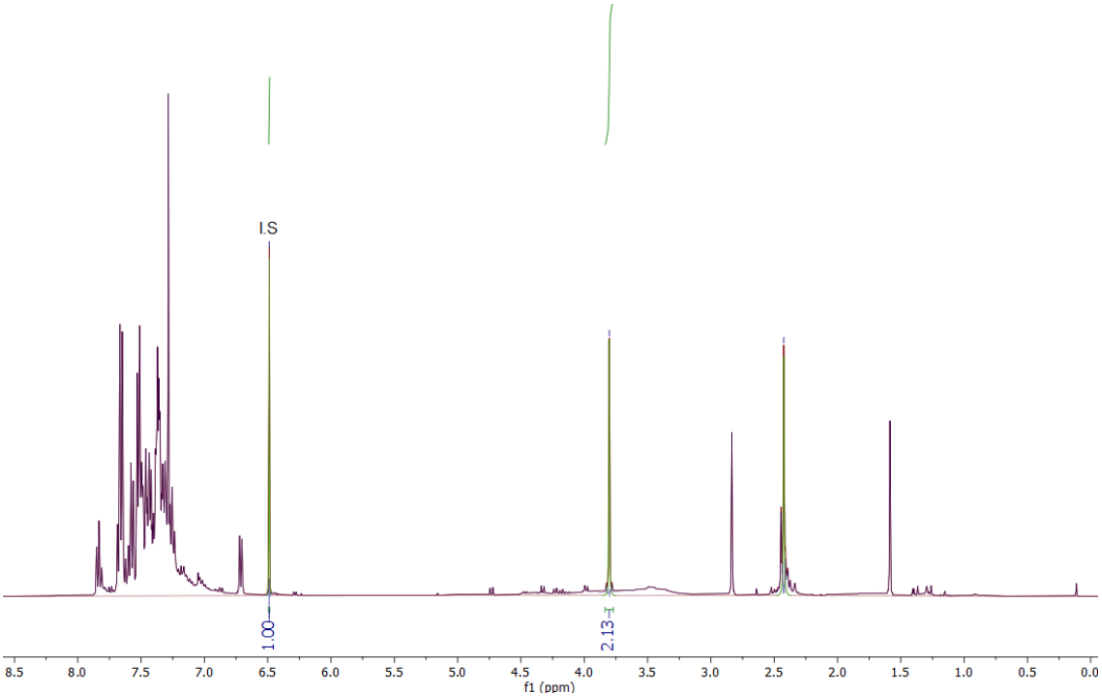

Figure 11. *Example of a reaction crude after the addition of the internal standard.*

Additionally, the optimization of the procedure could lead to a more inert and dry condition in the reaction vials, to avoid the presence of traces of oxygen and most importantly water to minimize the formation of the hydrolysis product (**46C**).

2.2 *Reaction optimization*

The optimization of parameters in a photochemical reaction is a crucial step to explore the full potential of photocatalysis for organic synthesis. [75] Each parameter can significantly impact the reaction outcome, selectivity, and efficiency. [76],[77] In this work, to optimize the key parameters of the photochemical transformations, a screening of different conditions was tested, keeping all the parameters constant except the one that is under investigations:

A) Solvent

Solvent screening is a crucial step in optimizing a photochemical reaction. The choice of solvent can significantly impact reaction efficiency, selectivity, and even the mechanism of the photochemical process. [78],[79] Conducting a systematic solvent screening is essential to identify the most suitable solvent for the desired photochemical transformation. During a solvent screening, some key features that are discussed in the next lines have to be considered:

Reactant solubility: The nature of the solvent plays a vital role in solubilizing the reactants and photocatalyst, this is necessary to have all the species in solution, and to make possible the formation of the encounter complex between the photocatalyst and the substrate that is going to be sensitized.

Absorption Spectrum: The solvent's absorption spectrum should also be taken into account, particularly if the photochemical reaction involves the use of UV or visible light. The solvent should not compete with the photocatalyst or reactants for light absorption, as this may reduce the overall efficiency of the process. Choosing a solvent with a low absorbance at the irradiation wavelength ensures that the maximum amount of light is available for the photochemical reaction.

Photostability: Some solvents can be photoreactive or prone to photodegradation under the irradiation conditions. This can lead to side reactions or interference with the photochemical process, if this is the case, more side-products should be observed in the reaction crude. A photostable solvent is preferred to maintain the integrity of the reaction and avoid undesired side products.

Dexter EnT efficiency: As explained in the introduction, the solvent could play a role on the efficiency of the Dexter EnT process in solution, since it should favour the formation of the exciplex between the photocatalyst and the substrate (**45**).

In some cases, solvent mixtures can be advantageous, combining the benefits of different solvents to optimize reaction outcomes. Mixtures can improve solubility, tune the solvent polarity, or minimize solvent absorbance at the irradiation wavelength.

Strategies for solvent screening involve evaluating a range of solvents with varying polarities, assessing their absorbance spectra, and investigating their photostability under the reaction conditions. Additionally, comparing the reaction yield and selectivity in different solvents can provide insight about how the solvent effects on the photochemical process.

Table 1 summarizes the outcome of the solvent screening, the choice of the best solvent for the reaction depicted in Scheme 22, was based on the highest NMR yield of **46A**, indicating a major efficiency with respect to the other tested solvents.

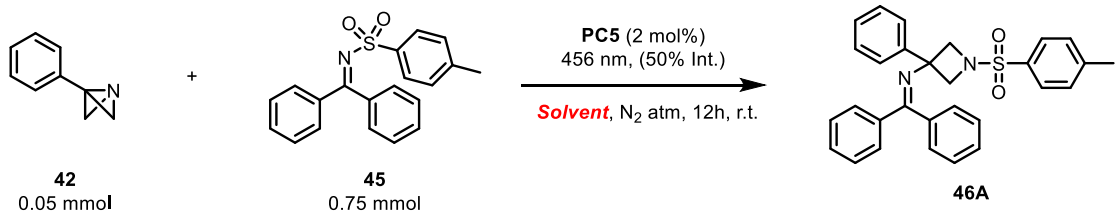

Scheme 22. *Model reaction for solvent screening.*

Entry	Solvent	NMR Yield of 46A (%)
1	Dimethylcarbonate (DMC)	**21**
2	Acetone	**5**
3	Ethyl Acetate (AcOEt)	**31**
4	Methyl-*t*-Butyl-ether (MTBE)	**18**
5	Dimethylformamide (DMF)	**0**
6	Toluene ($PhCH_3$)	**32**
7	Pentane/AcOEt (1:3)	**25**
8	Chlorobenzene (PhCl)	**32**
9	Dichloromethane (DCM)	**0**
10	Trifluorotoluene ($PhCF_3$)	**38**

Table 1. *Results of solvent screening (Scheme 22).*

The outcome of the experiments demonstrates that the best solvent for the transformation under study is trifluorotoluene, entry 9.

B) Stoichiometry

The molar ratio of reactants plays a vital role in determining the reaction yield and product selectivity. [80] Careful consideration of stoichiometry is essential to achieving the desired outcome. An excess of one reactant may lead to side reactions or waste of materials, while insufficient amounts can limit product formation. Systematic studies, using various stoichiometries, can help identify the optimal molar ratio for the highest yield and selectivity. In Table 2, the results of the stoichiometry optimization of the reaction (Scheme 23) are summarized.

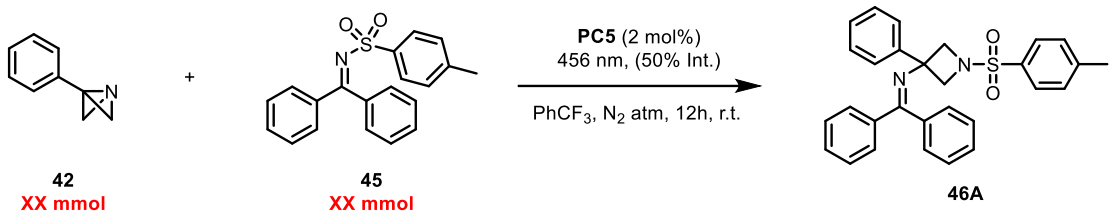

Scheme 23. *Model reaction for stoichiometry optimization.*

Entry	mmol of 42	mmol of 45	Molar ratio (42:45)	NMR Yield of 46A (%)
1	0.05	0.075	1:1.5	**38**
2	0.075	0.05	1.5:1	**40**
3	0.1	0.05	2:1	**42**
4	0.05	0.1	1:2	**33**
5	0.15	0.05	3:1	**31**

Table 2. *Results of stoichiometry optimization (Scheme23).*

The experiments lead to the understanding of the best stoichiometry ratio between the two reactants, a scenario which implied a 2:1 ratio, entry 3, between substrate **42** and **45** respectively. This is probably due to the fact that, after the energy transfer process, the two formed radicals are more easily

trapped by **42** if the latter is in higher concentration, leading to higher yields **46A** and less homocoupling product **46B**.

C) Reaction Time

Changing the reaction time could give important information about the rate of the process, and to investigate the desired product stability in the reaction conditions. [75] The reaction time must be sufficient in order the reaction to occur, additionally, a too long reaction time risks to give stability issues towards the final product. The possible decomposition or degradation could lead to lower yields and a more complicated reaction crude.

The reaction time was investigated (Scheme 24), the results are shown in Table 3.

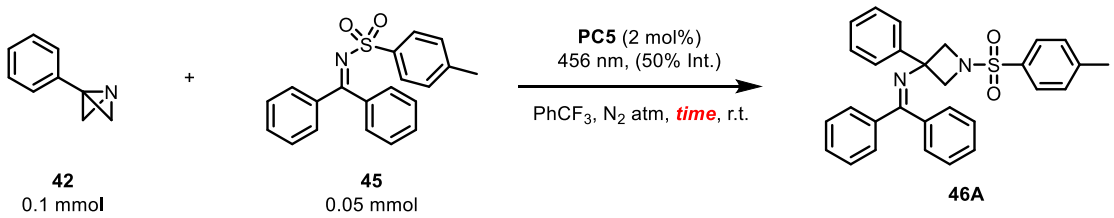

Scheme 24. *Model reaction for reaction time optimization.*

Entry	Reaction time (h)	NMR-yield of 46A (%)
1	4	**31**
2	12	**42**
3	22	**46**
4	36	**45**

Table 3. *Results of reaction time optimization.*

The results demonstrate that the best reaction time is 22 h. A further increase of the reaction time didn't lead to a higher yield, for this reason we assume that after 22 h the reaction could be considered finished.

D) Substituent effect on N-sulfonylimine

An aromatic substituent could have a huge impact on a chemical transformation, due to the fact that it changes the electronic distribution on the aromatic ring. [81] This depends on the electro-withdrawing or electro-donating nature of the substituent and most importantly from the sensitivity of the reaction to the electronic distribution on the aromatic ring. We started investigating the effect of the substituent on the two aromatic rings of the N-sulfonylimine, to understand the most favourable substrate for the reaction. After the synthesis of the N-sulfonylimine derivatives depicted in Figure 12, we performed the reaction on the so far best conditions to understand if a difference on the electronic nature of the substrate could impact the overcome of the photochemical transformation.

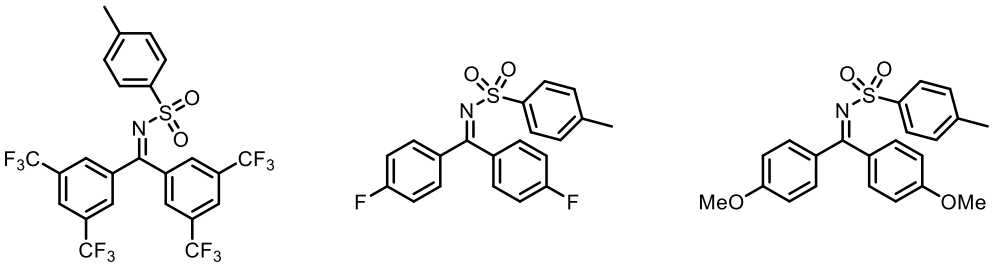

47 **48** **49**

Figure 12. *Structures of N-sulfonylimine derivatives to investigate the substituent's effect.*

The results of the photochemical reactions (Scheme 25) are shown in Table 4:

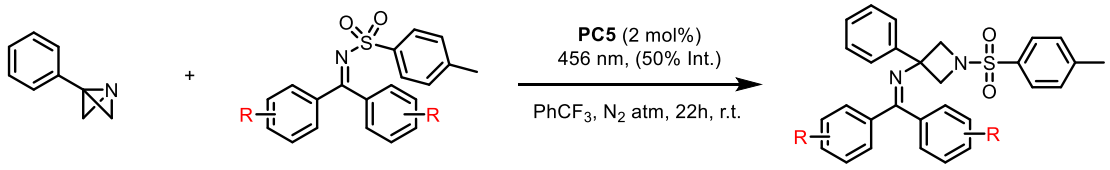

42
0.1 mmol

XX
0.05 mmol

50 (R = 3,5-CF_3)
51 (R = 4-F)
52 (R = 4-OMe)

Scheme 25. *Model reaction for investigation of N-sulfonylimine substituent's effect.*

Entry	N-sulfonylimine	NMR Yield of product (XX)
1	**45**	**46%** (46A)
2	**47**	**0 %** (50)
3	**48**	**41 %** (51)
4	**49**	**49 %** (52)

Table 4. *Results of N-sulfonyllimine substituent's influence (Scheme 25).*

The results proved that substrate (**49**) with the electron-donating substituent in the *para* position of the iminyl aromatic rings lead to the highest NMR-yield of the final azetidine (**52**) with respect to the non-substituted one (**46A**), and to the *para*-F one (**51**). Surprisingly, the reaction didn't work with two *meta*-CF_3 electron-withdrawing groups (**47**), the expected product (**50**) was not observed. The optimization process proceeded with the photocatalyst screening. From now on, N-sulfonylimine **49** was used as model substrate.

E) <u>Photocatalyst nature and loading, light wavelength and intensity</u>

The photocatalyst optimization is probably the most important parameter to enhance the quality of the transformation. The selection of the most suitable photocatalyst directly impacts reaction efficiency, selectivity, and the range of accessible transformations. [82],[40] The photocatalyst should efficiently absorb light at the desired irradiation wavelength [83], and usually those with broad absorption profiles that cover a wide range of wavelengths are particularly advantageous, since they allow the use of different light sources. For the PCs that possess broad absorption spectra, different wavelengths were tested to investigate the best one for the process. In this regard, another important parameter is the light intensity, that plays a role on the rate of the process. A higher light intensity gives a higher number of available photons for the photocatalyst excitation resulting in a faster process. [84] However, it could also lead to undesired side reactions and photodegradation of the reaction components. [85] Additionally, the absorption of the substrates should not

overlap with the selected irradiation source, but exclusively the photocatalyst's one, securing selective excitation of the photocatalyst. The fine tuning of all these parameters would aid to avoid photodegradation of the starting materials, enlarge the tolerance of functional groups and limit the possible pathways of the reaction. [18] Moreover, the photocatalyst must be stable under the reaction condition, avoiding significant photodegradation or photodecomposition and it should be regenerated at the end of each catalytic cycle in order to start with another one. Moreover, it should be soluble in the reaction solvent, in order to favour the formation of the encountered complex in solution with the subsequent energy transfer process. To do so, it is necessary to have a PC with feasible properties. According to the literature, in order to witness an efficient TTEnT activation, the PC should have a higher E_T with respect to the substrate, a high rate for the ISC process to reach the triplet excited state that has to be long-lived enough to make possible the EnT process. [40],[48] Another important parameter is the catalyst loading, that must be optimized to discover the right amount in the reaction media to efficiently promote the reactivity.

For the process under study, several PCs (Figure 13) were tested starting from the commonly used in TTEnT photocatalysis with both organic and metal-based nature, and then investigating the behaviour of fully organic TADF compounds. [48],[70],[86],[87]

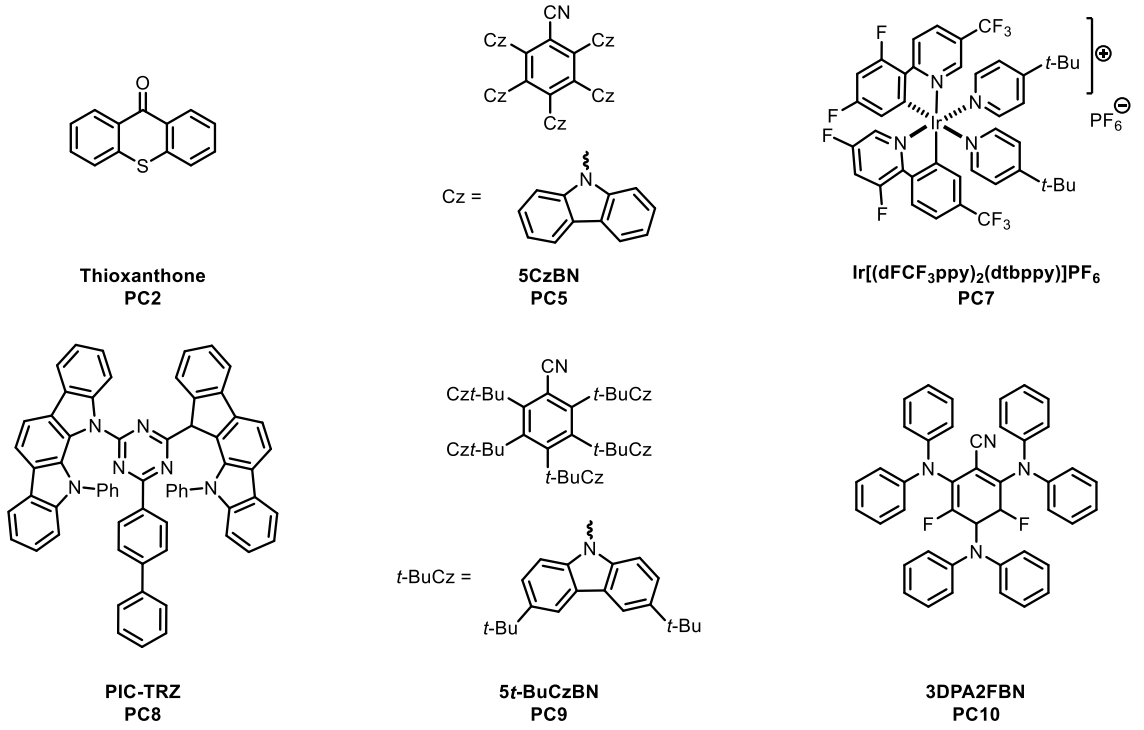

Figure 13. *Structures of the investigated photocatalysts*

The results of the photochemical tests (Scheme 26) are shown in Table 5:

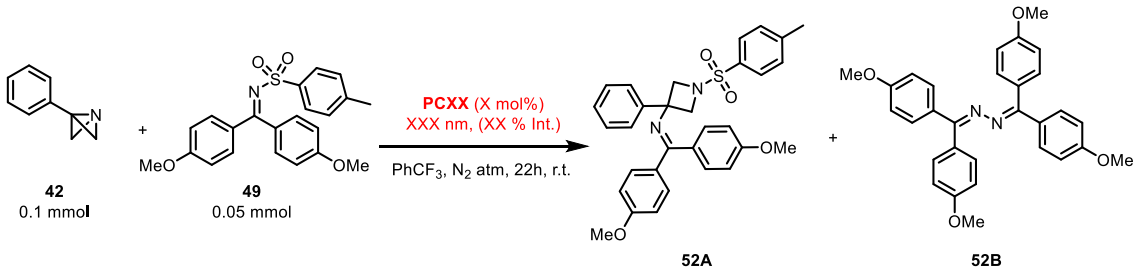

Scheme 26. *Model reaction for photocatalysts screening*

Entry	PC	λ (nm)	Intensity	Catalyst loading	NMR yield of 52A (%)
1	**PC5**	456	50%	2 mol %	**49**
2	**PC2**	427	50%	5 mol %	Only **52B**
3	**PC7**	456	50%	1 mol %	**42**
4	**PC8**	427	50%	2 mol %	**52**
5	**PC9**	456	50%	2 mol %	**53**
6	**PC9**	456	50%	1 mol %	**56**
7	**PC9**	456	50%	0.25 mol %	**63**
8	**PC9**	456	100%	0.25 mol %	**48**
9	**PC10**	427	50%	2 mol %	**37**

Table 5. *Results of photocatalysts screening*

The results of the PC screening were certainly unexpected, starting from entry 2, with the use of **PC2**, that is frequently used in TTEnT processes, in which the formation of the product **52A** was not observed and the main product was the homocoupling product **52B**. The formation of **52B** demonstrate that the **PC2** is able to undergo the energy transfer process, however the desired product was not observed. The use of an Iridium-based PC (**PC7**), entry 3, leads to the formation of the product **52A** in 42% NMR yield. However, **PC7** was not able to reach the result initially obtained with **PC5** (5CzBN), that bears TADF properties. After this, we started questioning this apparent effectiveness of TADF compounds and what could be favouring the transformation under study. Since these compounds possess a small energy difference between the singlet and the triplet excited state, they are prompt to undergo reverse intersystem crossing from the triplet to the singlet excited state. Consequently, the T_1 state of the photocatalyst would never be too much populated, resulting in a less efficient TTEnT. This means that the formation of the two radical intermediates after σ bond dissociation of substrate **49** is less favourable, as the consequent formation of the homocoupling product **52B**. The combination of all these concepts suggests a favourable scenario for the formation of the desired product **52A,** resulting in higher yields of the process. To investigate

this hypothesis, some TADF compound were tested. The best result was obtained with **PC9** (5*t*-BuCzBN) with a final 63% of NMR-yield for product **52A**, entry 7 after the optimization of the catalyst loading. Interestingly, a lower amount of **PC9** lead to a higher yield, and this is in accordance with the previous hypothesis. Another evidence in support of this concept come from entry 8, where increasing the light intensity led to a lower yield of the desired product.

During the photocatalyst optimization, we performed some test in order to improve the reaction conditions, in particular to avoid the presence of oxygen and water. To do so, we decided to try to use Argon atmosphere instead of Nitrogen. Additionally, we tried to add independently silica and molecular sieves (4Å) to the reaction vial in order to trap the water traces that were lowering the yield of the desired product. However, the NMRs of the reaction crudes, in both cases, were difficult to analyse and less clean with respect to the usual condition. Lastly, we performed the freeze-pump-thaw technique, after the addition of all the reaction components, to degas completely the vial and remove the traces of water. After that, the reaction vial was fill up with Argon atmosphere. This approach results in an improvement of the quality of the reaction crude NMR and in a lower formation of the hydrolysis product. For this reason, from now on, the photochemical reactions were performed using this strategy.

F) <u>Reaction Temperature</u>

The reaction temperature is a key parameter for every chemical transformation. [75] We envisioned that the construction of a home-made setup (see *Section 4.5*), and the possibility to use or not use the fan to cool down the temperature could lead to significant differences in the reaction temperature. Our purpose was to investigate the impact of the temperature on the reaction yield and selectivity. The temperature was measured with an infrared thermometer at the end of the reaction time, before removing the vials from the light source. Due to a transient unavailability of $PhCF_3$, the experiments

were conducted using toluene (Scheme 27). Table 6 summarizes the effect of the temperature over the reaction.

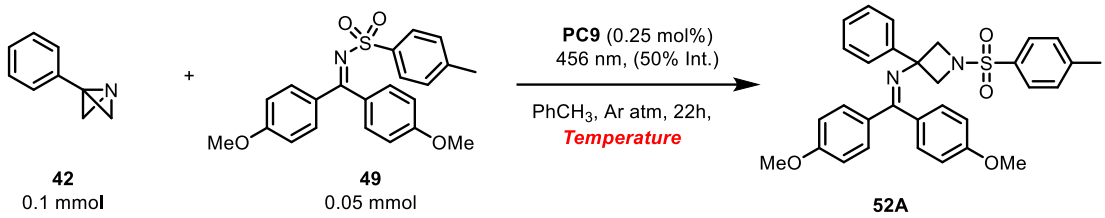

Scheme 27. *Model reaction to evaluate the impact of the reaction temperature.*

Entry	Place	Fan	T_{end} (°C)	NMR yield of 52° (%)
1	Box	On	28.7	**63**
2	Box	Off	41.7	**68**
3	Out	On	25.0	**55**
4	Out	Off	32.1	**65**

Table 6. *Results of Temperature investigation tests.*

The results show how the temperature has a certain impact on the reaction yield, and an increase of the reaction temperature leads to an enhanced yield, this was possible with the use of the designed photochemical setup excluding the use of the fan.

However, since the final optimization experiments and the reaction scope were conducted during the summer period, we noticed that the reaction temperature went above 50°C, leading to unreproducible results, so we decided to continue the investigations using the fan in order to keep the temperature around 35-40°C. We repeated the experiment with $PhCF_3$ as solvent reaching 70 % of yield and we made sure of the reproducibility of the optimized system, conducting the reactions by triplicate.

2.3 *Investigation of a new class of TADF compounds as photocatalysts*

Before closing the optimization process, aiming to enhance the reaction's yield we questioned ourselves the use of a more advanced selection of the photocatalyst. For this reason, we got interested in a class of TADF compounds that have never been used in photocatalysis. [88] The core-structure is depicted in Figure 14.

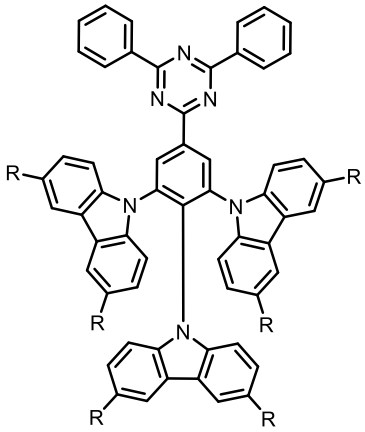

TCzTRZ (R = H) **PC11**
TMeCzTRZ (R = Me) **PC12**
T*t*-BuCzTRZ (R = *t*-Bu) **PC13**

Figure 14. *Structures of the TADF compounds under investigation.*

These compounds are characterized by the presence of a diphenyltriazine acceptor moiety and three carbazole derivative donor systems. They possess an extraordinarily small ΔE_{ST}, even lower from the **PC9**, so we hypothesized that they could enhance the yield of our process. We proceeded to synthesize the reported structure with the unsubstituted carbazole (**PC11**) and the methyl-substituted one (**PC12**), also we were able to get the *t*-butyl-derivative (**PC13**), which was not reported in the literature, since the *t*-butyl group has been demonstrated to reduce the self-quenching, and enhancing the photoluminescence efficiency and the solubility.[89],[90],[91] These compounds were finally tested for the process under investigation (Scheme 28), and the results are summarized in Table 7.

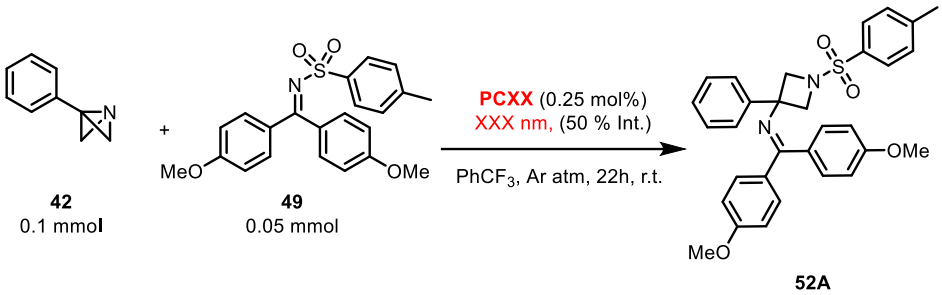

Scheme 28. *Model reaction for the investigation of the photocatalytic behaviour of the new class of TADF compounds.*

Entry	PC	λ (nm)	Intensity	NMR yield of 52° (%)
1	**PC11**	390	50%	**46**
2	**PC12**	456	50%	**55**
3	**PC13**	456	50%	**72**

Table 7. *Results of the new class of TADF photocatalysts*

The results obtained were exciting, the PCs were able to perform the transformation with quite good yields, in particular **PC 13**, entry 3, was found to be the best of all the tested PCs, reaching 72% of NMR yield and 66% of isolated yield . Most interestingly, the main difference between the previous best catalyst **PC 9** and **PC 12** (as example, this behaviour is the same for all this class of PCs) is observed in the ^{1}H NMR of the photocatalyzed reaction's crude, shown in Figure 15.

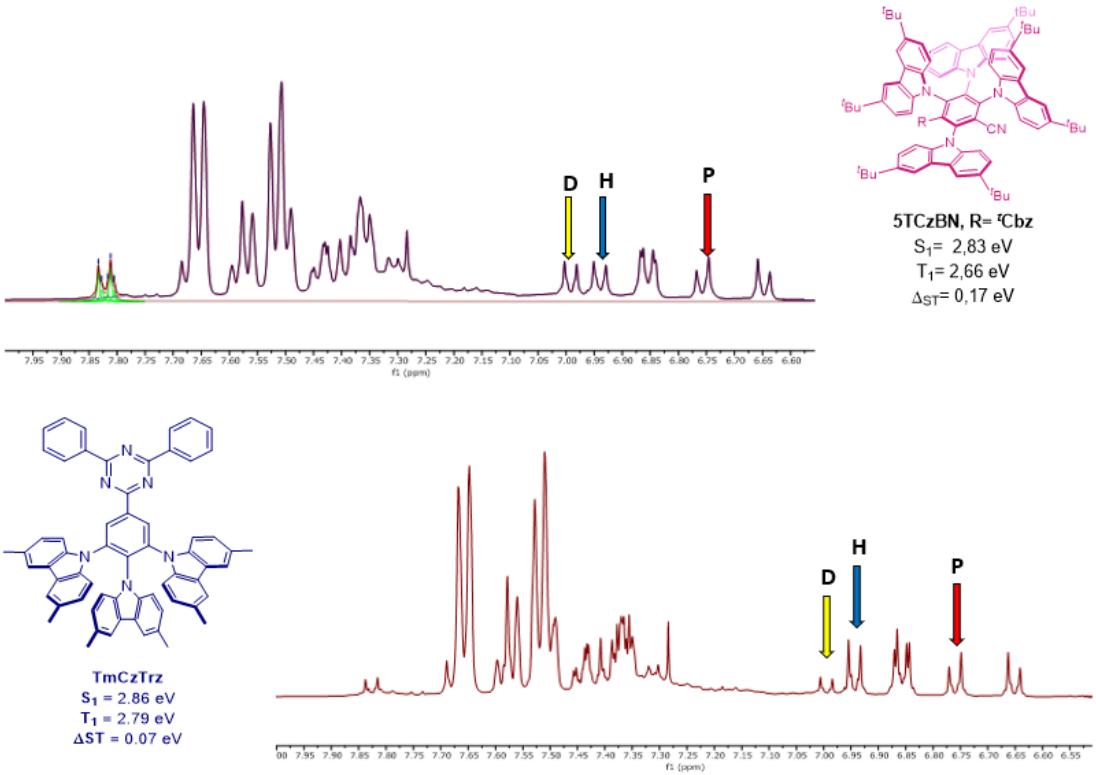

Figure 15. *Comparison of the NMR-crudes of the reaction (Scheme 28) with* ***PC9*** *and* ***PC12****. The yellow arrow corresponds to the dimerization product (D), the blue arrow corresponds to the hydrolysis product (H) while the red arrow corresponds to the desired product (P).*

From the NMR spectra, it can be noticed that when using **PC12** there's a less amount of the homocoupling product (**52B)** with respect to **PC9**. This might be correlated to the smaller ΔE_{ST} for **PC12**, which consequently leads to a minor formation of iminyl radicals (**VII**) (see *Section 2.6*), which are then less prone to undergo homodimerization.

The higher yields of the desired product, the enhanced selectivity of the transformation and the fact that **PC13** was not reported in the literature were the main reasons why we decided to utilize **PC13** for the reaction scope and the mechanistic investigations, after the investigation of the photophysical properties of the new PC.

With this in hand, we defined the overall optimized conditions of the photocatalytic process, summarized in Scheme 29.

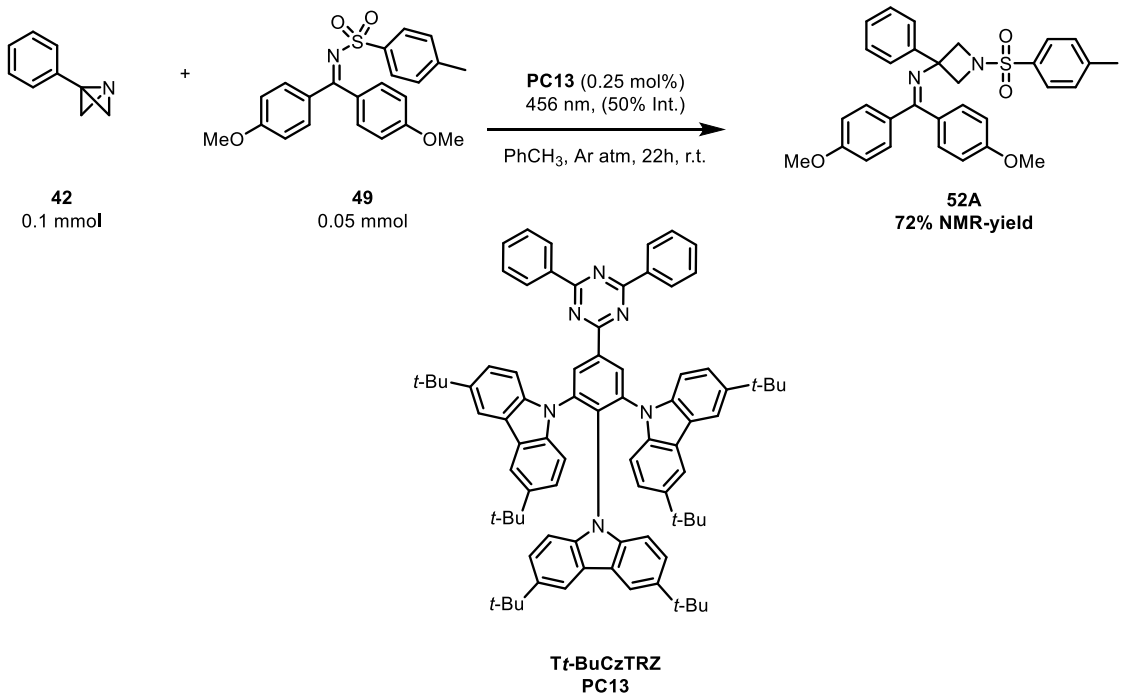

Scheme 29. *Optimized conditions of the transformation under study and structure of the best photocatalyst for the process.*

2.4 *Photo-physical characterization of the best photocatalyst*

Once the optimized reaction scenario was established, the evaluation of the best photocatalyst for the process under study gives as result **PC13**, the Tt-BuCzTRZ. The subsequent step was then to conduct the full characterization of all the relevant properties, starting from the confirmation of the structure followed by the investigation of the photo-physical properties. The latter would guarantee the feasibility of the process not only with the experimental evidence, but also from a theoretically point of view. Since the **PC13** has not been reported in the literature, the characterization was performed for also **PC12**, the TMeCzTRZ, the one with the methyl instead of the *t*-butyl as substituent on the Carbazole moiety, to have a direct comparison with the values reported in the literature.

With the structure in our hand (see *Section 4.4*), the subsequent step for the characterization is the investigation of the photophysical properties, with the further experimental evaluation of the relevant parameters herein described:

- *Absorption max and edge*

The two values create the range of wavelength that can be used to excite the PC. Theoretically, the reaction wavelength should be the closest possible to the maximum of absorption, to guarantee an efficient excitation of the PC with a subsequent population of the PC's triplet state after the ISC. This general rule could not be followed in the transformation under study, since we hypothesized that a high absorption would be translated into a highly populated PC's triplet state, that, after the energy transfer process could lead to the generation of radical intermediates (**VI** and **VII**) in a greater extent (see *Section 2.6*). This could be a problem for the product generation, since if many iminyl radicals (**VII**) are formed, they are more prompt to undergo recombination, generating the homocoupling by-product, and, as a direct consequence, to a lower yield of the desired product.

Figure 16 shows the overlap of the absorption profiles of **PC12** and **PC13**, the relevant values are summarized in Table 8.

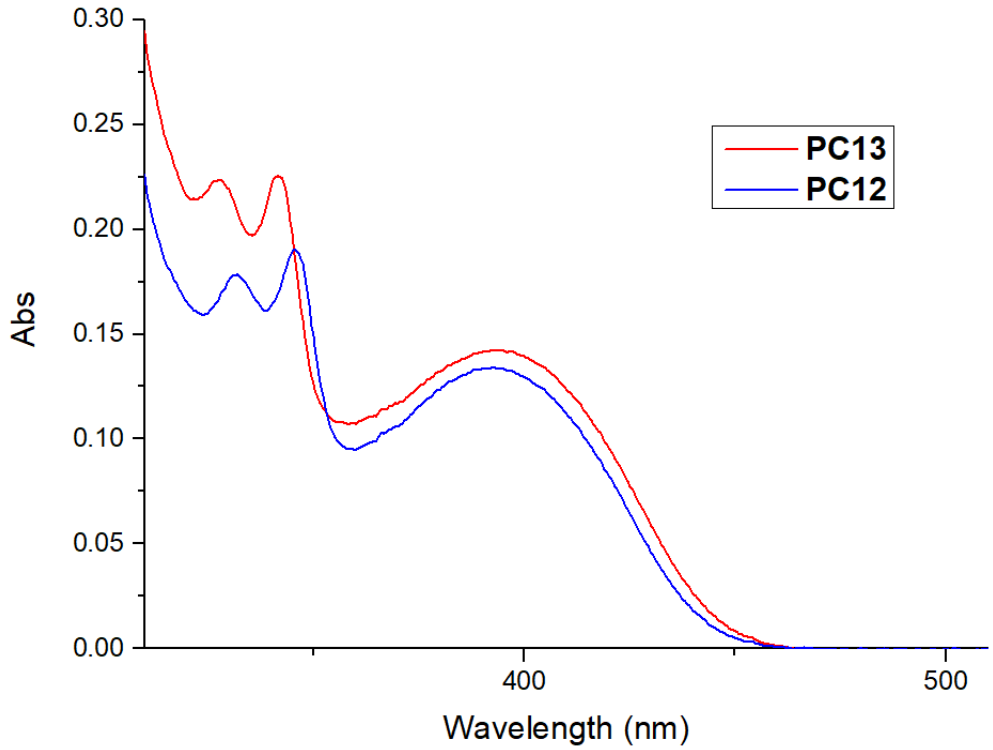

Figure 16. *Overlap of the absorption profiles of* ***PC12*** *and* ***PC13****.*

	Abs Max	Abs Edge
PC12	390 nm	449 nm
PC13	394 nm	460 nm

Table 8. *Relevant parameters obtained from the absorption spectra of* ***PC12*** *and* ***PC13****.*

The spectra show similar profiles for the two compounds, as expected since they have the same core-structure. Both have an absorption band in the UV-Vis region with the maximum localized at 390 nm and 394 nm for **PC11** and **PC12** respectively. The results for **PC11** are in accordance with the reported ones. [88]

The spectra confirmed that the **PC12** can be excited at the reaction wavelength (456 nm), and it is also important to notice that we are working at the very edge of the absorption profile, this agrees with what was anticipated before, that in this way it is feasible to diminish the iminyl radical formation by exciting less efficiently the PC. This favours the reaction of the sulfonyl radical (**VI**) with the ABB (**VIII**), and most importantly the PRE of iminyl radical (**VII**), that has less radicals to undergo the homocoupling forming the unwanted dimer (see *Section 2.6* for details).

- Excited states energies $E_{0,0}(S_1)$ and $E_{0,0}(T_1)$

In order to know the feasibility of a TTEnT process, it is mandatory to know the energy of the excited states. Firstly, the $E_{0,0}(T_1)$ of the PC should be compatible with the $E_{0,0}(T_1)$ of the substrate, in particular it should be higher to ensure the occurring of the TTEnT process. [40]

The determination of the $E_{0,0}(S_1)$ is usually conducted to calculate the redox properties of the S_1 excited state of the photocatalyst. The synthetic transformation does not proceed through an oxidative/reductive quenching cycle, however. In our case, it is crucial to investigate both, $E_{0,0}(S_1)$ and $E_{0,0}(T_1)$, making possible the calculation of the energy gap between the singlet and the triplet excited state (ΔE_{ST}), which for our purposes is important to look

for a correlation between these parameters and the final yield of the reaction. More precisely, the ratio between the product and the homocoupling by-product.

In principle, the lower the ΔE_{ST} is the RISC process from the T_1 to the S_1 excited state of the PC is more favourable. This would mean that the T_1 state will never be too much populated, consequently the generation of the radical intermediates (**VI**) and (**VII**) will not be very efficient, however, this could lead to a cleaner reaction, with less formation of the homocoupling by-product and higher yields.

The $E_{0,0}(S_1)$ is usually obtained from the crossing point of the normalized absorption and emission spectra. [92]

The determination of the $E_{0,0}(T_1)$ was not trivial, since it required the measurement of the phosphorescence spectra at cryogenic conditions, immerging the sample tube in liquid nitrogen at 77 K. [93] The phosphorescence spectrum was then recorded with a delay on the acquisition time in the order of ms, ensuring that the fluorescence contribution was not recorded (since the fluorescence has a lifetime in the order of ns or µs), having only the phosphorescence contribution. The $E_{0,0}(T_1)$ is then determined by the onset of the phosphorescence spectra.

Figure 17 and 18 shows the overlap of the normalized absorption, emission and phosphorescence spectra of **PC12** and **PC13**, respectively. The experimental obtained key parameters are summarized in Table 9, for both **PC12** (with the reported values from the literature) and the new **PC13**.

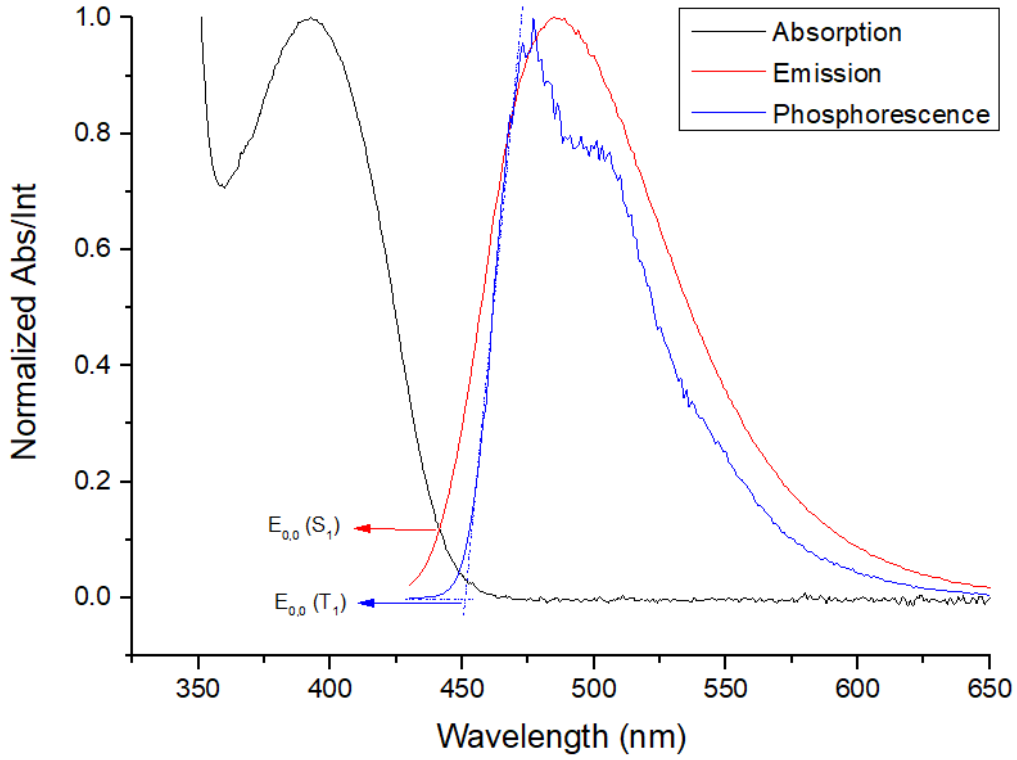

Figure 17. *Normalized absorption (black), emission (red) and phosphorescence (blue) profiles of* ***PC12****.*

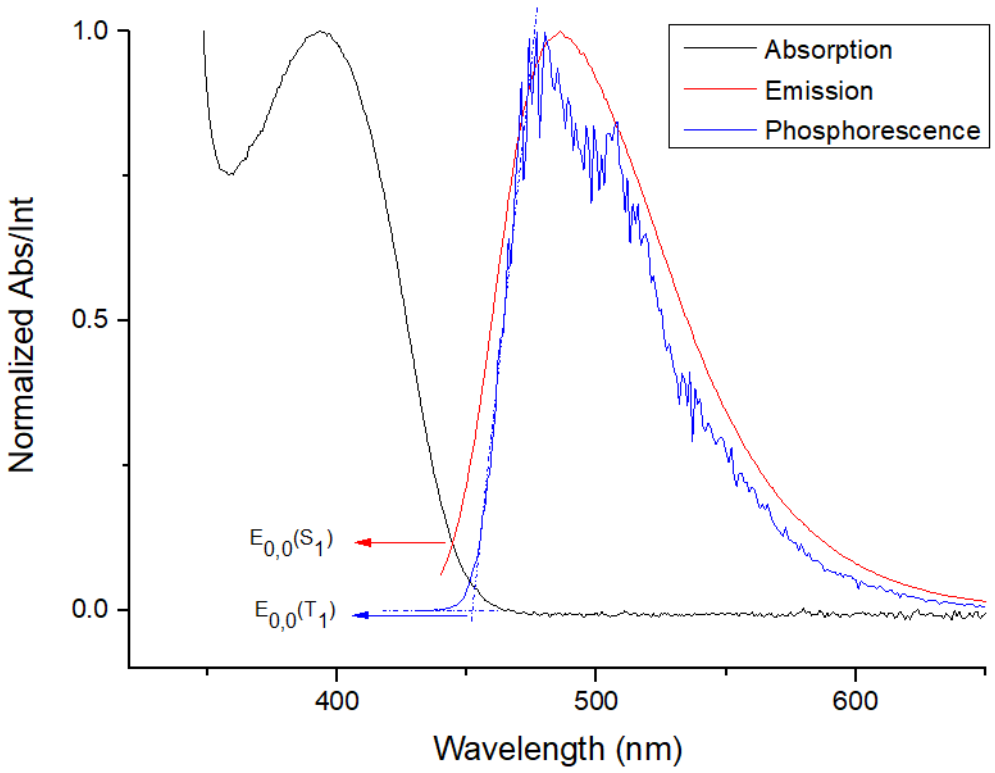

Figure 18. *Normalized absorption (black), emission (red) and phosphorescence (blue) profiles of* ***PC13****.*

Property	PC12	PC13
$E_{0,0}\ (S_1)_{exp}$	2.81 eV	2.79 eV
$E_{0,0}\ (S_1)_{lit}$	2.86 eV	/
$E_{0,0}\ (T_1)_{exp}$	2.75 eV 451 nm	2.74 eV 452 nm
$E_{0,0}\ (T_1)_{lit}$	2.79 eV	/
$\Delta E_{ST\ exp}$	0.06 eV	0.05 eV
$\Delta E_{ST\ lit}$	0.07 eV	/

Table 9. *Resulting values from the determination of* $E_{0,0}$ (S_1) *and* $E_{0,0}$ (T_1) *for* ***PC12*** *and* ***PC13****, and comparison with the reported values for* ***PC12*** *[88].*

The obtained values are in agreement with the literature's ones, [88] and a small difference between the **PC12** and **PC13** could be noticed. Notably, the emission and phosphorescence spectra are almost perfectly overlapped, this behaviour is characteristic for TADF compounds.

2.5 *Reaction Scope*

In order to demonstrate the generality and broadness of the designed methodology, we proceeded to evaluate the reaction scope. As depicted in Figure 19, several positions offer the possibility to be tuned, either in the ABB scaffold (**A**) and in the N-sulfonylimine core (**B**).

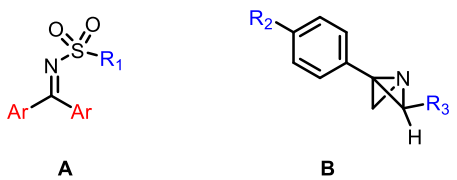

Figure 19. *Substitution pattern strategy for reaction scope.*

After the preparation of the substrates, we performed the reaction employing the optimized conditions (Scheme 30). The results are summarized in Figure 20.

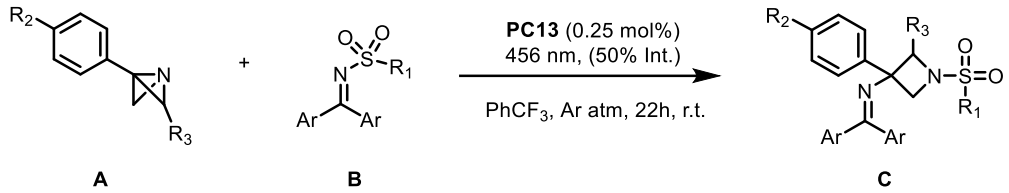

Scheme 30. *General reaction scheme for the scope.*

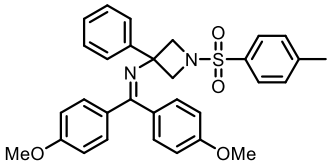

72% NMR yield

52A

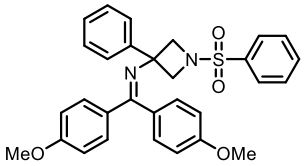

59% NMR Yield

53

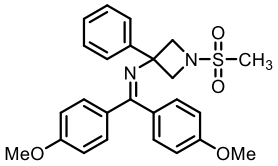

44% NMR Yield

54

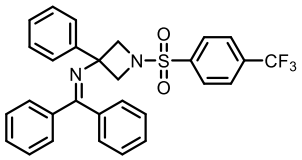

51% NMR Yield

55

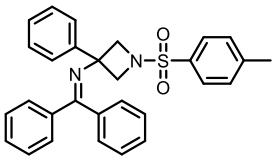

64% NMR Yield

46

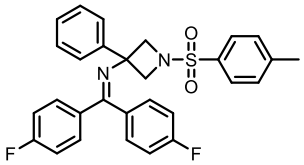

44% NMR Yield

51

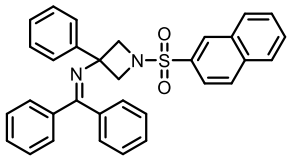

81% NMR Yield

56

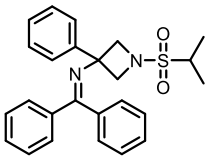

68% NMR Yield

57

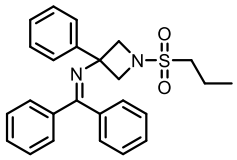

59% NMR Yield

58

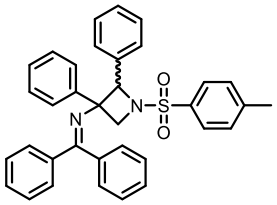

82% NMR Yield
1:1 dr

59

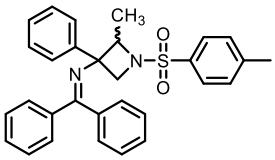

72% NMR Yield
2:1 dr

60

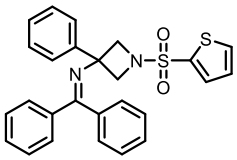

44% NMR Yield

61

Figure 20. *Reaction Scope*

The results of the reaction scope demonstrated that the reaction is working fine also changing the nature of the substituent. Changing the Ar group on the iminyl moiety is not hardly affecting the final result (**52, 46, 51**). As evidence from the experimental results, it seems that electron donating groups on the aromatic favour the overall reaction (**52**). Additionally, the reaction worked well with different substituent (R_1) on the sulfonyl moiety, for aromatic (**53, 55, 56**), hetero-aromatic (61) and aliphatic substituents (**54, 57, 58**). Moreover, we were able to perform the reaction adding a substituent on position 2 (R_3) of the ABB moiety, resulting in quite high yield but with low diastereomeric control (**59, 60**), this was expectable since the PC does not possess any chirality. Studies on the effect of the aromatic substituent on the phenyl of the ABB (R_2) are still ongoing.

2.6 *Mechanistic Investigations*

Obtaining experimental and theoretical evidence of a reaction mechanism is crucial to confirm or discard the mechanistic hypothesis on the process under study. This is relevant to understand how the molecules are interacting with each other, leading to a better optimization of the reaction conditions and reactants. These studies are usually not trivial in the context of photocatalytic reactions, since they often proceed through highly reactive radical intermediates which are not easily, or even impossible to isolate. Some information can be obtained with transient absorption spectroscopy (TAS) and electron paramagnetic resonance (EPR) measurements but is not always possible because of relatively short lifetime and low concentration (catalytic order) of the highly reactive radicals, that are not easily accumulated in the media making possible their detection by the instrument. Luminescence quenching studies are also powerful tools to gain information on the decay of the photocatalyst's excited state. Additionally, in the recent years, DFT calculations are gaining a huge importance to help to understand the energies and pathways of the reactant and intermediate species.
Regarding the process understudy, we hypothesize the catalytic cycle and the further reactivity depicted in Scheme 31.

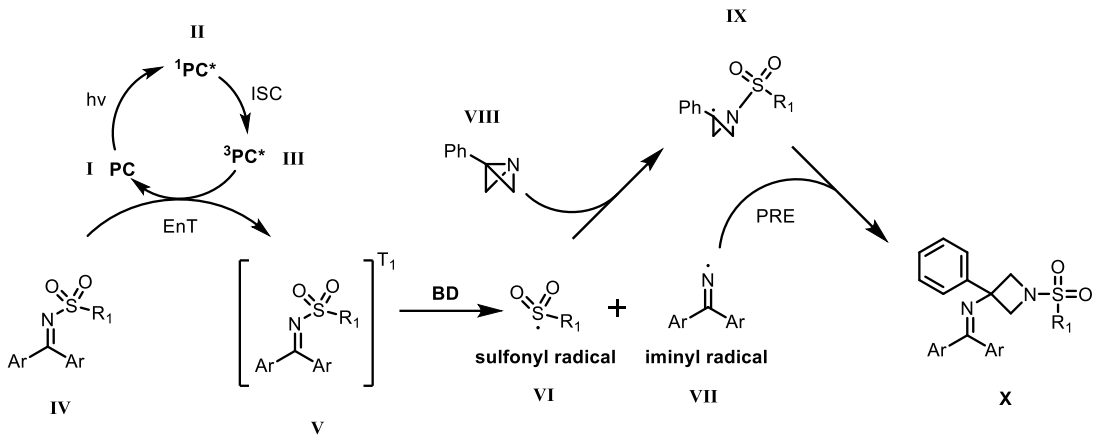

Scheme 31. *Proposed mechanism for the transformation under study.*

Firstly, the PC in the ground state form (**I**) is excited to its S_1 (**II**) excited state upon light irradiation. Subsequently, the ISC occurs in which the PC reaches its triplet excited state (**III**). After this, the triplet-triplet energy transfer from the photocatalyst to the sulfonylimine substrate (**IV**) leads to the regeneration of the ground state form of the photocatalyst (**I**) and to the population of the dark triplet state of the substrate (**V**), which undergoes N-S σ bond dissociation (BD) generating the correspond radical species, the sulfonyl radical and the iminyl radical (**VI** and **VII**, respectively). **VI** is then trapped by the ABB substrate (**VIII**), breaking the N-C3 bond of the bicycle and generating a tertiary and benzylic radical intermediate (**IX**), centred on the C3 atom. Subsequently, **VII** undergoes radical recombination with **IX**, that, due to a persistent radical effect (PRE), is long-lived enough to still be "available" in the reaction media (if it is not reacting with another molecule of **VII** leading to the homocoupling product). The final C-N bond formation leads to the neutral product **X**.

To demonstrate the validity of this hypothesis, we conducted the following studies:

- Experimental evidence

The sensitization of sulfonylaldimines was reported by Willis in 2022, [50] additionally, the generation of radical intermediates **VI** and **VII** upon σ bond dissociation has as experimental evidence the formation of the homocoupling product that could arise only from the radical dimerization of **VII**, following the mechanism depicted in Scheme 31.

- Control experiments

Some control experiments were conducted to investigate the behaviour of the reaction in absence of light and/or photocatalyst (Scheme 32). The results are summarized in Table 10.

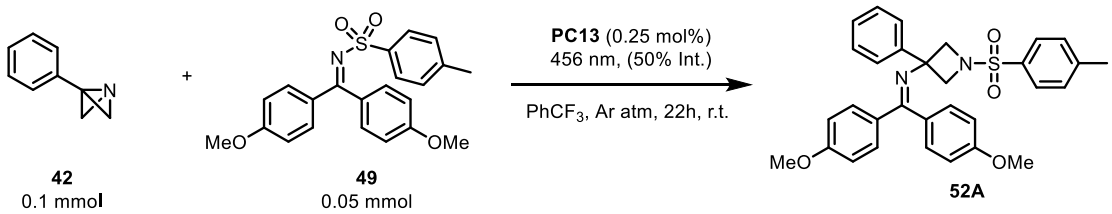

42
0.1 mmol

49
0.05 mmol

52A

Scheme 32. *Model reaction for control experiments.*

Entry	Wavelength	PC13	NMR yield (52A)
1	456 nm	Yes	**72 %**
2	No	Yes	**0 %**
3	456 nm	No	**0 %**
4	390 nm	No	**18 %**

Table 10. *Results of control experiments.*

As expected, the reaction did not occur in the absence of light, entry 2, corroborating that a light-promoted process was under study. Additionally, we tested the reaction without the use of the photocatalyst, at the usual wavelength (456 nm), entry 3, and at more energetic one (390 nm), entry 4.

As expected, the reaction at 456 nm didn't work, meaning that the photocatalyst is the active species under the standard reaction conditions. The reaction at 390 nm leads to the formation of the product, with a low yield (18%), entry 4. This is simply attributed to the fact that the sulfonylimine is able to partially absorb and consequently get excited at this wavelength thus, a merely photolysis of the N-S bond explains the formation of the required radical species. However, the efficiency and selectivity of the transformation is not as good as the result obtained in photocatalytic conditions.

- Luminescence quenching studies

Luminescence quenching studies were performed to demonstrate the reactivity between the triplet excited state of the photocatalyst and the substrates of the reaction. The experiment is based on the measure of the emission profile of the photocatalyst, firstly in the absence of substrates (I_0) (in this case they are named quenchers) and subsequently with increasing amounts of quenchers (I) while keeping constant the concentration of the photocatalyst. If the added quencher is reacting with the excited state of the photocatalyst, a decrease in the emission intensity should be observed. [94] This decrease should be correlated with the quencher concentration. For the construction of the Stern-Volmer plot [95], the ratio of the intensity maximums (I_0/I) is plotted against the quencher concentration ([Q]). This relationship should follow the Eq.4:

$$I_0/I = 1 + K_q[Q] \qquad \text{[Eq.4]}$$

In which I_0 is the emission maximum in the absence of any quencher, I is the emission's maximum point in the presence of quencher, *[Q]* is the quencher concentration and K_q is the quenching constant, this parameter is equal to the product of the excited state lifetime (τ_0) and the quencher rate coefficient k_q.

The experiment was conducted with the excitation of **PC13** at 456 nm to mimic the reaction conditions and to ensure that the measure is not affected by self-

quenching of the PC of its excited state, since at that wavelength the absorbance of the PC, at the applied concentration, is less than 0.1. Once the emission is recorded to obtain I_0, the quenchers are added (independently) following increasing pattern of concentration and keeping constant the amount of PC between each measure (Figure 21). The results of the experiments and the Stern-Volmer plot are shown in Figure 22, 23 and 24 respectively.

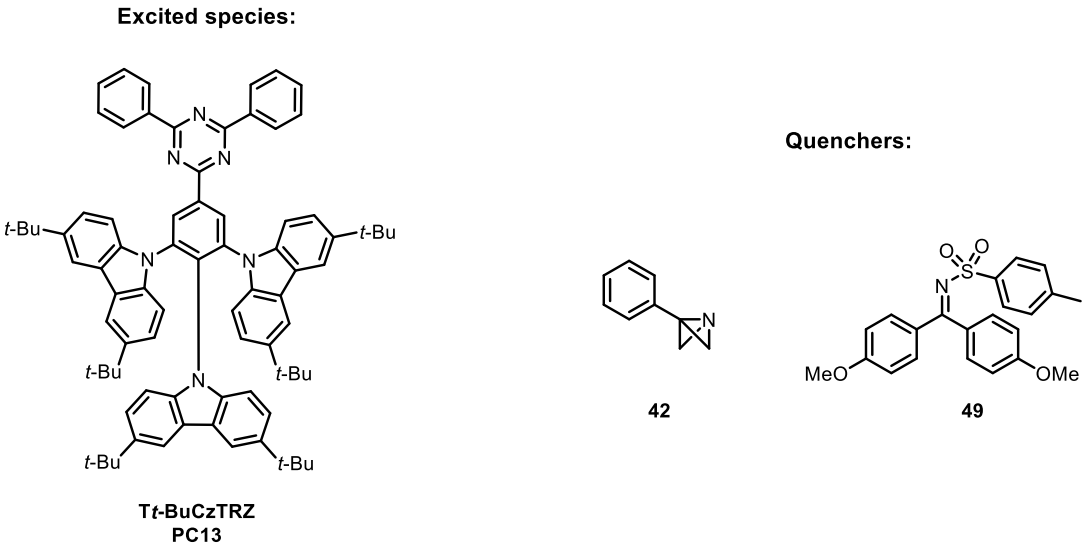

Figure 21. *Selected compounds for the luminescence quenching studies.*

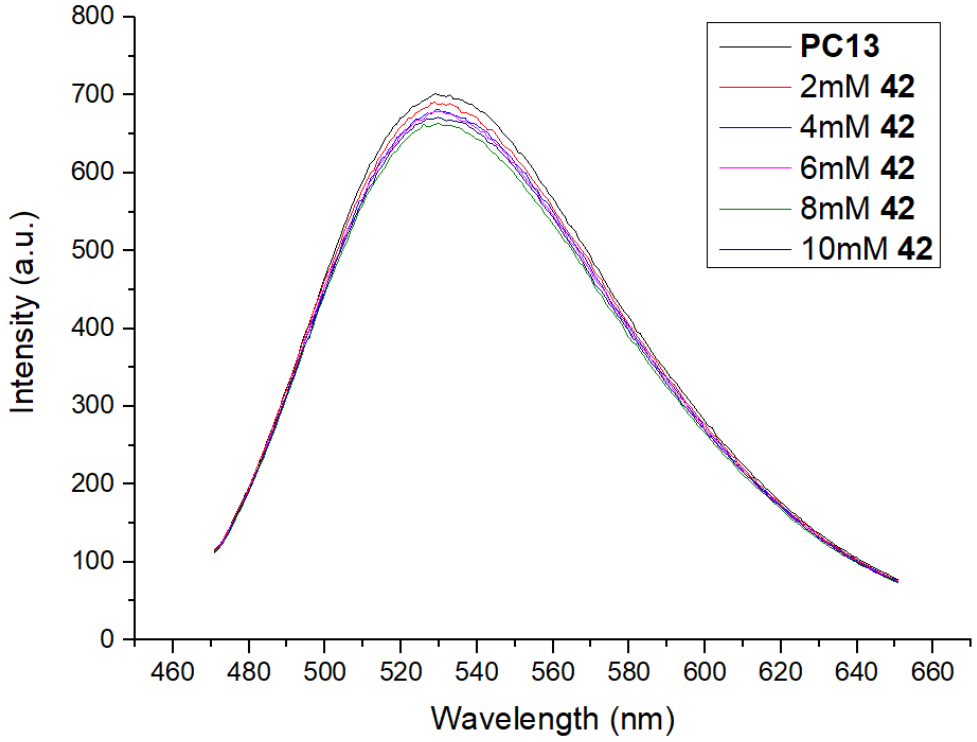

Figure 22. *Luminescence quenching experiment with quencher* ***42****. The spectrum was recorded in* $PhCF_3$.

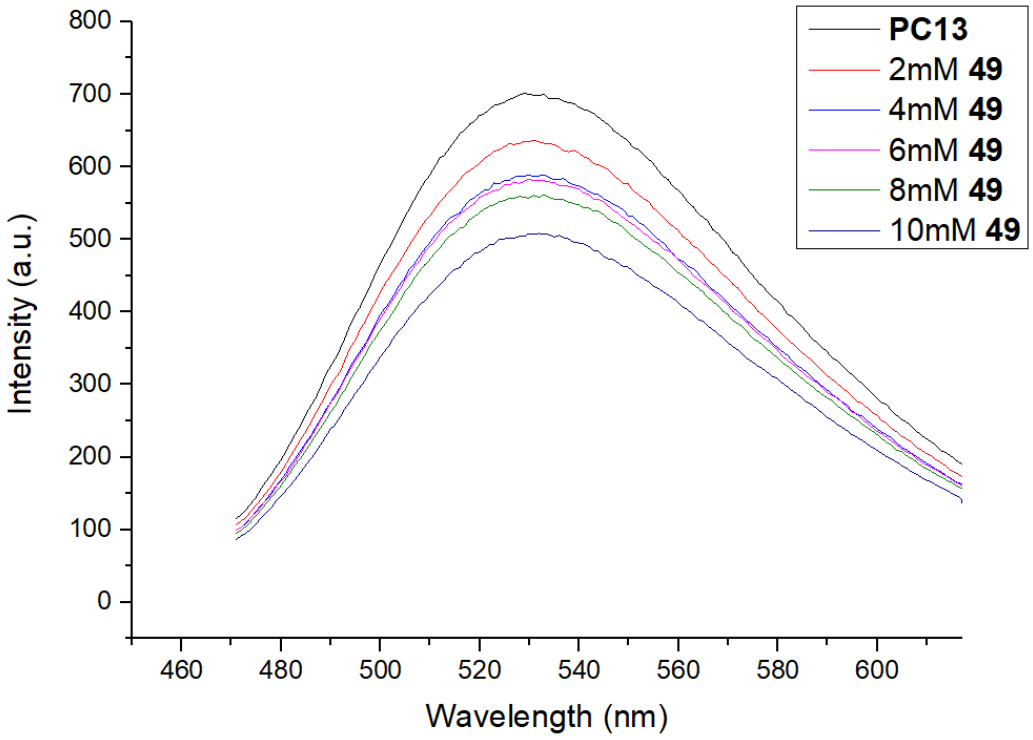

Figure 23. *Luminescence quenching experiment with quencher* ***49****. The spectrum was recorded in* $PhCF_3$.

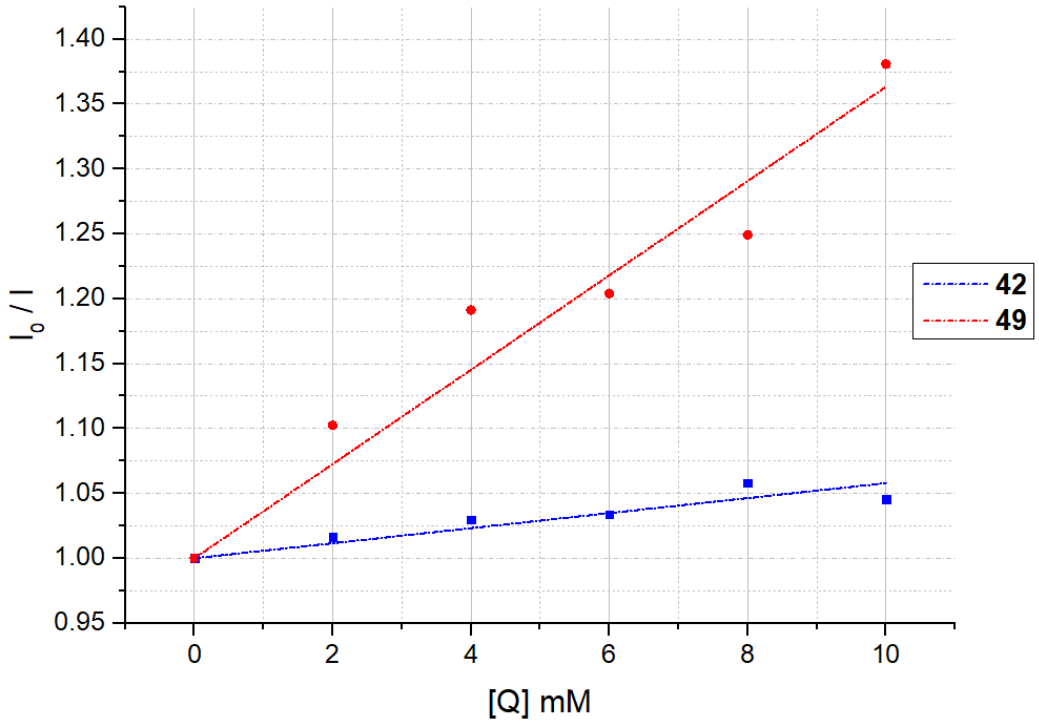

Figure 24. *Stern-Volmer plot resulting from the luminescence quenching studies.*

As expected from the emission spectra and the Stern-Volmer plot, it is clear that the substrate that has the strongest interaction and therefore is quenching the photocatalyst's excited state is the sulfonylimine. From this point, the sulfonylimine's dark triplet state gets populated and subsequently dissociates in the two radicals previously described. It is also clear from Figure 22 and from the Stern-Volmer plot that the ABB has practically any kind of influence on the PC's excited state since the slope of the plotted line is near to 0.

DFT calculations (in collaboration with Dr. Paolo Costa, University of Padova), TAS measurements (in collaboration with Prof. Mirco Natali, University of Ferrara), and EPR studies (in collaboration with Prof. Marco Bortolus, University of Padova) are ongoing, to get access to more detailed information about the mechanism of the transformation.

3 Conclusions and perspectives

In this thesis project, we exploited the advantages that photocatalysis offers in organic synthesis, reporting a new methodology to access the synthesis of 1,3-di-functionalized azetidines with the use of a fully organic photocatalyst in a visible light-mediated process. The obtained results are very promising since the preparation and functionalization of nitrogen containing four member-rings is still a quite hard challenge for the scientific community. Additionally, the use of 1-azabicyclo[1.1.0]butanes as starting materials, locates strain-release streamlining as a very powerful tool to achieve azetidines, obtained by a 100% atom economical process. In this project, for the very first time, the ABB ring was opened and functionalized through a photocatalytic reaction, accessing a new synthetic mechanistic route different from the commonly used polar chemistry. The transformation implies the use of mild conditions (room temperature) requiring the irradiation with visible light as energy source, resulting in an improvement with respect to the usually harsher conditions, longer reaction times, and lower selectivity. We expect that this strategy will provide a new platform for the synthetic community to achieve the preparation of 1,3-di-functionalized azetidines, which could be applicated in drug discovery programmes or agrochemical industries.

Additionally, we took advantage of the TTEnT activation mode to induce a σ bond dissociation generating two radicals, allowing us to utilize both highly reactive species to achieve an overall di-functionalization using only one reactant. This could be a very interesting example for the scientific community regarding the potentials of energy transfer catalysis.

Moreover, we showcased one of the potential applications of TADF emitters in photocatalysis. This concept is outstanding since these compounds, already known to have applications in OLED manufacturing, have been recently used also as photocatalyst. This dualism of possible application will generate a lot of interest and consequently developments on this class of compounds. In this work, a class of already known TADF emitters, based on a triazine core, was investigated for the first time in photocatalysis, resulting, after a derivatization of the structure reported in the literature, as the best for our process and

potentially for other transformations. The full characterization of the photocatalyst was performed to determine the relevant properties for a photocatalyst description.

In the project, the importance of the reaction optimization and the mechanistic investigations were underlined. These studies are necessary to achieve higher yields and selectivity of the desired transformation. The reaction optimization was obtained focusing on the key parameters of the reactions such as stoichiometry, solvent, photocatalyst, wavelength and intensity. By doing the latter, it was possible the increase of the yield up to 72% of the model reaction. The mechanistic investigations reinforced our mechanistic hypothesis of an TTEnT manifold with subsequent radical chemistry.

The perspectives of this project will involve a more accurate investigation of the mechanism, taking advantage of the DFT calculations, EPR and TAS measurements. DFT calculations could give evidence on the energies and the pathways of the species involved in the transformation. EPR studies could give informations on the radical species formed under the photocatalytic conditions. Additionally, TAS measurements could give some details on the lifetime of the active species involved. Moreover, the reaction scope will be extended, exploiting the full potential of the transformation. In this regards, different radical sources will be tested, to investigate the possibility to access to different functionalization patterns, based on the σ bond nature of the sensitized starting material.

4 Experimental methods

4.1 *General Informations*

NMR spectra were recorded on Bruker AVANCE Neo 400 Nanobay equipped with a BBFOATM-z grad probehead. The chemical shifts (δ) for ^{1}H and ^{13}C are given in ppm relative to residual signals of the solvents ($CHCl_3$ @7.29 ppm ^{1}H-NMR, 77.16 ppm ^{13}C NMR, CH_2Cl_2 @5,32 ppm ^{1}H-NMR, 53,84 ppm ^{13}C, $(CH_3)_2CO$ @2,05 ppm ^{1}H-NMR, 29,84 ppm ^{13}C NMR). Coupling constant are given in Hz. The following abbreviations are used to indicate the multiplicity; s, singlet; d, doublet; t, triplet; q, quartet; m, multiplet; bs, broad signal.

Chromatographic purification of products was accomplished using flash chromatography on silica gel (SiO2, 0.04-0.063 mm) purchased from Machery-Nagel, with the indicated solvent system according to the standard techniques. Thin-layer chromatography (TLC) analysis was performed on pre-coated Merck TLC plates (silica gel 60 GF254, 0.25 mm). Visualisation of the developed chromatography was performed by checking UV absorbance (254 nm). Organic solutions were concentrated under reduced pressure on a Büchi rotary evaporator.

Steady-state absorption spectroscopy studies were performed at room temperature on a Varian Cary 50 UV-vis double beam spectrophotometer; 10 mm and 1 mm path length Hellma Analytics 100 QS quartz cuvettes were used. Steady-state fluorescence spectra, Phosphorescence spectra and luminescence quenching studies were recorded on a Varian Cary Eclipse Fluorescence spectrophotometer; 10 mm path length Hellma Analytics 117.100F QS quartz cuvettes (for Fluorescence and luminescence quenching studies) or glass tubes (for Phosphorescence).

The ESI-MS analysis were performed in Flow Injection Analysis with an HPLC system (Agilent Technologies 1100 series, flux 0.5 mL/min, MeOH (1% HCOOH)) connected to a mass spectrometer detector (MSD Trap SL, model G2245D). The ionization was performed within the electrospray (ESI) source in positive under the following conditions: nebulizer 20 psi, dry gas flow rate 5

L/min, dry gas temperature 325 °C, capillary voltage 3.5 kV, capillary exit 117.5-212 V (depending on the mass), and skimmer 40 V.

DFT calculations were carried out by Dr. Paolo Costa using the Gaussian-16 suit of programs. Geometry optimizations were performed with M06-2X functional using def2TZVP as basis set. Frequency calculations were also carried out to ensure that the structures optimized are true relative minima of energy. The energy values reported include the thermal correction to Gibbs Free Energy.

4.2 *Materials*

Commercial grade reagents and solvents were purchased at the highest commercial quality from Sigma Aldrich, FluoroChem or BLDpharma and used as received, unless otherwise stated.

4.3 *Synthesis of substrates*

- General procedure for the synthesis of N-sulfonylimines

Sulfonylimines were prepared following the reported procedure, [97] depicted in Scheme 33:

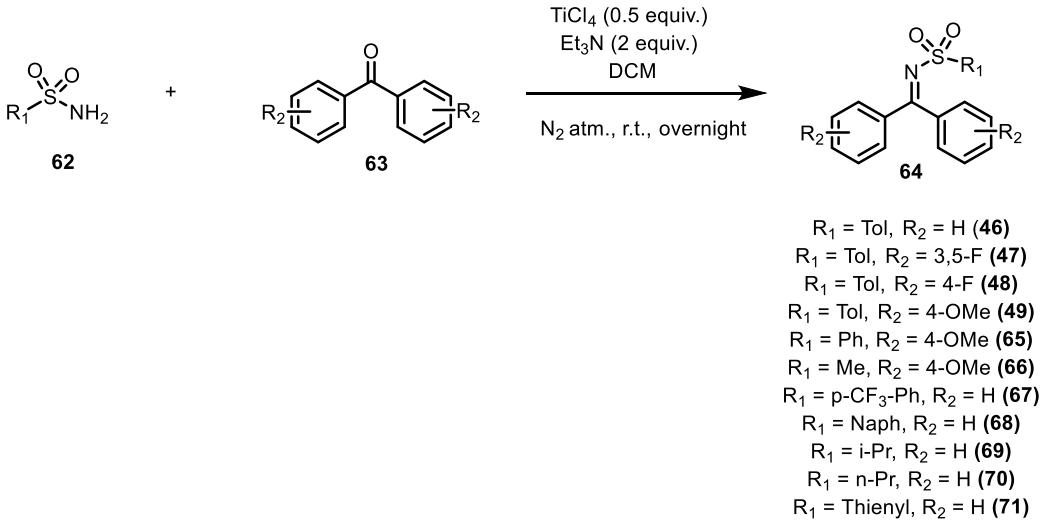

Scheme 33. *General procedure for the synthesis of N-sulfonylimines.*

The proper sulfonamide (**62**) 1 equiv. (5 mmol) and the corresponding benzophenone derivative (**63**) 1 equiv. (5 mmol) were added in a 50 mL round bottom flask and dissolved with 20 mL of dichloromethane (DCM). Triethylamine (NEt_3) 2 equiv. (10 mmol) was added under nitrogen atmosphere, then Titanium (IV) tetrachloride ($TiCl_4$) 0.5 equiv. (2.5 mmol) was added dropwise. The solution was stirred overnight at room temperature. The reaction mixture was checked by TLC (eluent: petroleum ether-ethyl acetate 7:3), then the reaction crude was filtrated over celite, and concentrate with rotary evaporator. The resulting solid was purified by flash column chromatography with the proper eluent mixture of petroleum ether-ethyl acetate leading to the final N-sulfonylimine derivative (**64**). All the spectroscopic data of the synthesized N-sulfonylimine were in agreement with the literature.

- <u>Synthesis of 3-phenyl-1- azabicyclo[1.1.0]butane</u>

The model ABB starting material was prepared from a reported multi-step synthesis [98] depicted in the following schemes:

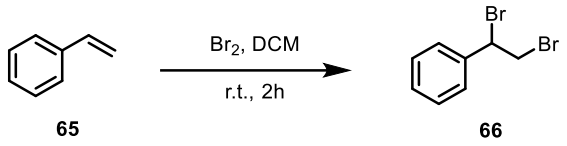

Scheme 34. *1st step of the synthesis of 3-phenyl-1-azabicyclo[1.1.0]butane.*

Styrene (**65**) 1 equiv. (20 mmol) was added in a 50 mL round bottom flask and dissolved in 16 mL of DCM, Br_2 1 equiv. (20 mmol) was added dropwise, then the mixture was stirred for 2h at room temperature, after that the solvent and the not reacted bromine were evaporate with rotary evaporator, the resulting orange solid (**66**) was directly used in the next step without further purification.

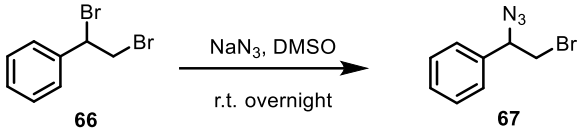

Scheme 35. *2nd step of the synthesis of 3-phenyl-1-azabicyclo[1.1.0]butane.*

(1,2-dibromoethyl) benzene (**66**) 1 equiv. (20 mmol) was added to a 50 mL round bottom flask and dissolved in 28 mL of dimethylsulfoxide (DMSO), then sodium azide (NaN_3) 1.5 equiv. (30 mmol) was slowly added to the solution, then the mixture was stirred overnight at room temperature, and the mixture containing **67** was directly used for the next step.

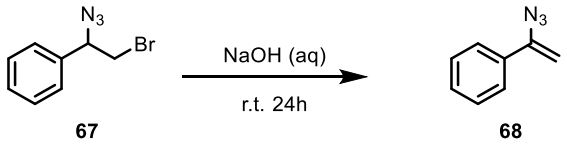

Scheme 36. *3rd step of the synthesis of 3-phenyl-1-azabicyclo[1.1.0]butane.*

Sodium hydroxide (NaOH) 1 equiv. (20 mmol) was smashed and dissolved in 6 mL of water ([6.66 M] solution), then the solution was added to the reaction mixture containing 1-bromo-2-azido-1-phenylethane (**67**) and stirred for 24h at room temperature. The mixture was then poured into 20 mL of a $NaHCO_3$ solution (5 mL of saturated solution + 15 mL of water). The organic phase was collected, and the aqueous phase was extracted with DCM. The combined

organic phase was then washed with brine, dried with $MgSO_4$, filtrate and concentrated with rotary evaporator obtaining a brownish liquid (**68**) that was directly used for the next step.

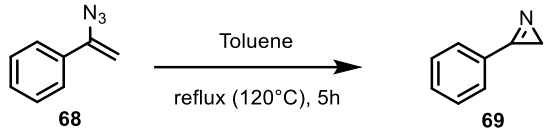

Scheme 37. *4th step of the synthesis of 3-phenyl-1-azabicyclo[1.1.0]butane.*

1-azido-styrene (**68**) was dissolved in 50 mL of Toluene in a 250 mL round bottom flask, the latter was equipped with a condensator and the mixture was refluxed at 120°C for 5h. The solvent was then removed with rotary evaporator and the final product (**69**) was dried under vacuum and used in the last step.

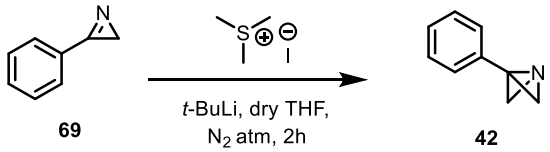

Scheme 38. *Last step of the synthesis of 3-phenyl-1-azabicyclo[1.1.0]butane.*

Trimethylslfonium iodide 1.1 equiv. (17.0 equiv.) were added in a 250 mL two neck round bottom flask, under nitrogen conditions, and dissolved in 120 mL of dry tetrahydrofuran (THF). The mixture was cooled to -30°C with a acetonitrile-dry ice bath, then tert-butyllithium *t*-BuLi (1.7M) 1.1 equiv. (17 mmol) was added dropwise with an addition funnel. The mixture was stirred for 30 min then a solution of 3-phenyl-2H-azirine (**69**) 1 equiv. (15.5 mmol) in 9 mL of dry THF was added dropwise the addition funnel, the mixture was stirred for 1h at -30°C, then the reaction was quenched with 20 mL of ice-cold water. The organic and the aqueous phase were separated, and the aqueous one was extracted with DCM, then the organic phases were collected, dried with $MgSO_4$, filtrate and concentrated at the rotary evaporator to remove the solvent and the dimethylsulfide by-product. Finally the 3-phenyl-1azabicylo[1.1.0]butane (**42**) was obtained through distillation with Kugelrohr

apparatus. It appears as a colourless and viscous liquid. The characterization of the obtained compound **42** was in agreement with the literature.

- Synthesis of 3-phenyl-2-substituted-1-azabicyclo[1.1.0]butane

The 2-substituted ABB was prepared following the reported procedure: [99]

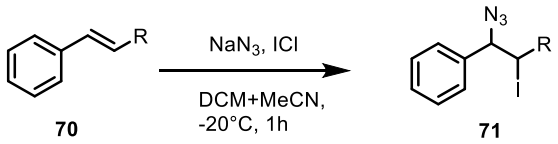

Scheme 39. *1st step for the synthesis of 3-phenyl-2-substituted-1-azabicyclo[1.1.0]butane.*

A suspension of NaN_3 2.5 equiv. (11 mmol) in acetonitrile (3 mL) was added dropwise to a solution of iodine monochloride 1.14 equiv. (4.97 mmol) in DCM (6 mL) at −20 °C, and the mixture was stirred at the same temperature. After 30 min, a solution of appropriate olefin (**70**) 1 equiv. (4.36 mmol) in DCM (2 mL) was added slowly, and the mixture was stirred for 1 h. The reaction was quenched with saturated aqueous $Na_2S_2O_3$ solution, and the organic materials were extracted two times with Et2O. The combined extracts were washed with brine and dried over $MgSO_4$. After evaporation of solvents with rotary evaporator, the resulting crude materials (**71**) were used immediately for the next step without further purification.

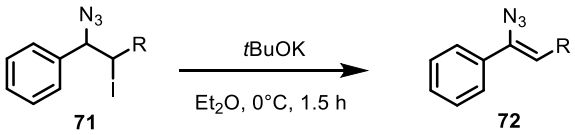

Scheme 40. *2nd step for the synthesis of 3-phenyl-2-substituted-1-azabicyclo[1.1.0]butane.*

To a solution of the obtained compounds (**71**) in Et_2O (10 mL) tBuOK 1.2 equiv. (5.23 mmol) was added at 0 °C, and the mixture was stirred for 1.5 h. The reaction mixture was filtered through filter paper and the solvent from the filtrate was removed under vacuum. The resulting crude materials were

purified by column chromatography (silica gel; hexane) to give vinyl azide (**72**) that was directly used for the next step.

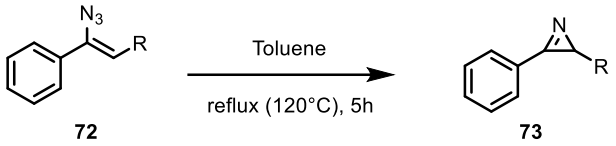

***Scheme 41**. 3rd step for the synthesis of 3-phenyl-2-substituted-1-azabicyclo[1.1.0]butane.*

Vinyl azide (**72**) was refluxed (oil bath) in toluene for 4 h. After the removal of the solvent the corresponding 2-substituted 3-phenyl-2H-azirine was obtained, and the corresponding ABB was prepared with the procedure previously described (Scheme 38), obtaining the 2 substituted ABB derivative, as shown in Scheme 42.

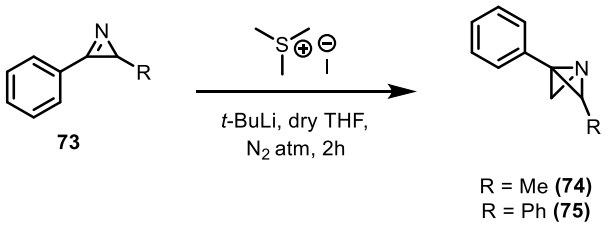

***Scheme 42.** Last step for the synthesis of 3-phenyl-2-substituted-1-azabicyclo[1.1.0]butane.*

Compound **74** was obtained through distillation with Kugelrohr apparatus, while **75** didn't require further purification. The characterization of the two ABB derivatives is shown in *Section 4.4.*

4.4 *Synthesis of photocatalysts*

- Synthesis of benzonitrile derivatives

PC5 and **PC9**, 5CzBN and 5TCzBN respectively, were prepared following the reported procedure shown the reaction scheme XX: [70]

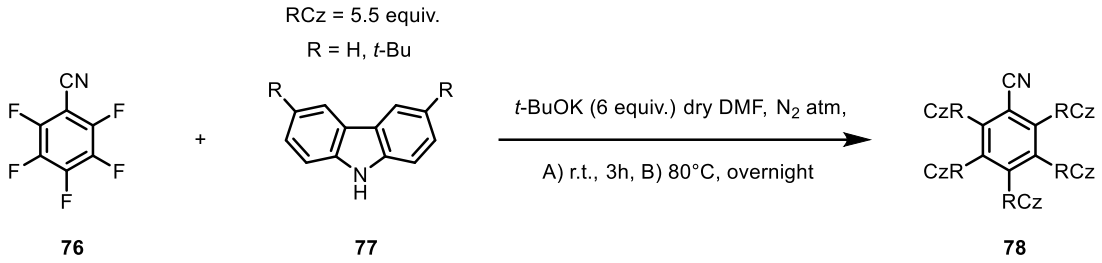

Scheme 43. *Synthesis of benzonitrile PCs.*

6 equiv. (60 mmol) of potassium tert-butoxide (*t*-BuOK) were added to a round bottom dry flask, under N_2 atmosphere, and dissolved with 20 mL of dry dimethylformamide (DMF). A solution of the proper Cz derivative (**77**), 5.5 equiv. (55 mmol) in 20 mL DMF was added dropwise with an addition funnel for 15 min. The mixture gets yellowish. Stir for 3h at r.t., then a solution of 2,3,4,5,6-pentafluorobenzonitrile (**76**) 1 equiv. (10 mmol) in 10 mL of dry DMF was added dropwise for 15 min, then the reaction was stirred overnight at 80°C in an oil bath.

After the night, water was added to force precipitation, then the mixture was filtrated under vacuum and subsequently dried under vacuum, obtaining a yellow solid. The compound was purified by flash column chromatography (eluent: petroleum ether-ethyl acetate 95:5) to remove the excess of the Cz derivative, resulting in the corresponding product (**78**), in particular **PC5** (R = H) and **PC9** (R = *t*-Bu), they both appear as yellow solids.

- Synthesis of triazine derivatives

The triazine derivative photocatalysts were obtained with the following procedure reported in the literature: [88]

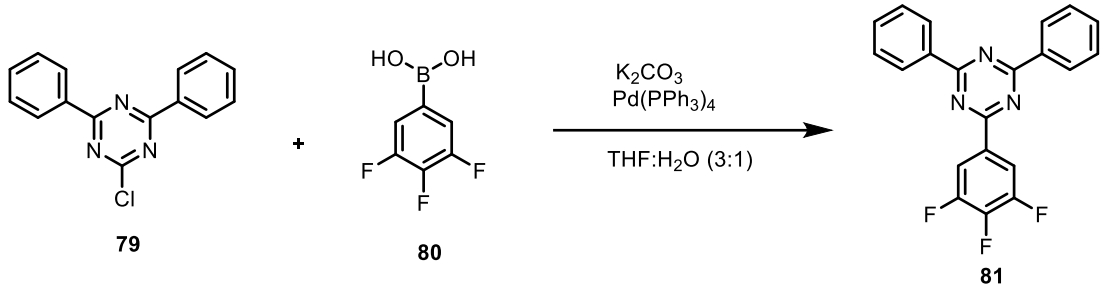

Scheme 44. *1st step fot the synthesis of triazine PCs.*

2-chloro-4,6-diphenyl-1,3,5-triazine (**79**), 1 equiv. (19.9 mmol), (3,4,5-trifluorophenyl)boronic acid (**80**) 1 equiv. (19.9 mmol) and potassium carbonate 3 equiv. (59.7 equiv.) were dissolve in a mixture of THF and water 3:1 (150 mL and 50 mL, respectively), After 20 min. of nitrogen bubbling tetrakis(triphenylphosphine)palladium(0), 1 mmol(5mol%), was added to the solution. The mixture was refluxed for 8 h under nitrogen atmosphere, then cooled down to room temperature. The mixture was filtered, and the residue (**81**) was washed with ethyl acetate and acetone and used in the further step.

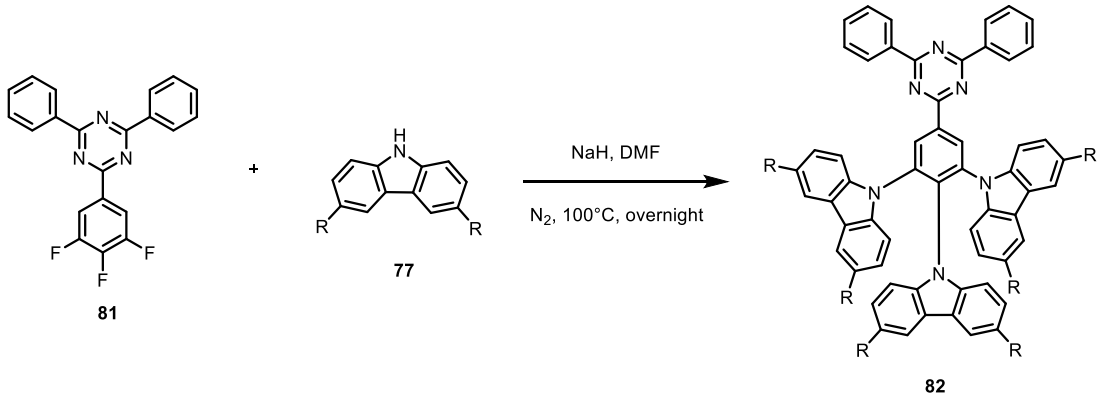

Scheme 45. *2nd step for the synthesis of triazine PCs.*

Sodium hydride (NaH-60% in mineral oil), 4.5 equiv. (4.95 mmol) were added in a 100 mL round bottom flask and washed three times with hexane. A solution of the proper carbazole derivative (**77**) 3.3 equiv. (3.63 mmol) in 25 mL of dry DMF was added and the mixture was stirred for 30 min. 2,4-diphenyl-6-(3,4,5-trifluorophenyl)-1,3,5-triazine (**81**) was then added, then the reaction flask was equipped with a condensator under nitrogen atmosphere. The mixture was stirred at 100°C overnight. The reaction was quenched with water, and the

product extracted with diethyl ether. The organic phase was washed with brine, dry with MgSO4, filtrate and concentrate with the rotary evaporator. The obtained solid was redissolved in diethyl ether and put in the fridge to force the precipitation. Then the precipitate was filtered under vacuum and the final product (**82**) was recovered, in particular **PC11** (R = H), **PC12** (R = Me) **PC13** (R = *t*-Bu). The compounds all appear as yellow solids. **PC12** and **PC13** shown interesting emission properties in the solid state under a UV-lamp (Figure 25).

Figure 25. *Emission of* ***PC12*** *(right) and* ***PC13*** *(left) in the solid state under a UV lamp.*

All the NMR and ESI-MS spectra of **PC11** and **PC12** were in accordance with the procedures followed from the literature. The characterization of the unreported **PC13** (T*t*-BuCzTRZ) is described in *Section 4.6*

4.5 *Photochemical setup and procedure*

The photochemical setup is shown in figure 26, it consists in a box with two holes on the walls at two opposite sides, one for the accommodation of the light source (Kessil lamp) and the other for a fan, to control the temperature.

The box is placed over a stirring plate and the walls were covered with aluminium foil to reflect the light inside the box. With this homemade setup, three reaction vials can be placed at the same time.

Figure 26. *Homemade photochemical setup.*

The photocatalytic reactions schematized in Scheme 46, were performed using the following procedure:

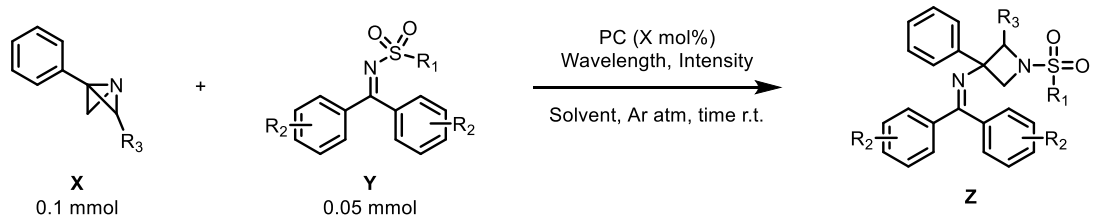

Scheme 46. *General photocatalytic reaction scheme.*

In a 4 mL vial, the corresponding ABB derivative (**X**) 2 equiv. (0.1 mmol) was weighted, then the photocatalyst solution (0.25 mol% of the PC in 0.5 mL of solvent) was added to the vial, followed by the addition of the corresponding N-sulfonylimine (**Y**) 1 equiv. (0.05 mmol) under Ar atmosphere. After that, the freeze-pump-thaw (FPT) method was performed to remove the presence of oxygen and water traces. After that, the reactions were stirred under the Kessil lamp for the reaction time with the proper selection of wavelength and intensity. Finally, the solvent was removed with the use of a centrifuge and the reaction crude was analysed by ^{1}H NMR after the addition of the internal standard. The desired product (**Z**) and the by-products were isolated and purified by flash column chromatography with the proper eluent mixture of petroleum ether and ethyl acetate.

4.6 *Characterization of Compounds*

4.6.1 *Spectroscopic Data*

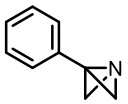

42

42. Colorless oil

^{1}H NMR (400 MHz, $CDCl_3$): δ 7.47 – 7.30 (m, 5H), 2.80 (bs, 2H), 1.55 (bs, 2H).

^{13}C NMR (100 MHz, $CDCl_3$): δ 134.8, 128.4, 127.9, 127.4, 53.9.

[ESI-MS]: 132 (M+1)

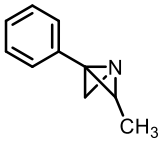

74

74. Colorless oil

^{1}H NMR (400 MHz, $CDCl_3$): δ 7.45 – 7.40 (m, 2H), 7.38 – 7.28 (m, 3H), 2.52 (d, *J* = 2.7 Hz, 1H), 1.71 (q, *J* = 5.1 Hz, 1H), 1.52 (dd, *J* = 2.7, 0.7 Hz, 1H), 1.16 (d, *J* = 5.5 Hz, 3H).

^{13}C NMR (101 MHz, $CDCl_3$): δ 133.1, 128.7, 128.3, 127.9, 62.2, 54.1, 35.1, 13.6.

[ESI-MS]: 146 (M+1)

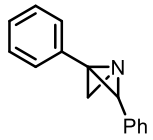

75

75. Clear yellow oil

^{1}H NMR (400 MHz, $CDCl_3$) δ 7.30 – 7.20 (m, 10H), 2.72 (d, *J* = 2.7 Hz, 1H), 2.67 (s, 1H), 1.73 (d, *J* = 2.7 Hz, 1H).

^{13}C NMR (100 MHz, $CDCl_3$) δ 134.5, 132.2, 128.4, 128.1, 128.0, 127.9, 127.8, 67.4, 52.1, 37.4.

[ESI-MS]: 208 (M+1)

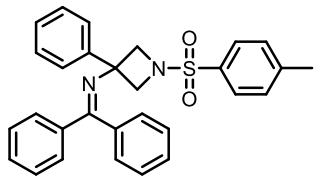

46. White crystals

^{1}H NMR (400 MHz, CD_2Cl_2) δ 7.59 (d, *J* = 8.2 Hz, 2H), 7.43 – 7.33 (m, 9H), 7.33 – 7.26 (m, 5H), 7.24 (apparent t, *J* = 7.6 Hz, 2H), 6.66 (dd, *J* = 7.9, 1.5 Hz, 2H), 3.74 (d, *J* = 8.4 Hz, 2H), 3.70 (d, *J* = 8.5 Hz, 2H), 2.37 (s, 3H).

^{13}C NMR (100 MHz, CD_2Cl_2) δ 167.6, 145.5, 144.5, 140.0, 137.0, 130.5, 130.5, 129.8, 129.5, 128.8, 128.7, 128.6, 128.3, 128.0, 127.9, 127.3, 125.2, 65.1, 60.9, 21.4.

[ESI-MS]: 467 (M+1)

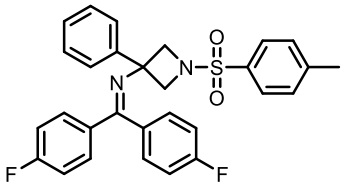

51. Colourless oil

^{1}H NMR (400 MHz, $CDCl_3$) δ 7.66 (d, *J* = 8.2 Hz, 2H), 7.46 (apparent d, *J* = 5.6 Hz, 1H), 7.44 (apparent d, *J* = 5.5 Hz, 1H), 7.41 – 7.36 (m, 2H), 7.34 (d, *J* = 7.7 Hz, 3H), 7.32 – 7.27 (m, 2H), 7.01 (t, *J* = 8.6 Hz, 2H), 6.93 (t, *J* = 8.6 Hz, 2H), 6.68 (apparent d, *J* = 5.4 Hz, 1H), 6.65 (apparent d, *J* = 5.4 Hz, 1H), 3.82 (d, *J* = 8.4 Hz, 2H), 3.76 (d, *J* = 8.5 Hz, 2H), 2.40 (s, 3H).

^{13}C NMR (400 MHz, $CDCl_3$) δ 165.6, 164.4 (d, *J* = 251.9 Hz), 163.1 (d, *J* = 251.1 Hz), 145.2, 144.2, 135.9, 132.6 (d, *J* = 3.9 Hz), 131.3, 130.8 (d, *J* = 8.7 Hz), 129.9 (d, *J* = 8.2 Hz), 129.6, 128.8, 128.5, 127.4, 125.0, 115.5 (d, *J* = 48.3 Hz), 115.2 (d, *J* = 48.5 Hz), 64.8, 60.7, 21.6.

^{19}F NMR (377 MHz, $CDCl_3$) δ -109.80, -109.87.

[ESI-MS]: 503 (M+1)

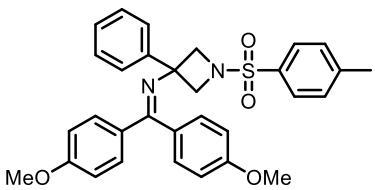

52. Yellow solid

^{1}H NMR (400 MHz, $CDCl_3$) δ 7.64 (d, *J* = 8.0 Hz, 2H), 7.47 (d, *J* = 7.7 Hz, 2H), 7.38 (d, *J* = 8.5 Hz, 2H), 7.33 (dd, *J* = 8.0, 3.5 Hz, 4H), 7.28 (d, *J* = 7.3 Hz, 1H), 6.82 (d, *J* = 8.7 Hz, 2H), 6.72 (d, *J* = 8.5 Hz, 2H), 6.61 (d, *J* = 8.4 Hz, 2H), 3.83 (s, 3H), 3.80 (s, 3H), 3.77 (d, *J* = 8.4 Hz, 2H), 3.74 (d, *J* = 8.4 Hz, 2H), 2.39 (s, 3H).

^{13}C NMR (100 MHz, $CDCl_3$) δ 166.7, 161.5, 160.3, 145.9, 144.1, 133.1, 130.9, 129.6, 129.5, 129.2, 128.7, 128.6, 127.2, 125.1, 113.5, 113.2, 65.3, 60.7, 55.4, 55.3, 21.6.

[ESI-MS]: 527 (M+1)

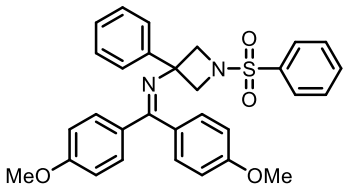

53. Yellow oil

^{1}H NMR (400 MHz, $CDCl_3$) δ 7.76 (d, *J* = 8.0 Hz, 2H), 7.64 – 7.58 (m, 1H), 7.55 (dd, *J* = 8.2, 6.6 Hz, 2H), 7.50 – 7.45 (m, 2H), 7.38 (d, *J* = 8.8 Hz, 2H), 7.34 (t, *J* = 7.4 Hz, 2H), 7.28 (d, *J* = 6.9 Hz, 1H), 6.82 (d, *J* = 8.8 Hz, 2H), 6.73 (d, *J* = 8.7 Hz, 2H), 6.60 (d, *J* = 8.7 Hz, 2H), 3.83 (s, 3H), 3.81 (s, 3H), 3.79 (d, *J* = 8.4 Hz, 2H), 3.74 (d, *J* = 8.4 Hz, 2H).

^{13}C NMR (100 MHz, $CDCl_3$) δ 166.7, 161.5, 160.3, 145.8, 133.9, 133.2, 133.0, 130.5, 129.5, 129.2, 128.9, 128.7, 128.5, 127.2, 125.1, 113.6, 113.3, 65.3, 60.7, 55.4, 55.3.

[ESI-MS]: 513 (M+1)

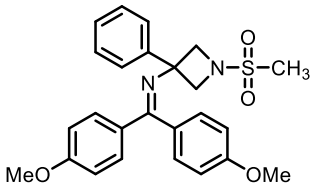

54. Colourless oil

^{1}H NMR (400 MHz, $CDCl_3$) δ 7.61 (d, *J* = 8.7 Hz, 2H), 7.58 – 7.51 (m, 2H), 7.37 (t, *J* = 7.5 Hz, 2H), 7.31 (d, *J* = 7.3 Hz, 1H), 6.88 (d, *J* = 8.7 Hz, 2H), 6.75 (collapsed dd, 4H), 4.11 (d, *J* = 7.9 Hz, 2H), 3.85 (s, 3H), 3.80 (s, 3H), 3.76 (d, *J* = 7.9 Hz, 2H), 2.83 (s, 3H).

^{13}C NMR (100 MHz, $CDCl_3$) δ 167.1, 161.6, 160.2, 145.9, 132.9, 130.6, 129.6, 129.2, 128.7, 127.3, 125.1, 113.6, 113.4, 64.5, 60.3, 55.4, 55.2, 36.2.

[ESI-MS]: 451 (M+1)

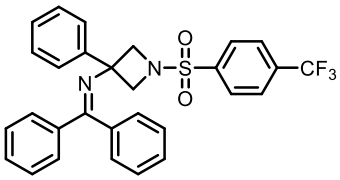

55. Clear oil

1H NMR (400 MHz, CDCl3) δ 7.92 (d, J = 8.2 Hz, 2H), 7.84 (d, J = 8.2 Hz, 2H), 7.51 – 7.46 – 7.38 (m, 9H), 7.42 (dt, J = 8.1, 1.6 Hz, 1H), 7.38 – 7.30 (m, 6H), 7.26 (t, J = 7.6 Hz, 2H), 6.70 (d, J = 7.9 Hz, 2H), 3.89 (d, J = 8.5 Hz, 2H), 3.84 (d, J = 8.5 Hz, 2H).

13C NMR (100 MHz, CDCl3) δ 168.18, 145.07, 138.28, 135.1, 134.7, 130.72, 129.59, 128.83, 128.80, 128.75, 128.32, 128.13, 127.82, 127.47, 126.15 (q, J = 3.7 Hz), 125.02, 123.3 (q, J = 274 Hz), 65.1, 60.8.

19F NMR (377 MHz, CDCl3) δ -63.1.

[ESI-MS]: 521 (M+1)

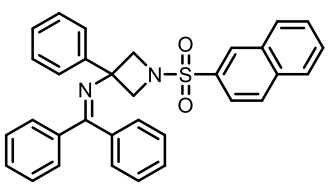

56. Orange crystals

1H NMR (400 MHz, CD2Cl2) δ 8.34 (d, J = 1.9 Hz, 1H), 8.07 (dd, J = 9.2, 3.3 Hz, 2H), 8.00 – 7.93 (m, 1H), 7.77 (dd, J = 8.6, 1.9 Hz, 1H), 7.71 (dt, J = 6.3, 3.4 Hz, 2H), 7.45 (dt, J = 6.1, 1.5 Hz, 2H), 7.43 – 7.20 (m, 11H), 6.56 (d, J = 6.9 Hz, 2H), 3.85 (collapsed AB system, 4H).

13C NMR (75 MHz, CD2Cl2) δ 167.4, 145.3, 139.8, 136.9, 135.1, 132.1, 130.7, 130.2, 130.0, 129.4, 129.2, 129.0, 128.6, 128.5, 128.2, 127.9, 127.8, 127.7, 127.2, 125.1, 65.1, 60.8.

[ESI-MS]: 503 (M+1)

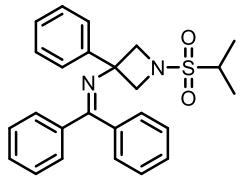

57. Colorless oil

1H NMR (400 MHz, CDCl3) δ 7.65 (d, J = 7.0 Hz, 2H), 7.54 – 7.47 (m, 2H), 7.40 – 7.34 (m, 5H), 7.31 (dd, J = 7.0, 2.0 Hz, 2H), 7.22 (t, J = 7.6 Hz, 2H), 6.82 (d, J = 7.1 Hz, 2H), 4.31 (d, J = 8.4 Hz, 2H), 3.62 (d, J = 8.4 Hz, 2H), 3.08 (h, J = 7.4, 6.8 Hz, 1H), 1.31 (d, J = 6.9 Hz, 6H).

13C NMR (100 MHz, CDCl3) δ 167.9, 146.1, 139.9, 137.1, 130.5, 129.2, 128.9, 128.7, 128.2, 128.1, 128.0, 127.2, 125.0, 64.8, 60.5, 53.5, 26.9, 16.4.

[ESI-MS]: 419 (M+1)

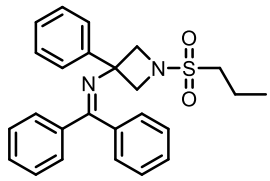

58. Colorless oil

1H NMR (400 MHz, CD2Cl2) δ 7.70 (dt, J = 7.0, 2H), 7.55 – 7.50 (m, 2H), 7.50 – 7.45 (m, 1H), 7.40 (ddd, J = 9.0, 7.0, 1.9 Hz, 5H), 7.29 (t, J = 7.7 Hz, 2H),

7.33 – 7.26 (m, 1H), 6.87 (d, J = 6.9 Hz, 2H), 4.22 (d, J = 8.4 Hz, 2H), 3.69 (d, J = 8.4 Hz, 2H), 2.93 – 2.87 (m, 2H), 1.80 (sext, J = 7.5 Hz, 2H), 1.04 (t, J = 7.5 Hz, 3H).

13C NMR (100 MHz, CD2Cl2) δ 167.8, 145.8, 139.9, 137.1, 130.5, 129.1, 128.8, 128.6, 128.2, 128.0, 127.9, 127.2, 63.8, 60.4, 52.4, 16.9, 12.7.

[ESI-MS]: 419 (M+1)

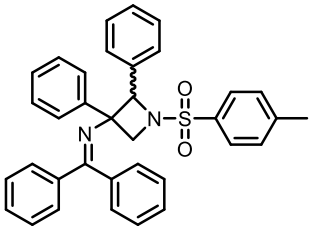

59. Major diastereoisomer. Yellowish oil

1H NMR (400 MHz, CDCl3) δ 7.57 (d, J = 7.8 Hz, 4H), 7.46 – 7.39 (m, 1H), 7.35 (t, J = 7.4 Hz, 2H), 7.29 – 7.27 (m, 4H), 7.22 (t, J = 7.6 Hz, 2H), 7.15 – 7.05 (m, 4H), 7.06 – 6.98 (m, 5H), 6.62 (d, J = 7.6 Hz, 2H), 5.07 (s, 1H), 3.54 (d, J = 8.7 Hz, 1H), 3.47 (d, J = 8.7 Hz, 1H), 2.39 (s, 3H).

13C NMR (100 MHz, CDCl3) δ 166.8, 144.2, 141.2, 139.5, 137.1, 135.6, 130.5, 129.5, 129.2, 128.8, 128.7, 128.1, 128.0, 128.0, 127.7, 127.3, 127.3, 127.1, 126.8, 126.8, 79.6, 68.0, 59.0, 29.7, 21.6.

[ESI-MS]: 543 (M+1)

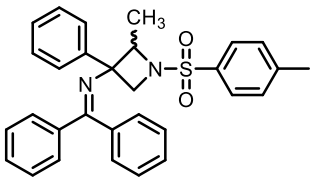

60. Crystalline solid

^{1}H NMR (400 MHz, $CDCl_3$) δ 7.68 (dd, *J* = 8.3, 1.7 Hz, 4H), 7.47 – 7.42 (m, 1H), 7.40 – 7.35 (m, 2H), 7.37 (m, 2H), 7.19 (t, *J* = 7.7 Hz, 2H), 7.16 – 7.12 (m, 1H), 7.09 (t, *J* = 7.4 Hz, 2H), 6.76 – 6.72 (m, 2H), 6.70 (d, *J* = 6.9 Hz, 2H), 4.24 (q, *J* = 6.4 Hz, 1H), 3.81 (d, *J* = 9.6 Hz, 1H), 3.72 (d, *J* = 9.6 Hz, 1H), 2.47 (s, 3H), 1.73 (d, *J* = 6.4 Hz, 3H).

13C NMR (100 MHz, CDCl3) δ 168.6, 145.9, 143.7, 140.7, 137.7, 133.1, 130.4, 129.7, 128.9, 128.8, 128.4, 128.1, 128.1, 127.8, 126.6, 125.0, 75.9, 63.0, 58.8, 21.6, 16.7.

[ESI-MS]: 481 (M+1)

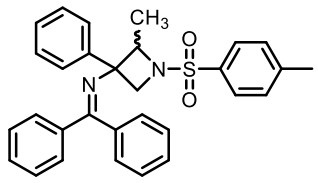

60. Crystalline solid

1H NMR (400 MHz, CDCl3) δ 7.63 (d, J = 8.3 Hz, 2H), 7.46 (d, J = 6.9 Hz, 2H), 7.41 – 7.37 (m, 3H), 7.37 – 7.27 (m, 8H), 7.19 (t, J = 7.6 Hz, 2H), 6.58 (d, J = 6.8 Hz, 2H), 4.05 (q, J = 6.4 Hz, 1H), 3.37 (d, J = 8.8 Hz, 1H), 3.23 (d, J = 8.8 Hz, 1H), 2.41 (s, 3H), 0.96 (d, J = 6.4 Hz, 3H).

13C NMR (100 MHz, CDCl3) δ 167.1, 144.1, 141.9, 139.8, 137.2, 130.9, 130.3, 129.5, 129.2, 128.6, 128.6, 128.3, 128.1, 128.0, 127.9, 127.2, 126.7, 72.9, 65.2, 60.3, 21.6, 16.4.

[ESI-MS]: 481 (M+1)

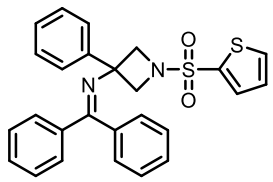

61. Yellow oil

1H NMR (400 MHz, CDCl3) δ 7.68 (dd, J = 5.0, 1.3 Hz, 2H), 7.57 (dd, J = 3.8, 1.3 Hz, 1H), 7.50 (tt, J = 7.9, 1.2 Hz, 4H), 7.46 – 7.42 (m, 2H), 7.42 – 7.31 (m, 5H), 7.26 – 7.19 (m, 3H), 6.72 (d, J = 6.9 Hz, 1H), 3.88 (d, J = 8.7 Hz, 2H), 3.85 (d, J = 8.6 Hz, 2H).

13C NMR (100 MHz, CDCl3) δ 167.7, 145.3, 139.8, 136.8, 133.9, 132.9, 130.5, 130.1, 129.6, 128.8, 128.8, 128.7, 128.3, 128.1, 127.8, 127.7, 127.4, 127.3, 125.1, 65.6, 60.6.

[ESI-MS]: 459 (M+1)

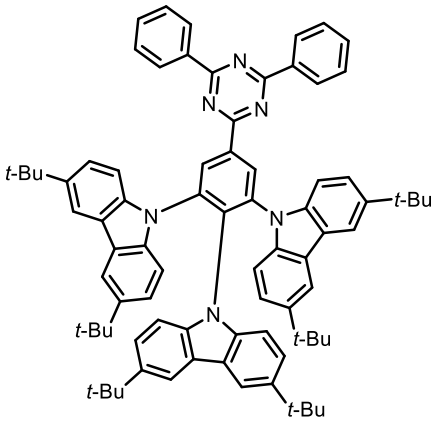

PC13. Yellow solid

1H NMR (400 MHz, CDCl3) δ 9.19 (s, 2H), 8.75 (d, J = 7.0 Hz, 4H), 7.80 (d, J = 1.8 Hz, 2H), 7.66 – 7.58 (m, 2H), 7.55 (dd, J = 8.2, 6.6 Hz, 4H), 7.30 (d, J = 1.9 Hz, 2H), 7.13 (d, J = 8.6 Hz, 2H), 7.08 (dd, J = 8.7, 1.9 Hz, 4H), 6.78 (d, J = 8.6 Hz, 2H), 6.61 (dd, J = 8.6, 1.9 Hz, 2H), 1.39 (s, 36H), 1.26 (s, 18H).

[ESI-MS]: 1141 (M+1)

4.6.2 Characterization spectra of model reaction products

In this section, the NMR and ESI-MS spectra of the model reaction products (Scheme 29, Figure 27) are reported.

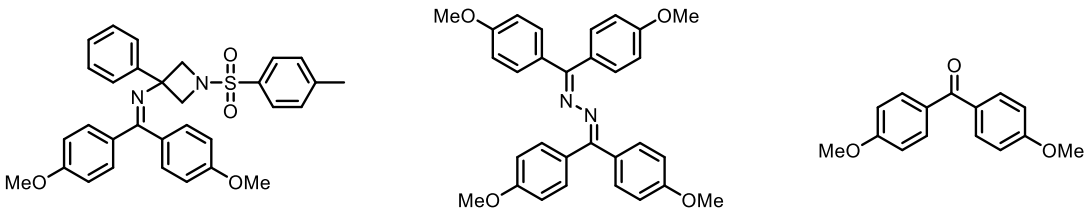

Exact Mass: 526.19 | Exact Mass: 480.20 | Exact Mass: 242.09

52A | **52B** | **52C**

Figure 27. *Model reaction products: desired product (**52A**), homocoupling product (**52B**) and hydrolisis product (**52C**)*

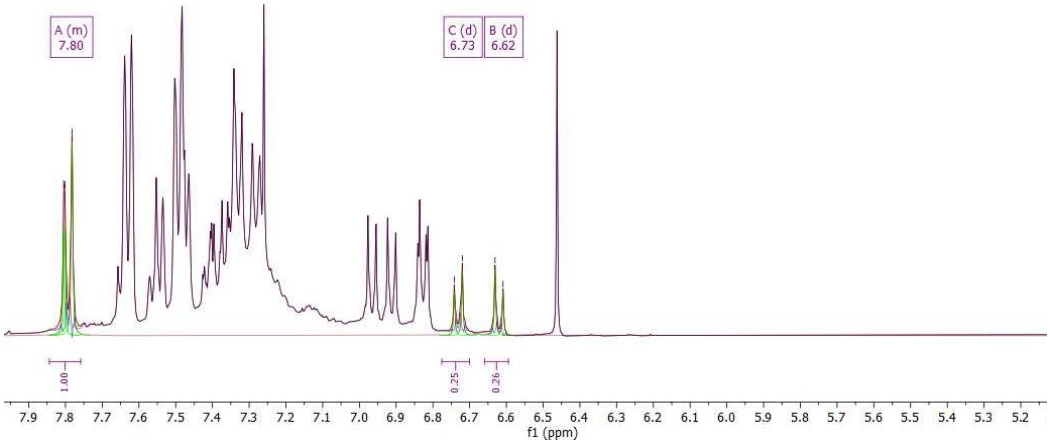

Figure 28. *Aromatic ^{1}H NMR region of the model reaction crude.*

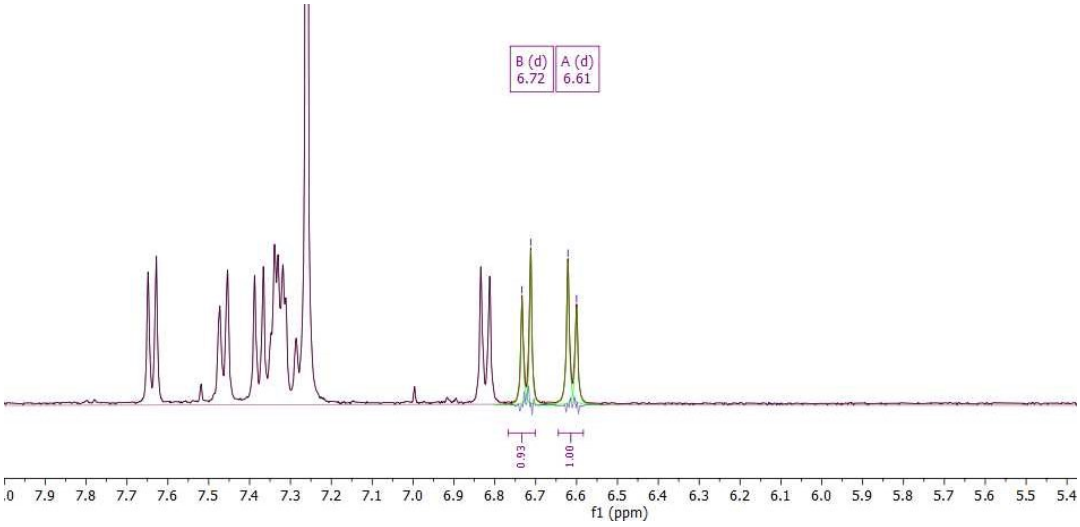

Figure 29. *Aromatic ^{1}H NMR region of **52A**.*

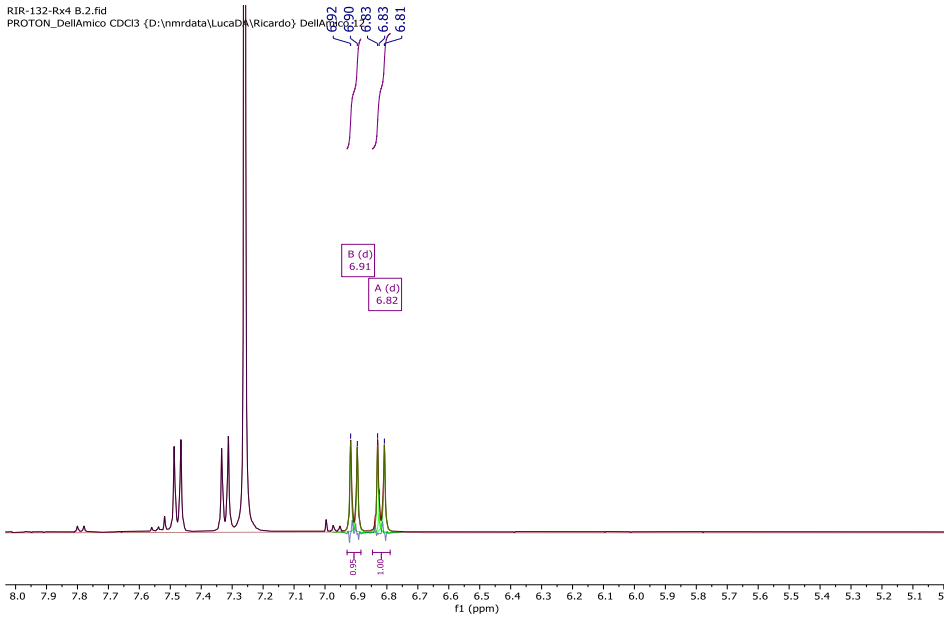

Figure 30. *Aromatic ^{1}H NMR region of* ***52B****.*

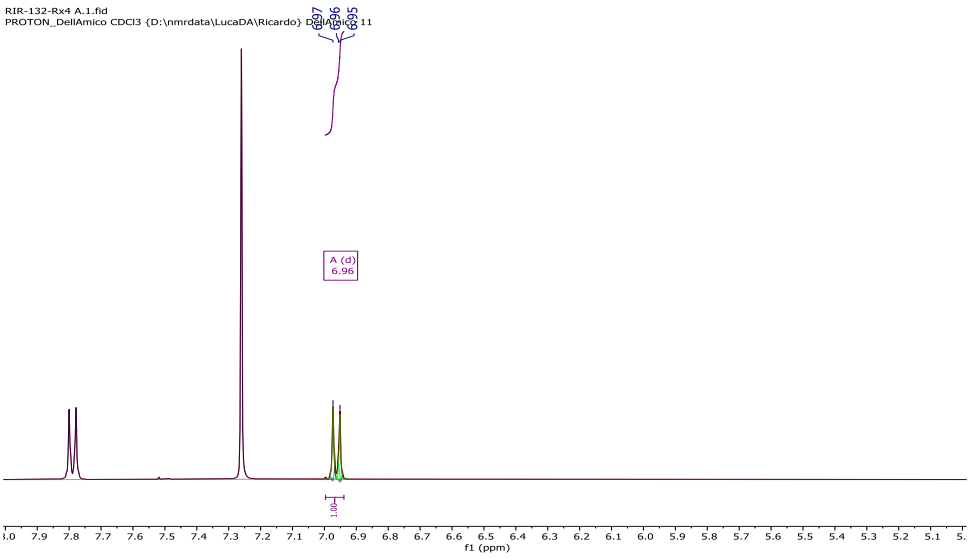

Figure 31. *Aromatic 1H NMR region of* ***52C****.*

The ESI-MS spectra were performed eluting the analytes with a mixture 100:1 methanol / formic acid and scanning in positive polarity.

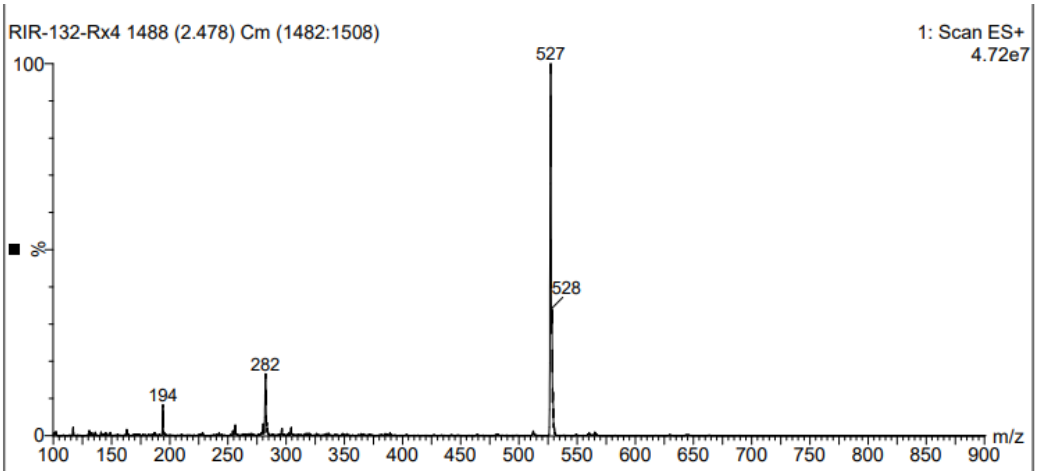

***Figure 32**. ESI-MS spectrum of compound **52A**. [M+1] = 527.*

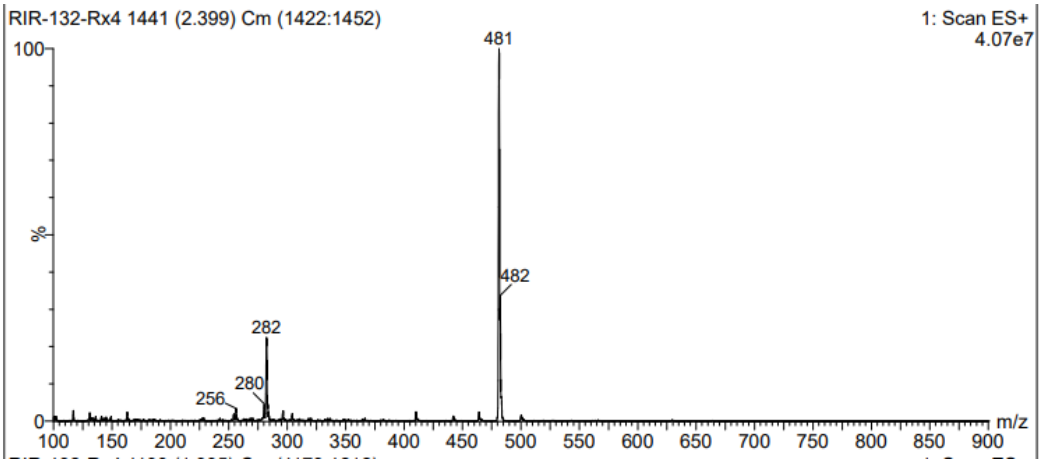

***Figure 33.** ESI-MS spectrum of compound **52B**. [M+1] = 481.*

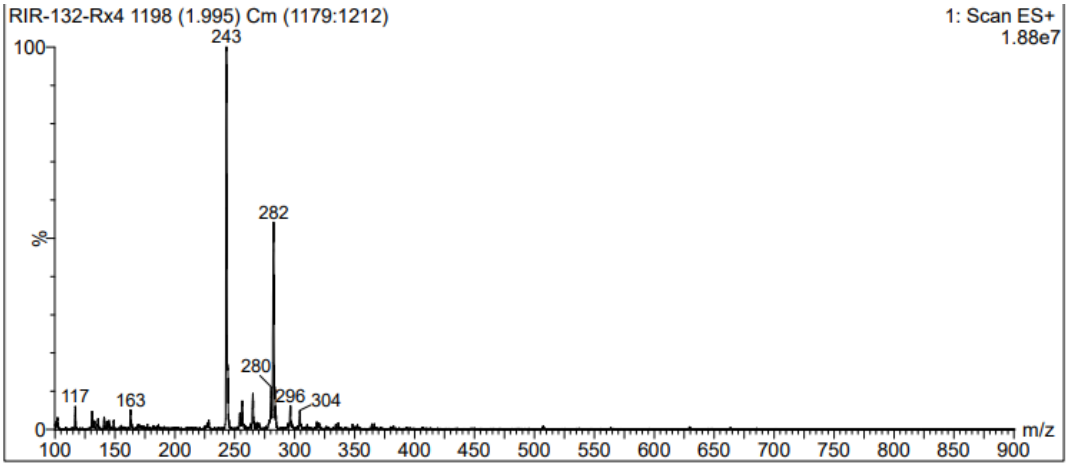

***Figure 34.** ESI-MS spectrum of compound **52C**. [M+1] = 243.*

4.6.3 Absorption, Emission and Phosphorescence Spectra of TRZPCs

In this section, Absorption, Emission and Phosphorescence spectra of **PC12** and **PC13** are reported.

- *Absorption Spectra*

All the UV-Vis spectra were recorded from a PC solution ([PC] = 10^{-4}M) in Toluene.

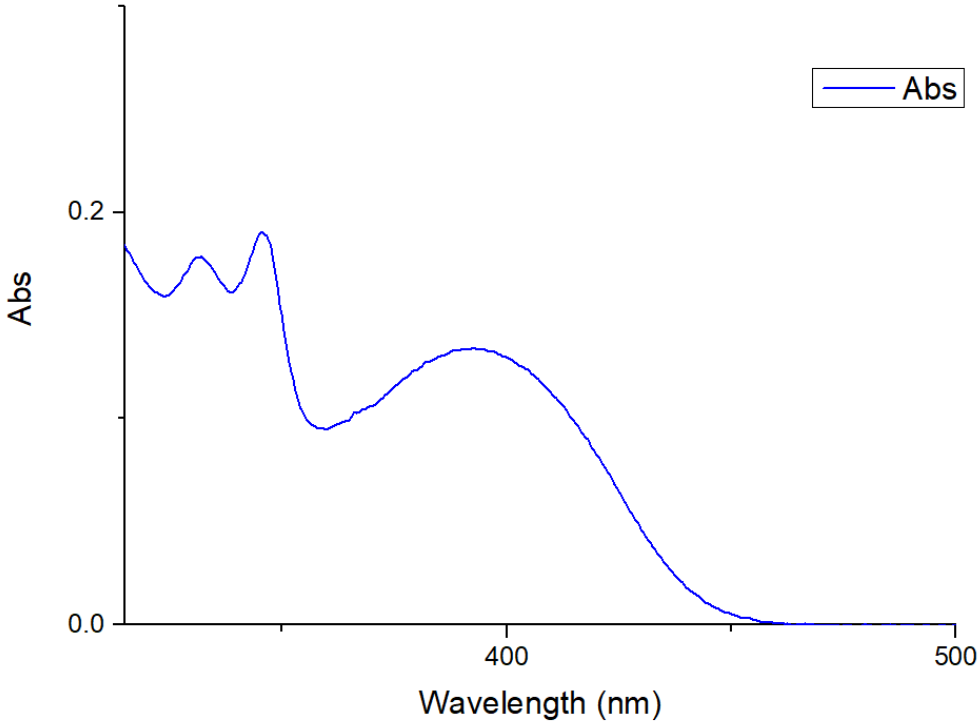

Figure 35. *Absorption profile of* ***PC12***

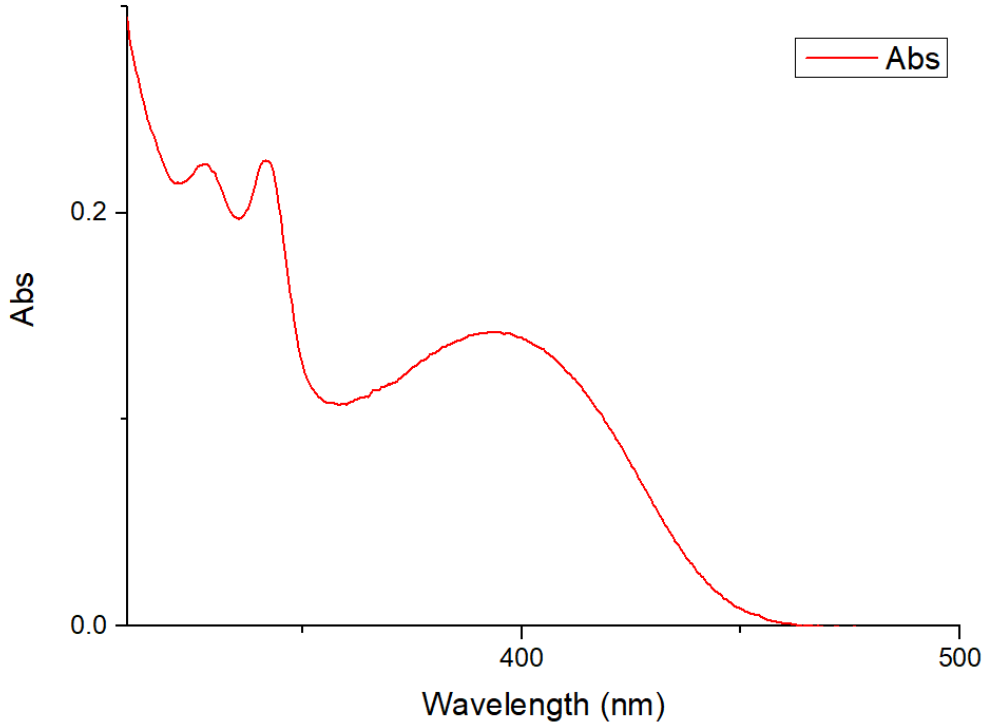

Figure 36. *Absorption profile of* ***PC13***

- *Emission Spectra*

All the emission spectra were recorded from a PC solution ([PC] = 10^{-4}M) in Toluene.

The choice of the excitation wavelength was based on the absorption spectra, in particular at the selected wavelength, the absorbance of the analyte must not exceed 0.1, to avoid self-absorption of the PC of its the emitted radiation.

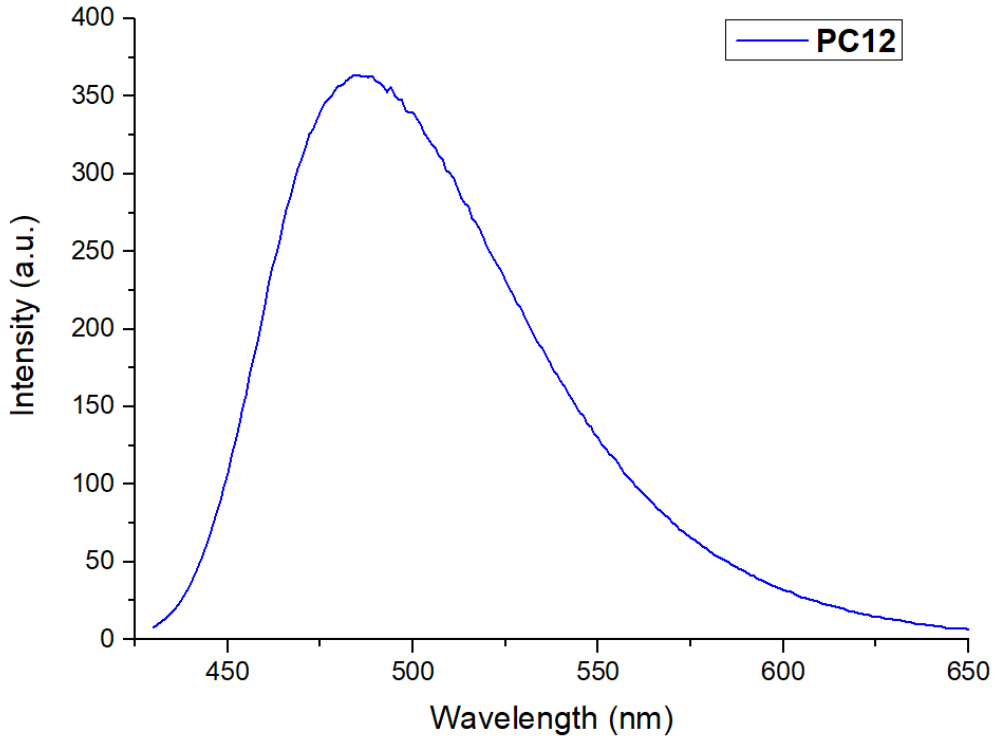

Figure 37. *Emission profile of* ***PC12****.*

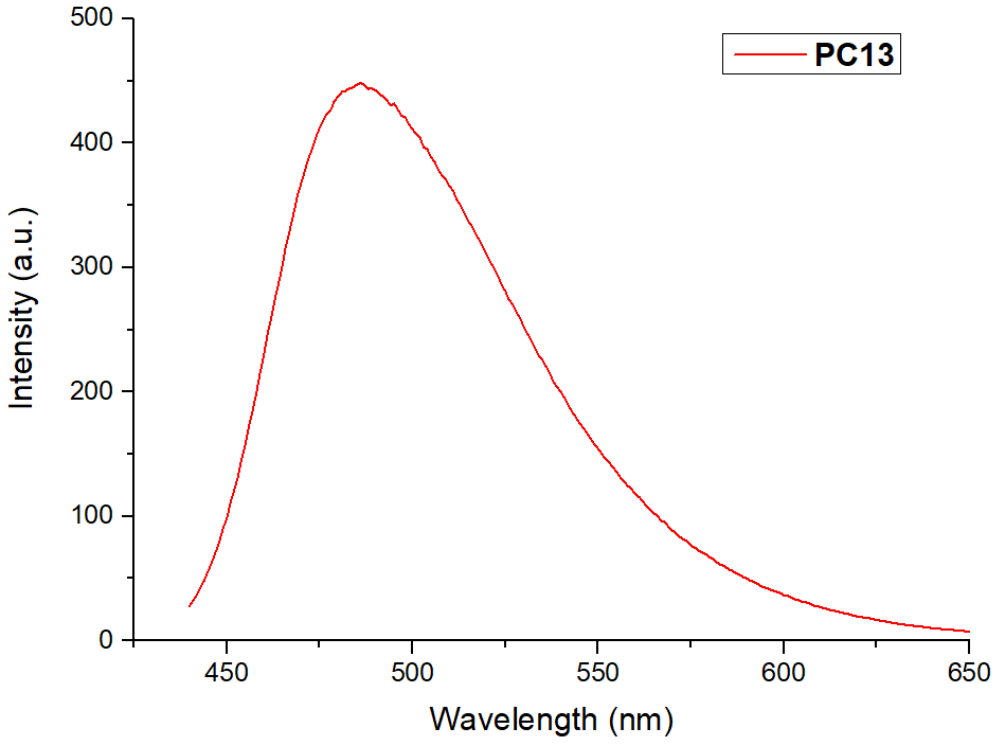

Figure 38. *Emission profile of* ***PC13****.*

- *Phosphorescence Spectra*

Phosphorescence spectra were recorded from a PC solution ([PC] = 10^{-3}M) in Toluene. The solution was placed inside the glass tube, then the tube was placed in liquid nitrogen to freeze the solution, taking care of avoiding the 'crack' of the solvent. Then the tube was placed inside the instrument and the spectra was recorded with a delay in the acquisition time of 5 ms, to avoid the fluorescence contribution.

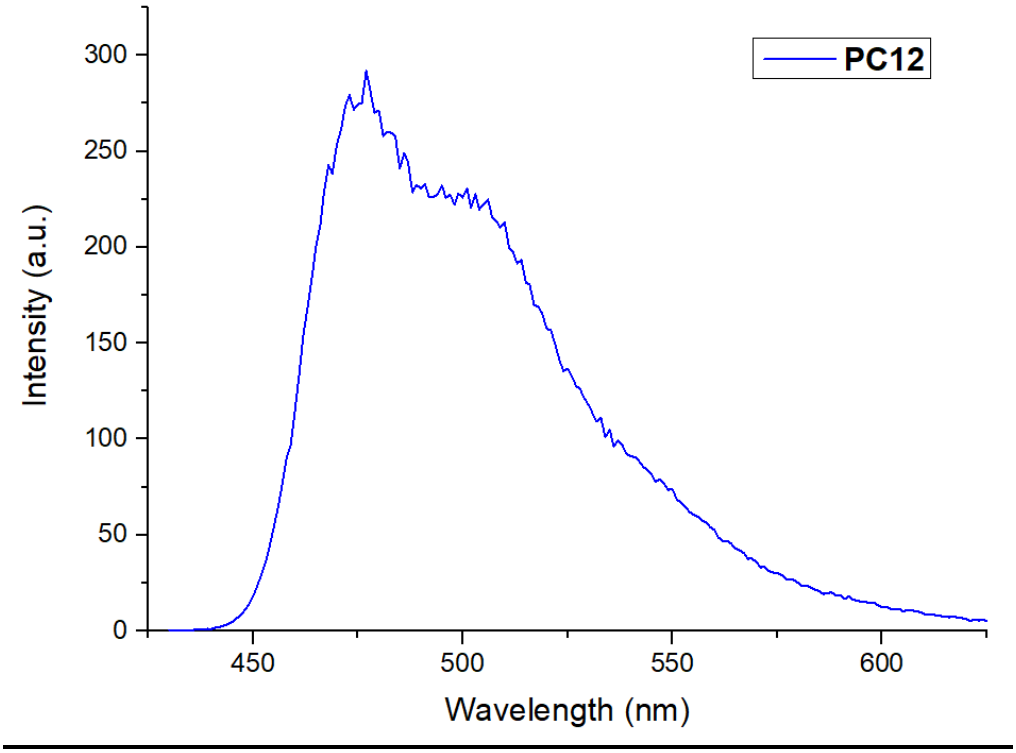

Figure 39. *Phosphorescence profile of* ***PC12***

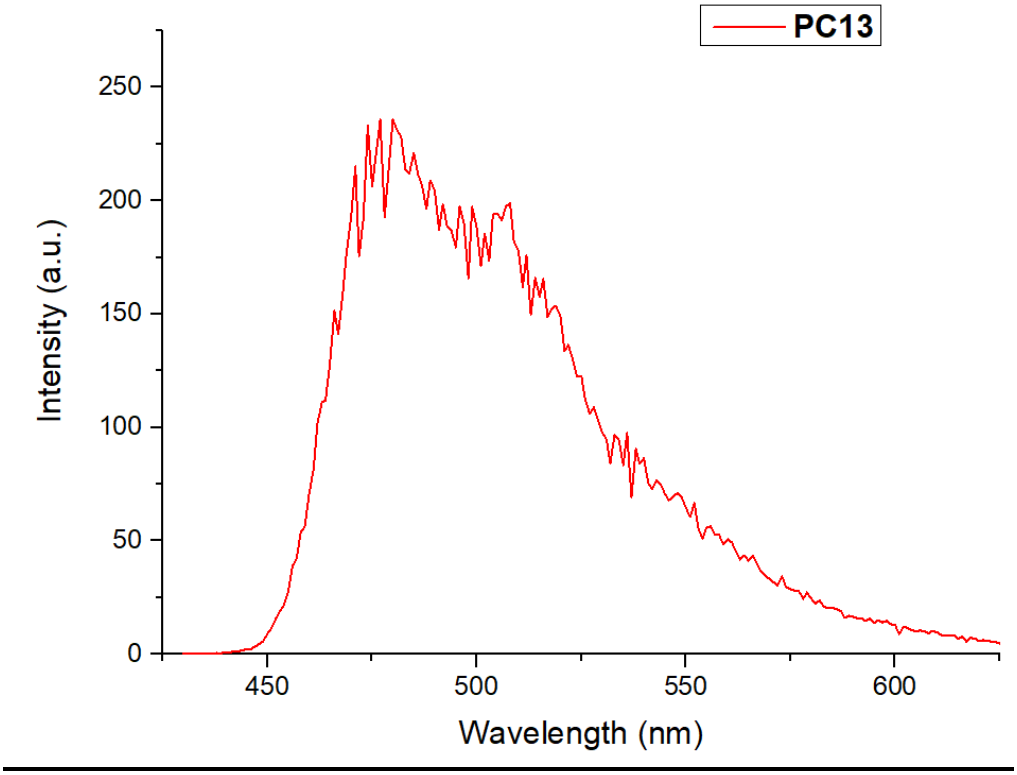

Figure 40. *Phosphorescence spectrum of* ***PC13***

5 References

[1]: A.B. Beeler *Chem. Rev.* **2016**, *116*, 9629

[2]: B. König Eur. *J. Org. Chem.* **2017**, 1979

[3]: Laura Buglioni, F. Raymenants, A. Slattery, S. D. A. Zondag and T. Noël *Chem. Rev.* **2022**, *122*, 2752

[4]: H.D. Roth Angew. *Chem. Int. Ed. Engl.* **1989**, *28*, 1193

[5]: G. Ciamician *Science* **1912**, *36*, 385

[6]: L. A. Coldren, S. W. Corzine, M. L. Mašanović *Diode Lasers and Photonic Integrated Circuits* **2012**

[7]: H. H. Jaffe and Albert L. Miller *J. Chem. Educ.* **1966**, *43*, 469

[8]: M. Luis, D.M. Bishop, B. Kirtman. *J. Chem. Phys.* **2004**, *120*, 813

[9]: Kahler, *Arch. Pharm.* **1830**, *34*, 318.

[10] Alms, *Arch. Pharm.* **1830***, 34*, 319.

[11] H. Trommsdorff, *Ann. Chem. Pharm.* **1834**, 190

[12]: F. Sestini, *Bull. SOC. Chim.* **1866**, *2*, 202

[13]: S. Cannizzaro, F. Sestini *Gazz. Chim. Ital.* **1873**, *3*, 241

[14]: D. Ravelli, D. Dondi, M. Fagnonia and A. Albini *Chem. Soc. Rev.* **2009**, *38*, 1999

[15]: M. H. Shaw, J. Twilton and D. W. C. MacMillan *J. Org. Chem.* **2016**, *81*, 6898

[16]: S. Reischauer and B. Pieber *iScience* **2021**, *24*, 102209

[17]: P. Melchiorre *Chem. Rev.* **2022**, *122*, 1483

[18]: N. A. Romero and D. A. Nicewicz *Chem. Rev.* **2016**, *116*, 10075

[19]: L. Buzzetti, G. E. M. Crisenza and P. Melchiorre Angew. *Chem. Int. Ed.* **2019**, *58*, 3730

[20]: T. Bortolato, G. Simionato, M. Vayer, C. Rosso, L. Paoloni, E. M. Benetti, A. Sartorel, D. Lebœuf, and L. Dell'Amico *J. Am. Chem. Soc.* **2023**, *145*, 1835

[21]: L. Capaldo and D. Ravelli Eur. *J. Org. Chem.* **2017**, 2056

[22]: J. W. Verhoeven, *Pure Appl. Chem.* **1996**, *68*, 2223

[23]: F. Strieth-Kalthoff, M. J. James, M. Teders, L. Pitzer and F. Glorius *Chem. Soc. Rev.* **2018**, *47*, 7190

[24]: T. Forster, *Ann. Phys.*, **1948**, *437*,55

[25]: M. Beutler, R. Heintzmann, *Encyclopedic Reference of Genomics and Proteomics in Molecular Medicine* Springer, Berlin, Heidelberg, **2005**, 594

[26]: Amrita Kaur, Pardeep Kaur and Sahil Ahuja *Anal. Methods* **2020**, *12*, 5532

[27]: J. SzöllÖsi, D. R. Alexander, *Methods in Enzymology*, *Academic Press* **2003**, *366*, 203,

[28]: Y. Qiao, Y. Luo, N. Long,Y. Xing, J.Tu, *Micromachines* **2021**, *12*, 492

[29]: D. L. Dexter, *J. Chem. Phys.* **1953**, *21*, 836

[30]: R. A. Marcus, *Rev. Mod. Phys.* **1993**, *65*, 599

[31]: J. B. Birks, *Nature* **1967**, *214*, 1187

[32]: S. Bai, P. Zhang, P. Antoniou, S. S. Skourtis and D. N. Beratan *Faraday Discuss.* **2019**, *216*, 301

[33]: M. A. Bryden and E. Zysman-Colman *Chem. Soc. Rev.* **2021**, *50*, 7587

[34]: X. Yin, Y. He, X. Wang, Z. Wu, E. Pang, J. Xu and J. Wang *Front. Chem.* **2020**, *8*, 725.

[35]: A. Endo, M. Ogasawara, A. Takahashi, D. Yokoyama, Y. Kato and C. Adachi, *Adv. Mater. Weinheim* **2009**, *21*, 4802

[36]: T. Hatakeyama, K. Shiren, K. Nakajima, S. Nomura, S. Nakatsuka, K. Kinoshita, J. Ni, Y. Ono and T. Ikuta *Adv. Mater.* **2016**, *28*, 2777

[37]: H. Uoyama, K. Gouschi, K. Shizu, H. Nomura and C. Adachi *Nature* **2012**, *492*, 234

[38]: A. Endo, K. Sato, T. Kai, A. Kawada, H. Miyazaki, C. Adachi *Appl. Phys. Lett.* **2011**, *98*, 083302

[39]: C. Zang, S. Liu, M. Xu, R. Wang, C. Cao, Z. Zhu, J. Zhang, H. Wang, L. Zhang, W. Xie and C.S. Lee *Science & Applications* **2021**, *10*, 116

[40]: F. Strieth-Kalthoff and F. Glorius *Chem* **2020**, *6*, 1888

[41]: Q. Liu and L.Z. Wu National *Science Review* **2017**, *4*, 359

[42]: S. Poplata, A. Tröster, Y.Q. Zou and T. Bach *Chem. Rev.* **2016**, *116*, 9748

[43]: D. Sarkar, N. Bera and S. Ghosh *Eur. J. Org. Chem.* **2020**, 1310

[44]: M. Zhu, C. Zheng, X. Zhang and S. You *J. Am. Chem. Soc.* **2019**, *141*, 2636

[45]: J. J. Molloy, T. Morack and R. Gilmour *Angew. Chem. Int. Ed.* **2019**, *58*, 13654

[46]: J. B. Metternich and R. Gilmour *J. Am. Chem. Soc.* **2016**, *138*, 1040

[47]: A. G. Walker, G. K. Radda *Nature* **1967**, *215*, 1483

[48]: M. Teders, C. Henkel, L. Anhäuser, F. Strieth-Kalthoff, A. Gómez-Suárez, R. Kleinmans, A. Kahnt, A. Rentmeister, D. Guldi and F. Glorius *Nature Chemistry* **2018**, *10*, 981

[49]: T. Patra, S. Mukherjee, J. Ma, F. Strieth-Kalthoff and F. Glorius *Angew. Chem. Int. Ed.* **2019**, *58*, 10514

[50]: M. J. Tilby, D. F. Dewez, L. R. E. Pantaine, A. Hall, C. Martínez-Lamenca, and M. C. Willis *ACS Catal.* **2022**, *12*, 6060

[51]: D. Antermite, L. Degennaro and R. Luisi *Org. Biomol. Chem.* **2017**, *15*, 34

[52]: A. Brandi, S. Cicchi, and F. M. Cordero *Chem. Rev.* **2008**, *108*, 3988

[53]: D. Enders, J. Gries *SYNTHESIS* **2005**, *20*, 3508

[54]: Z. Hong, A. Bolard, C. Giraud, S. Prevost, G. Genta-Jouve, C. Deregnaucourt, S. Hussler, K. Jeannot, and Y. Li Angew. *Chem. Int. Ed.* **2019**, *58*, 3178

[55]: F. Lovering, J. Bikker, and C. Humblet *J. Med. Chem.* **2009**, *52*, 6752

[56]: F. Lovering Med. *Chem. Commun.* **2013**, *4*, 515

[57]: G.S. Singh, M. Dhooghe, N. De Kimpe, *Comprehensive Heterocyclic Chemistry III*, *2*, Elsevier, **2008**

[58]: F. Couty, G. Evano and N. Rabasso *Tetrahedron: Asymmetry* **2003**, *14*, 2407

[59]: L. Degennaro, M. Zenzola, P. Trinchera, L. Carroccia, A. Giovine, G. Romanazzi, A. Falcicchio and R. Luisi *Chem. Commun.* **2014**, *50*, 1698

[60]: B. Alcaide, P. Almendros and C. Aragoncillo *Chem. Rev.* **2007**, *107*, 4437

[61]: A. D. Richardson, M. R. Becker and C. S. Schindler *Chem. Sci.* **2020**, *11*, 7553

[62]: M. R. Becker, A. D. Richardson, C. S. Schindler *Nat Commun.* **2019**, *10*, 5095

[63]: M. Andresini, L. Degennaro and R. Luisi *Org. Biomol. Chem.* **2020**, *18*, 5798

[64]: N. De Kimpe, A. Žukauskaitė, S. Mangelinckx and A. Šačkus *Heterocycles* **2014**, *88*, 731.

[65]: J. Dolfen, N. N. Yadav, N. De Kimpe, M. D'hooghe and H. J. Ha, *Adv. Synth. Catal.* **2016**, *358*, 3485

[66]: J. L. Kurz, B. K. Gillard, D. A. Robertson and A. G. Hortmann, J. *Am. Chem. Soc.* **1970**, *92*, 5008

[67]: B. K. Gillard and J. L. Kurz, *J. Am. Chem. Soc.* **1972**, *94*, 7199

[68]: R. Gianatassio, J. M. Lopchuk, J. Wang, C. M. Pan, L. R. Malins, L. Prieto, T. A. Brandt, M. R. Collins, G. M. Gallego, N. W. Sach, J. E. Spangler, H. Zhu, J. Zhu and P. S. Baran, *Science* **2016**, *351*, 241

[69]: R. Gianatassio and D. Kadish, *Org. Lett.* **2019**, *21*, 2060

[70]: D. Zhang, M. Cai, Y. Zhang, D. Zhang and L. Duan *Mater. Horiz.* **2016**, *3*, 145

[71]: H. Uoyama, K. Coushi, K. Shizu, H. Nomura and C. Adachi, *Nature* **2012**, *492*, 234

[72]: A. A. Abdel-Shafi and David R. Worrall, *Journal of Photochemistry and Photobiology A: Chemistry* **2005**, *172*, 170

[73]: C. Schweitzer, R. Schmidt, *Chem. Rev.* **2003**, *103*, 1685

[74]: T.Rundlöf, M. Mathiassona, S. Bekiroglub, B. Hakkarainena, T. Bowdenc, T. Arvidsson *Journal of Pharmaceutical and Biomedical Analysis* **2010**, *52*, 645

[75]: C. J. Taylor, A. Pomberger, K. C. Felton, R. Grainger, M. Barecka, T. W. Chamberlain, R. A. Bourne, C. N. Johnson and A. A. Lapkin *Chem. Rev.* **2023**, *123*, 3089

[76]: A. Y. S. Lam and V. O. K. Li *Memetic Comp.* **2012***, 4*, 3

[77]: K. D. Collins, T. Gensch and F. Glorius *Nature Chemistry* **2014**, *6*, 859

[78]: T. Zhou, Z. Qi, and K. Sundmacher *Chemical Engineering Science* **2014**, *115*, 177

[79]: C. Reichardt, T. Welton *Solvents and Solvent Effects in Organic Chemistry* **2010,** Wiley-VCH Verlag GmbH & Co. KGaA

[80]: S. I. A. Shah, L. W. Kostiuk, and S. M. Kresta International *Journal of Chemical Engineering* **2012**, 1

[81]: H. Szatylowicz, A. Jezuita and T. M. Krygowski *Structural Chemistry* **2019**, *30*, 1529

[82]: X. Yang and D. Wang *ACS Appl. Energy Mater.* **2018**, *1*, 6657

[83]: D. A. Nicewicz, D. W. C. MacMillan *Science* **2008**, *322*, 77

[84]: H. E. Bonfield, T. Knauber, F. Lévesque *Nat Commun* **2020**, *11*, 804

[85]: C. J. Easley, F. Tong, X. Dong, R. O. Al-Kaysi and C. J. Bardeen *Chem. Sci.* **2020**, *11*, 9852

[86]: H. Fukagawa, T. Shimizu, T. Kamada *Sci. Rep.* **2015**, *5*, 9855

[87]: E. Speckmeier, T. G. Fischer and K. Zeitler *J. Am. Chem. Soc.* **2018**, *140*, 15353

[88]: D. R. Lee, M. Kim, S. K. Jeon, S. H. Hwang, C. W. Lee and J. Y. Lee *Adv. Mater.* **2015**, *27*, 5861

[89]: K. R. Justin Thomas, J. T. Liu, Y. T. Tao and C. H. Chuen, *Adv. Mater*. **2002**, *14*, 822

[90]: Y. H. Kim, D. C. Shin, S. H. Kim, C. H. Ko, H. S. Yu, Y. S. Chae and S. K. Kwom, *Adv. Mater.* **2001**, *13*, 1690.

[91]: Y. J. Cho, K. S. Yook and J. Y. Lee, *Adv. Mater.* **2014**, *26*, 6642

[92]: A. Kikuchi, Y. Hata, R. Kumasaka, Y. Nanbu and M. Yagi *Photochemistry and Photobiology* **2013**, *89*, 523

[93]: F. Edhborg, A. Olesund and B. Albinsson *Photochem. Photobiol. Sci.* **2022**, *21*, 1143

[94]: M. N. Hopkinson, A. G. Suarez, M. Teders, B. Sahoo and F. Glorius *Angew. Chem. Int. Ed.* **2016**, *55*, 4361

[95]: M. H. Gehlen *Journal of Photochemistry and Photobiology C: Photochemistry Reviews* **2020**, *42*, 100338

[96]: F. Weigend, M. Häser, H. Patzelt, R. Ahlrichs, *Chem. Phys. Lett.* **1998**, *294*, 143

[97]: L. Wang, Y. Yu, L. Deng, K. Du *Org. Lett.* **2023**, *25*, 2349

[98]: L. Chen, H. Li, P. Li, L. Wang, *Org. Lett.* **2016**, *18*, 3646

[99]: F. Zhang, Y. Wang, G. H. Lonca, X. Zhu, S. Chiba, *Angew. Chem. Int. Ed.* **2014**, *53*, 4390.

Ringraziamenti

Per l’importante traguardo raggiunto vorrei ringraziare innanzitutto i miei genitori, che mi hanno permesso di compiere questo percorso sostenendomi in tutti i momenti, soprattutto quelli più difficili. Vorrei inoltre ringraziare le mie sorelle, grazie al loro affetto ho compiuto il percorso con più serenità.

Vorrei dire grazie al resto della mia famiglia, che è sempre stata al mio fianco.

Vorrei ringraziare la mia fidanzata, che mi ha accompagnato con amore e generosità in questi anni, sopportandomi e supportandomi in ogni momento.

Vorrei inoltre ringraziare i miei amici e i miei compagni di calcio, che mi hanno permesso di divertirmi e distrarmi lungo il corso degli studi, offrendo sostegno e una sana ignoranza per superare i momenti più cupi.

Infine, vorrei ringraziare il Prof. Dell’Amico per avermi dato l’opportunità di lavorare all’interno del suo gruppo di ricerca, e tutti i componenti del gruppo per essere stati disponibili e gentili dandomi un grande aiuto durante il progetto di tesi, in particolare il Dott. Ricardo Rodriguez Perez con cui ho lavorato per lo sviluppo del progetto.